AD-A173 137 BLAST INDUCED LIQUEFACTION POTENTIAL AND TRANSIENT POREWATER PRESSURE RES (U) COLORADO STATE UNIV FORT COLLINS DEPT OF CIVIL ENGINEERING W A CHARLIE ET AL

1/3

UNCLASSIFIED 15 OCT 85 AFOSR-TR-86-0946 AFOSR-80-0260 F/G 8/13 NL

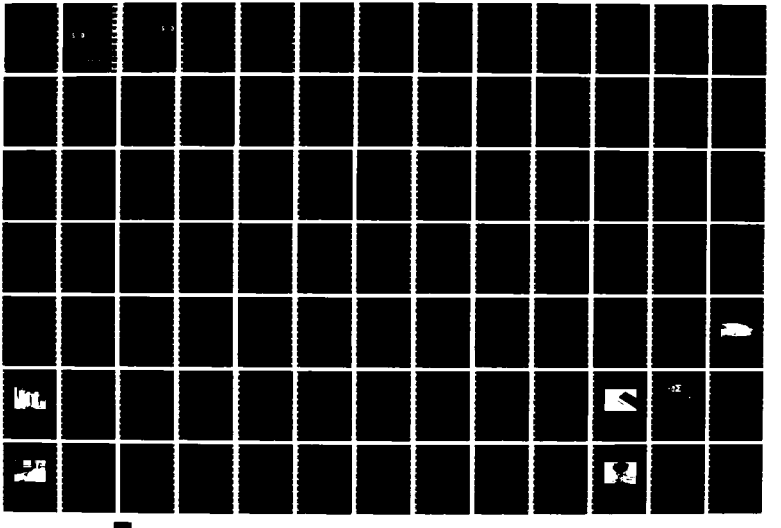

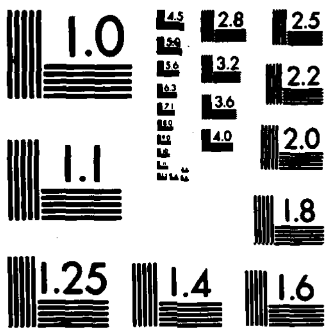

ICROCOPY RESOLUTION TEST CHART
NATIONAL BUREAU OF STANDARDS-1963-A

Geotechnical Engineering Program
Civil Engineering Department
Colorado State University

(2)

BLAST INDUCED LIQUEFACTION POTENTIAL AND TRANSIENT POREWATER PRESSURE RESPONSE OF SATURATED SANDS

15 Oct. 1985

Prepared for
Air Force Office of Scientific Research
Washington, D. C.

Under Grant
AFOSR-80-0260

Wayne A. Charlie
George E. Veyera
Donald O. Doehring
Steven R. Abt

Colorado State University
Department of Civil Engineering
Fort Collins, Colorado 80523

UNCLASSIFIED
SECURITY CLASSIFICATION OF THIS PAGE

AD-A173137

REPORT DOCUMENTATION PAGE

1a. REPORT SECURITY CLASSIFICATION: UNCLASSIFIED	1b. RESTRICTIVE MARKINGS
2a. SECURITY CLASSIFICATION AUTHORITY	3. DISTRIBUTION/AVAILABILITY OF REPORT: Approved for Public Release; Distribution Unlimited
2b. DECLASSIFICATION/DOWNGRADING SCHEDULE	
4. PERFORMING ORGANIZATION REPORT NUMBER(S)	5. MONITORING ORGANIZATION REPORT NUMBER(S): AFOSR-TR- 86-0946
6a. NAME OF PERFORMING ORGANIZATION: Dept. Civil Engineering, Colorado State University; 6b. OFFICE SYMBOL (If applicable)	7a. NAME OF MONITORING ORGANIZATION: AFOSR
6c. ADDRESS (City, State and ZIP Code): Fort Collins, Colorado 80523	7b. ADDRESS (City, State and ZIP Code): Bame AFB SA
8a. NAME OF FUNDING/SPONSORING ORGANIZATION: Air Force Office of Scientific Research; 8b. OFFICE SYMBOL (If applicable): AFOSR/NA	9. PROCUREMENT INSTRUMENT IDENTIFICATION NUMBER: Grant No. AFOSR-80-0260
8c. ADDRESS (City, State and ZIP Code): Building 410, Bolling AFB, DC 20332	10. SOURCE OF FUNDING NOS.

PROGRAM ELEMENT NO.	PROJECT NO.	TASK NO.	WORK UNIT NO.
61102F	2307	C1	

11. TITLE (Include Security Classification): (Blast Induced Liquefaction Potential and Transient Porewater Pressure Response of Saturated Sands) (u)

12. PERSONAL AUTHOR(S): Wayne A. Charlie, George E. Veyera, Jr.; Donald O. Doehring, Steven R. Abt

13a. TYPE OF REPORT	13b. TIME COVERED	14. DATE OF REPORT (Yr., Mo., Day)	15. PAGE COUNT
FINAL	FROM 1980 TO 1985	1985 Oct. 15	208

16. SUPPLEMENTARY NOTATION

17. COSATI CODES		
FIELD	GROUP	SUB. GR.

18. SUBJECT TERMS (Continue on reverse if necessary and identify by block number): Liquefaction, Porewater Pressure, Dynamic Testing, Blast Loading, Soil Mechanics, Laboratory Testing, Material Modelling.

19. ABSTRACT (Continue on reverse if necessary and identify by block number)

A new experimental apparatus has been developed to investigate the transient and long-term porewater pressure responses of saturated soils. The facility is capable of generating compressive shock loadings on the order of 35000 KPa with millisecond rise times to peak stress. This experimental investigation represents an effort to examine and establish an understanding of compressionally-induced liquefaction. Samples of water saturated Monterey No. 0/30 sand were examined at various relative densities and effective stresses. Boundary conditions used for the experiments were one-dimensional, confined, compressive loadings without drainage. Results indicate that it is possible to liquefy Monterey No. 0/30 sand under these conditions. Significant porewater pressure increases were possible even at high densities and high effective stresses. Liquefaction was generally observed at compressive strains greater than about 1×10^{-1} percent. Threshold strain values, below which substantial porewater pressures increases generally did not occur, were about 1×10^{-2} percent.

(cont.)

20. DISTRIBUTION/AVAILABILITY OF ABSTRACT	21. ABSTRACT SECURITY CLASSIFICATION
UNCLASSIFIED/UNLIMITED ☒ SAME AS RPT. ☐ DTIC USERS ☐	UNCLASSIFIED

22a. NAME OF RESPONSIBLE INDIVIDUAL	22b. TELEPHONE NUMBER (Include Area Code)	22c. OFFICE SYMBOL
Lt. Col. Lawrence D. Hokanson	202/767-4935	AFOSR/NA

DD FORM 1473, 83 APR — EDITION OF 1 JAN 73 IS OBSOLETE.

UNCLASSIFIED
SECURITY CLASSIFICATION OF THIS PAGE

19. (Abstract Continued)

The data analysis has provided several empirical models that can be used to estimate liquefaction potential as a function of density, effective stress and applied compressive strain. One of the models uses an empirical scaling law for explosive loadings to predict the extent of porewater pressure increases in the field from buried, contained charges in saturated soils. A finite difference analysis that considers the saturated soil as a two-phase medium has been performed. The analysis accounts for the nonlinear, inelastic behavior of the soil skeleton and has shown that liquefaction is dependent upon the unloading constrained modulus of the soil. Results agree with the experimental observations of peak and long-term porewater pressure responses.

ACKNOWLDGEMENTS

The Air Force Office of Scientific Research, Bolling Air Force Base, Washington, D.C. sponsored this research (Contract No. AFOSR-80-0260; Program Managers John J. Allen, Lt. Col., USAF and Lawrence D. Hokanson, Lt. Col., USAF). Wayne A. Charlie and Steven R. Abt, Associate Professors of Civil Engineering at Colorado State University, Fort Collins, Colorado were the Principal and Co-Principal Investigators. George E. Veyera, Jr. conducted the laboratory research and his Ph.D. dissertation represents this report. Wayne A. Charlie, Steven R. Abt, Donald O. Doehring and J. W. N. Fead served on George E. Veyera's graduate committee. Eric J. Rinehart, AFWL; Scott E. Blouin and James D. Shinn, II of Applied Research, Inc.; and S. Melzer of Civil Systems, Inc. provided technical assistance and insight in the research. Jon Payne, Robert Kiesel and Walt Patzer fabricated many of the items required for the development of the shock loading laboratory equipment.

TABLE OF CONTENTS

LIST OF TABLES

LIST OF FIGURES

LIST OF SYMBOLS

B_{mix} = bulk modulus of the soil-water mixture (KPa)

B_{pvc} = bulk modulus of polyvinylchloride (PVC) (KPa)

B_s = bulk modulus of the soil particles (KPa)

B_w = bulk modulus of water (KPa)

C = damping coefficient

c' = effective cohesion (KPa)

cc = cubic centimeters

D = damping coefficient

D_c = soil skeleton constrained modulus

D_l = soil skeleton constrained modulus for loading (KPa)

D_r = relative density (decimal or %)

D_u = soil skeleton constrained modulus for unloading (KPa)

d = depth of buried explosive charge (M)

ES = effective stress (KPa)

e = void ratio

e_{min} = minimum void ratio

e_{max} = maximum void ratio

F(t) = applied force as a function of time (KN)

f = ground shock coupling factor

G_s = specific gravity of solids

g = acceleration of gravity = 9.81 M/sec^2

g_i = the components of the gravitational constant (M/sec^2)

h_b = depth of liquefied soil for a contained explosion (M)

h_o = optimum charge placement depth for maximum radius of liquefaction at the ground surface (M)

h_s = depth of liquefied soil for a surface explosion (M)

K = empirical scaling constant

Kg = kilograms

KPa = kilopascals

k = Darcy's coefficient of permeability (M/sec)

k = spring constant (N/M)

k_3 = empirical scaling constant

k_4 = empirical scaling constant

L_c = liquefaction coefficient

log = denotes logarithm to the base 10

M = mass (Kg)

M = meters

MPa = megapascals

m = empirical scaling exponent

N = Newton

n = empirical scaling exponent

n = porosity of the solid skeleton

P = pore pressure (KPa)

$P_{,i}$ = pore pressure tensor (KPa)

PPR = porewater pressure ratio

PWP Ratio = porewater pressure ratio

R = radial distance from a buried charge (M)

R^2 = coeffecient of determination (%)

R_{eff} = effective radius of influence of a contained explosion (M)

R_{max} = maximum radius of liquefied soil for a contained explosion (M)

S = standard error of estimate

s = indexing parameter

t = time

u = porewater pressure (KPa)

u = displacement vector of the solid skeleton (M)

$\ddot{u}_i$ = acceleration vector of the solid skeleton (M/sec^2)

u_{pk} = peak porewater pressure (KPa)

u_r = residual excess porewater pressure (KPa)

V_c = compressive stress wave propagation velocity (M/sec)

V_{mix} = compressive stress wave propagation velocity in a soil-water mixture (M/sec)

V_p = particle velocity (M/sec)

V_{pk} = peak particle velocity (M/sec)

V_w = compressive stress wave propagation velocity in fresh water (M/sec) fresh water (M/sec)

VDP = volume decrease potential

W = charge weight in kilograms per delay for concentrated charges

W = charge weight in kilograms per delay per meter for row charges

$\dot{w}_i$ = velocity vector of the fluid (M)

$\ddot{w}_i$ = acceleration vector of the fluid (M/sec^2)

$w_{i,i}$ = displacement vector of the fluid with respect to the solid skeleton (M)

y = displacement (M)

$\dot{y}$ = velocity (M/sec)

$\ddot{y}$ = acceleration (M/sec^2)

Greek Symbols

β = kinetic energy correction factor

Δ = denotes change in

$\Delta\varepsilon^p$ = increment of inelastic volumetric strain (decimal)

$\delta_{i,j}$ = the Kronecker delta

ε_c = compressive strain (decimal or %)

ε_{pk} = peak compressive strain (decimal or %)

$\varepsilon_{i,j}$ = strain tensor of the solid skeleton (decimal)

ϕ' = effective angle of internal friction (degrees)

ρ = mass density (Kg/M^3)

ρ_t = total mass density (Kg/M^3)

ρ_w = mass density of water (Kg/M^3)

Σ = denotes summation

σ' = effective stress (KPa)

σ'_o = initial effective stress (KPa)

σ_c = compressive stress (KPa)

$\sigma_{ij,j}$ = total stress tensor (KPa)

$\sigma'_{ij,j}$ = effective stress tensor (KPa)

σ_{pk} = peak compressive stress (KPa)

σ'_r = residual effective stress (KPa)

σ_{pw} = peak compressive stress in water (KPa)

τ_{max} = shear strength (KPa)

Θ = variation in the fluid content

I. INTRODUCTION

A. Statement of the Problem

Nearly all materials, including soil, lose strength with repeated loadings. The number of repeated loadings required to reach failure increases with decreasing cyclic stress intensity. When a dry, loose sand is subjected to stresses sufficient to cause intergranular slip or particle fracture, the rearrangement of grains leads to volumetric compaction. Volumetric compaction can be induced by a single large loading or a series of loadings of smaller intensity. When a saturated, loose sand is subjected to stresses of sufficient intensity to cause intergranular slip or grain fracture, compaction is inhibited because the water cannot drain instantaneously to accommodate the potential volume change. As a result, the porewater pressure increases since the water must support the gravity loading. The larger the increase in porewater pressure, the greater the loss in strength of a cohesionless soil. Depending on drainage conditions, the residual excess porewater pressure can persist for minutes, hours or even days until enough drainage occurs to accommodate the volume change.

Porewater pressure increases in loose, saturated sands can be produced by sustained low frequency, low amplitude, random ground motions. A complete loss of shear strength, as a consequence of reduced effective stress due to increased porewater pressures, is termed liquefaction. This behavior can lead to catastrophic consequences including landslides, foundation failures, ground

subsidence and embankment failures. Liquefaction as a result of earthquake-induced ground motions is well understood and has been documented by many researchers in both the field and laboratory. Liquefaction from explosive-induced ground motions is not well documented beyond its existence and the mechanism is not well understood. Field data are often limited in extent and incomplete in detail while dynamic experimental laboratory facilities are still in a developmental stage.

Recognition of the potential effects of explosive-induced liquefaction warrants a study of explosive-induced liquefaction phenomenon and related effects in the field. Damage disproportionate to the amount of explosive used or of a nature inconsistent with previous experience may be attributable to liquefaction. For example, recent re-examinations of the events at the Pacific Proving Grounds, where nuclear explosives were detonated in the 1950's, seem to suggest that liquefaction may be the primary factor causing the unusually broad, flat crater shapes and other phenomenon observed there. Other military high explosive tests, construction blasting and small scale field tests have also shown evidence of damage beyond the direct effects of the explosion.

Field observations and limited empirical relationships are the current basis for evaluating and predicting explosive-induced liquefaction. However, these empirical relationships do not have the benefit of a large data base or extensive theoretical foundation. Of prime importance is the development of a controlled, systematic experimental evaluation of liquefaction in both the laboratory and field. Such a study would vastly improve the understanding of the

behavior of saturated granular soils under dynamic loadings and will lead the way to a coherent, comprehensive theoretical analysis.

B. Objectives of This Study

The primary objective of this investigation was to experimentally and systematically evaluate the behavior of a saturated granular soil subjected to dynamic, one-dimensional, confined, compressive loadings in the laboratory. The experiments were conducted to simulate the field loading of a soil element located near the detonation point of an explosive. Intense compressive loadings having millisecond rise times occur in this region. The soil's porewater pressure response both during and after the passage of the stress wave was used to evaluate the liquefaction potential of the soil.

A large number of parameters have been observed to affect the onset of liquefaction. Some are associated with the soil and underlying bedrock while others are related to the explosive itself. In this study, the effect of variations in the initial relative density and the initial effective stress along with the intensity and number of applied loadings were investigated. A projectile was fired at a confined, water saturated sample with undrained loading conditions to simulate an explosive loading. Experimental measurements included the applied loading stress, the porewater pressure response and the projectile impact velocity.

All experimental runs were conducted on saturated samples of Monterey No. 0/30 sand at relative densities and effective stresses ranging from 0 to 80 percent and 86 to 690 KPa, respectively. Monterey sand was chosen because the performance of this material under static

and very low frequency (1 cycle per second) loadings is well documented in the literature.

Analysis of the data included an evaluation of the influence of several parameters on the peak and long-term porewater pressure response in the soil, the stress wave velocity and the peak particle velocity. These results were used to define liquefaction threshold limits and develop empirical relationships for predicting porewater pressure increases in saturated, cohesionless soils. This investigation has lead to the development of a new apparatus for studying the dynamic response of saturated soils and has provided a new approach for examining compressional liquefaction. This study has also derived and documented some important relationships between soil properties and compressional stress wave loading.

II. LITERATURE REVIEW

A. The Liquefaction Phenomenon

1. Effects of Liquefaction

Observations of the effects of liquefaction have been made in connection with earthquake loadings of soils. The 1964 Alaskan earthquake destroyed harbor facilities, roadways, buildings and homes in Valdez, Alaska, due in part to a large flow of liquefied soil (Seed, 1968). In 1964, an earthquake in Niigata, Japan, caused extensive structural damage as a result of bearing capacity failures. A number of buildings sank into the ground while a sewage treatment tank floated up above the ground and an apartment building rotated intact almost 80 degrees (Seed and Idriss, 1967). Informative reviews of earthquake-induced liquefaction phenomena and case histories are given by Gilbert (1976), Green and Ferguson (1971) and Seed (1968,1979).

Although such dramatic and widespread damage has not been reported for explosions, it is not unreasonable to expect that such catastrophic consequences as those associated with seismic ground motions from earthquake loadings are possible. The primary sources of information in this area are from indirect observations of construction, military and small scale field explosive events. Where liquefaction has been evidenced, water spouts, sand boils, ground subsidence and flow of soils have followed the explosion (Benson,1983; Blouin,1978; Blouin and Kim,1983; Carnes,1976; Charlie,1978a,b; Gilbert,1976; Melzer,1978a). It is also believed that the unusually broad, flat crater shapes

observed as a result of surface and near surface detonations in saturated soils may be indicative of liquefaction (Blouin,1978; Blouin and Kim,1983; Carnes,1976; Gilbert,1976). Explosive loadings pose a twofold potential for damage, including the direct effects of the explosion as well as the additional consequences of soil liquefaction. Reviews of explosive-induced liquefaction phenomena and experience are given by Charlie et al. (1980, 1985), Gilbert (1976), Marti (1978) and Rischbieter (1977).

Since the effects of liquefaction from explosive-induced ground motions are not restricted to surface damage, both above ground and buried structures are subject to potential damage. Therefore, the possibility of explosive-induced liquefaction is a significant consideration for nearby structures. The resulting damage primarily involves bearing capacity failures, including excessive settlements, upward movements and rotations. While such occurrences may not necessarily damage a facility structurally, as was observed in the Niigata earthquake, they may render it unusable from a practical point of view. Therefore, in examining the liquefaction potential of a given site, it is essential to maintain a proper perspective on site specific field conditions and structural considerations. This is especially true for high explosive events in areas where the groundwater table is within the depth of influence of explosively generated stresses.

2. Definition of Liquefaction

The term liquefaction has been generally associated with the response of loose, saturated sands to loading conditions that induce large strains resulting in flow slides, or to describe a state of

stress existing where the effective stress approaches zero or, when the reduction in soil shear strength is substantial enough that the soil behaves like a liquid. One of the first attempts at quantifying this phenomenon was made by Casagrande (1936). Since that time there has been increased awareness and interest in liquefaction, particularly by researchers investigating seismic soil response. Reviews of test procedures for dynamically loading soils and liquefaction analyses are given by Finn (1972,1981) and Whitman (1969).

From these investigations, a number of definitions and terms associated with liquefaction have been developed (Committee on Soil Dynamics,1978, Seed,1976). Several definitions of liquefaction and related observations are as follows.

Liquefaction: 'Denotes a condition where a soil will undergo continued deformation at a low residual stress or with no residual resistance due to the build-up of high porewater pressures which reduce the effective confining pressure to a very low value; pore pressure build-up leading to true liquefaction of this type may be due to either static or cyclic stress applications.' (Seed,1976).

Initial Liquefaction: 'Denotes a condition where, during the course of cyclic stress application, the residual porewater pressure on completion of any full stress cycle becomes equal to the applied confining pressure; the development of initial liquefaction has no implications concerning the magnitude of the deformations which the soil might subsequently undergo; however it defines a condition which is a useful basis for assessing various possible forms of subsequent soil behavior.' (Seed,1976).

Cyclic Liquefaction: 'Denotes a condition in which cyclic stress applications develop a condition of initial liquefaction and subsequent cyclic stress applications cause limited strains to develop either because of the remaining resistance of the soil to deformation or because the soil dilates, the pore pressure drops, and the soil stabilizes under the applied loads.' (Seed,1976).

> **Liquefaction**: 'The act or process of transforming any substance into a liquid. In cohesionless soil, the transformation is from a solid state to a liquefied state as a consequence of increased pore pressure and reduced effective stress....Liquefaction is thus defined as a changing of states which is independent of initiating disturbance that could be static, vibratory, sea wave, or shock loading, or a change in groundwater pressure. The definition also is independent of deformation or ground failure movements that might follow the transformation. Liquefaction always produces a transient loss of shear resistance but does not always produce a longer-term reduction of shear strength.' (Committee on Soil Dynamics,1978).

Since the work presented herein investigates the phenomenon of liquefaction as a result of impact loadings in terms of the porewater pressure response relative to the initial effective stress and initial soil density, the definition by Seed (1976) for 'initial liquefaction' and that for 'liquefaction' by the Committee on Soil Dynamics (1978) will be used in this paper. In this way liquefaction can be evaluated by comparing the amount of porewater pressure increase that occurs after the attenuation of an explosive-induced or shock-induced compressive stress wave. The porewater pressure increase above the hydrostatic pressure, remaining after the dissipation of the compressive stress wave, will be referred to as the 'residual excess porewater pressure.'

3. Effective Stress and Shear Strength

The behavior of soils under loads is governed by the principle of effective stress (Lambe and Whitman,1969; Terzaghi and Peck,1948). This concept was first presented by Terzaghi (1943) and is fundamental to understanding the response of soils under various loading conditions. The effective stress, σ' , is defined as:

$$\sigma' = \sigma - u \qquad \text{(Eq. 2.1)}$$

where, σ is the total stress and u is the porewater pressure.

The shear strength of a soil, τ_{max}, is proportional to the intergranular pressure and the internal frictional resistance which is expressed by:

$$\tau_{max} = c' + \sigma' \text{ Tan } \phi' \qquad \text{(Eq. 2.2)}$$

where, c' is the effective cohesion and ϕ' is the effective angle of internal friction. For cohesionless soils the effective cohesion, c', is zero by definition.

The condition of liquefaction requires a complete loss of shear strength as a result of a reduction in the effective stress to zero. The effective stress is zero when the *porewater pressure increases* in magnitude equal to the value of the total stress. It is this increase in porewater pressure from dynamic loadings which, whether from explosives, earthquakes or shock loadings, can induce liquefaction in a saturated, cohesionless soil.

B. Liquefaction Mechanisms

1. Explosive-Induced Ground Motions

An explosive event produces high amplitude, high frequency ground motions of relatively short duration. The intense compressive body waves generated by an explosion propagate outward from the source in a cylindrically or spherically diverging pattern, depending on the geometry of the source. These waves attenuate with radial distance, R,

from the disturbance. For cylindrical wave fronts the attenuation occurs according to $1/(R^{1/2})$ and for spherical wave fronts according to $1/R$ (Rinehart,1975). Surface waves are also generated and propagate from the source for some distance, attenuating with according to $1/(R^2)$ (Richart et al.,1970). Shear waves may also be produced by the reflection of compression waves from interfaces such as the ground surface, groundwater table, soil layers or underlying bedrock. From explosive field ground motion records, it is evident that compression, shear and surface waveforms exist but their exact interrelationship in producing liquefaction is not clear.

Near a contained (no crater) explosion, the soil is loaded under confined, uniaxial compression. This type of loading has been observed in strain path plots of field data from deeply buried tests with spherically shaped charges (Workman et al., 1981). Radial strains dominate and hoop strains are virtually nonexistant until after the compressive stress wave has sufficiently attenuated. When tensile hoop strains are developed in the soil, relative grain movements occur and may disrupt the soil fabric. If the magnitude of an explosively generated stress wave is large enough, the soil will fail in shear as the particles separate and lose grain-to-grain contact (Melzer,1978a,b). This complete loss of shear strength is consistent with the requirement for liquefaction, but this approach does not account for the water in the pores or the small hoop strains at distances away from the explosion.

The applied compressive load also produces a direct and immediate porewater pressure response in a saturated soil. Correspondingly, the soil grains and soil skeleton are also stressed, but for a saturated

soil the porewater carries a large part of the load increase. Shock pulses generated by explosions typically result in undrained loading conditions, particularly near the source, since the porewater pressures cannot dissipate until after the compressive stress wave attenuates and the system unloads. During unloading, the pressure in the grain matrix falls short of the static value due to hysteresis and has the effect of adding to the porewater pressure which reduces the effective stress. The onset of liquefaction probably occurs during the unloading phase as the system rebounds (Schaepermeier,1978a). The residual excess porewater pressure decreases the effective stress reduces the soil's shear strength. With time, the soil gradually regains strength as the residual excess porewater pressure dissipates and the effective stress is restored.

Seismic loading of the soil occurs in regions where the compressive stress waves have attenuated and the shear waves dominate. In these regions liquefaction may occur from repeated shearing strain reversals in a manner similar to that observed for earthquake-induced ground motions. For surface or near surface explosions, the stress distributions in the soil become more complicated by the presence of air overpressure stresses generated by the explosion (Melzer,1978b). However, in some cases the near surface soils may undergo a one-dimensional compressive loading from the air overpressure. This condition may be analyzed by the same approach suggested above for direct-induced explosive loadings.

2. Earthquake-Induced Ground Motions

A seismic event produces low amplitude, low frequency ground motions of relatively long durations and numerous cycles. Shear waves generated during an earthquake occur as a result of stress redistributions within the earth's crust that release energy proportional to the fault size and shear modulus. Shear waves are generally assumed to propagate upward from the underlying bedrock through the soil mass in an oscillatory manner involving a series of stress reversals. Under this action, the soil grains begin to rearrange themselves relative to one another in an attempt to reduce the volume of the soil skeleton and reach a condition of stable equilibrium. As a result of the corresponding reductions in fluid filled pore spaces, the porewater pressure increases and the effective stress decreases. The oscillatory nature of the earthquake loading causes the porewater pressure to gradually increase. Therefore, the duration and number of cycles are significant factors in producing liquefaction (Seed and Idriss,1971). Since the porewater is not capable of maintaining any shear, the shear stresses are carried by the individual grains of the soil skeleton. When liquefaction occurs, the intergranular friction is temporarily lost, and the soil is not capable of maintaining any shear strength. With time, the residual excess porewater pressure dissipates through fluid drainage, and the effective stress and shear strength are gradually regained.

3. Comparison of Liquefaction Mechanisms

From the nature and geometry of explosive loadings, both compressive and shear waves are generated. The compressive stress

waves are most significant near the explosion and generate intense compressive pulses. Shear stress waves dominate at distances away from the explosion and produce oscillatory motions. Seismic ground motions, similar to those produced by earthquake loadings, have been simulated in the field by controlled explosive tests (Bruce et al., 1979,1982). The effect of these stress waves in producing liquefaction is relative to their position and intensity as they attenuate away from the source.

It is not clear how the unloading and shearing actions are related near the explosion and it is difficult to precisely define the transition between them from field ground motion records. However, these actions are consistent with observations of relatively instantaneous liquefaction near the explosive source. At distances away from the explosion, seismic ground motions dominate and liquefaction may occur in a manner similar to that from earthquake loadings at some time after the explosion has occurred. The resulting cyclic shearing action gradually increases the porewater pressure until the effective stress goes to zero and the soil fails. These observations have been made by a number of investigators (Benson,1983; Charlie,1978b; Gilbert,1976; Langley et al.,1972; Melzer,1978a).

C. Factors Influencing Liquefaction

There are a significant number of factors that have been observed to influence the occurrence of liquefaction. Most of the experience with explosive loadings comes indirectly in the sense that soil densification was being attempted or field blasting programs were being conducted and liquefaction or liquefaction features may have been noted. The general observations of many researchers involved in both

laboratory and field experiments investigating compressional liquefaction from explosive loadings will be presented. Some references from earthquake researchers will also be given where similar observations have been made.

1. Soil-Water System

a. Degree of Saturation

Where the degree of saturation is less than 100 percent, liquefaction is difficult to induce. Even small amounts of air can significantly reduce the bulk modulus of the soil-water mixture and the compressive stress wave propagation velocity. Richart et al.(1970) used the equations for the compressibility of mixtures and the wave propagation velocity in mixtures to demonstrate that the presence of 0.01 percent air in a saturated quartz sand will reduce the bulk modulus of the soil-water system by a factor of 16, and reduce the wave propagation velocity by a factor of four.

While liquefaction of materials containing air bubbles may be difficult to induce by seismic loadings, it may be possible for liquefaction to occur from intense shock loadings associated with explosions. This can occur if the magnitude of the applied compressive stress or strain is large enough to force the air into solution and saturate the soil. These observations have been made by a number of investigators (Allen,1975; Allen et al.,1980; Damitio,1978b; Florin and Ivanov,1961; Perry,1972; Gilbert,1976; Ivanov,1967; Silver,1981; Studer and Kok,1980; True,1967,1969; Van der Kogel et al.,1981).

b. Relative Density

Liquefaction susceptible soils have a significant potential for volume decrease. Earthquake-induced liquefaction typically occurs in soils having relative densities of less than 65 percent. Loose soils have been successfully increased in relative density by as much as 40 percent by explosive loadings which generally results in a more stable soil mass. Some dense soils may even become loose and this has been mainly attributed to the dilative behavior of dense soils which exhibit a volume increase accompanied by a reduction in porewater pressure. These observations have been made by a number of investigators (Allen,1975; Allen et al.,1980; Damitio,1978b; D'Appolonia,1968; Drake,1978; Finn,1972; Florin and Ivanov,1961; Gilbert,1976; Ishihara and Watanabe,1976; Ivanov,1967; Klohn et al.,1981; Kok,1978a; Kummeneje and Eide,1961; Kurzeme,1971; Mitchell and Katti,1981; Rischbieter,1977; Seed and Idriss,1967; Studer and Hunziker,1977; Studer and Kok,1980; Studer and Prater,1977; Yamamura and Koga,1974).

c. Permeability

The duration of the liquefied state depends on the permeability, compressibility, stratum thickness and drainage path length. The rate of dissipation of the residual excess porewater pressure is primarily controlled by the soil permeability which is a function of soil type, density, grain size, packing, cementation and fluid properties. High permeability soils, such as coarse sands and gravels, tend to drain rapidly and reduce the residual excess porewater pressure quickly enough to inhibit liquefaction and restore the

effective stress. Low permeability soils, such as fine silts and low sensitivity clays, are not usually prone to liquefaction. Coarse silts and medium to fine sands have been observed to be liquefaction susceptible as they are not capable of relieving the residual excess porewater pressures in a short enough period of time. Surface features generally believed to be indicative of liquefaction include sand cones, sand boils, small geysers and water spouts that result from the dissipation of residual excess porewater pressures. These features have been observed at various times after the explosion at various distances away from the detonation point, depending on the soil permeability and other factors. These observations have been made by a number of investigators (Damitio,1978a; Das,1983; Florin and Ivanov,1961; Gilbert,1976; Ivanov,1967; Ivanov et al.,1981; Kok,1978a; Kurzeme,1971; Prater,1977; Prugh,1963; Seed and Booker,1976; Studer and Hunziker,1977; Studer and Kok,1980; Studer and Prater,1977; True,1967,1969).

d. Compressibility

The transient and long-term porewater pressure responses to applied compressive stress loadings are dependent upon the amplitude of the applied stress, the compressibility of the soil skeleton, the compressibility of the pore fluid (water and/or air) and drainage conditions. The presence of entrapped air increases the compressibility of the pore fluid, reducing the transient and long-term porewater pressure increases.

The tendency for volume decrease is a necessary requirement for liquefaction. In a saturated soil, a volume decrease causes an

increase in porewater pressure and a corresponding decrease in effective stress. As such, water saturated soils having a low relative density should have a high liquefaction potential. The potential for a soil to decrease in volume also depends on the stiffness of the soil skeleton which is a function of both density and effective stress. Soils having low effective stress conditions should have a high liquefaction potential.

The presence of entrapped air increases the compressibility of the system, reducing the potential for liquefaction and increasing the attenuation of the compressive stress wave. In a partially saturated soil, the tendency for volume decrease is resisted by the compressibility of the soil skeleton, the entrapped air and the water, whereas in a saturated soil the resistance is primarily due to the porewater. The pore air bubbles tend to act as a 'cushion' as they absorb the compressive stress during deformation. These observations have been made by a number of investigators (Florin and Ivanov,1961; Gilbert, 1976; Ishihara and Watanabe,1976; Ivanov,1967; Jackson et al.,1980; Lyakhov,1961; Richart et al.,1970; Studer and Kok,1980; Van der Kogel et al.,1981).

e. Static Overburden Pressure

In general, increasing the static overburden pressure increases the effective stress and decreases the potential for liquefaction. With increasing effective stress the stiffness of the soil skeleton is increased and the porewater pressure must reach a higher value before liquefaction can occur. These observations have been made by a number of investigators (Allen,1975; Allen et al.,1980;

Damitio,1978a,b; Florin and Ivanov,1961; Ivanov,1967; Mitchell and Katti,1981; Oriard,1976; Rischbieter,1977; Seed,1979; Seed and Idriss,1971; Studer,1978; Studer and Hunziker,1977; Studer and Prater,1977).

f. Cohesion

Observations from field blasting experience indicate that the presence of cohesion in soils tends reduce the liquefaction potential (Damitio,1978b; Gilbert,1976; Rischbieter,1977). It has generally been observed that granular soils with little or no cohesion are the most susceptible to liquefaction for seismic loadings. D'Appolonia (1968) suggests that less than 10 percent silt or clay size particles is sufficient for a granular soil to be considered cohesionless. Seed (1981) indicates that soils containing more than 10 percent clays are generally not sensitive to liquefaction from earthquake loadings.

g. Gradation

It has been recognized by most researchers that for explosive and seismic loadings, uniformly graded soils, having a narrow band of grain sizes, tend to be more liquefaction susceptible than soils having a variety of particle sizes. The distribution of particle sizes in a well graded soil are effective in filling pore spaces with soil grains which increases the particle-to-particle contact area and shearing resistance. These observations have been made by a number of investigators (Damitio,1978b; D'Appolonia, 1968; Klohn et al.,1981; Kummeneje and Eide,1961; Rischbieter,1977; Seed and Lundgren,1954;

Studer,1978; Studer and Hunziker,1977; Studer and Kok,1980; Studer and Prater,1977; True,1967,1969).

Studer and Kok (1980) have noted substantial porewater pressure increases in coarse granular soil under shock loadings in the laboratory. Florin and Ivanov (1961) have demonstrated in laboratory experiments that all sufficiently loose, cohesionless soils of any grain size can be liquefied under explosive loadings.

h. Particle Size and Shape

Fine sands have been found to be generally the most susceptible to liquefaction as compared to other grain sizes for both explosive and seismic loadings (Damitio,1978b; D'Appolonia, 1968; Gilbert,1976; Klohn et al.,1981; Kummeneje and Eide,1961; Seed and Lundgren,1954; Studer,1978; Studer and Hunziker,1977; Studer and Prater,1977; Yang,1973).

Studer and Kok (1980) have noted substantial porewater pressure increases in coarse granular soil under dynamic loadings in the laboratory. Florin and Ivanov (1961) have demonstrated in laboratory experiments that all sufficiently loose, cohesionless soils of any grain size can be liquefied under explosive loadings.

There is relatively little information available on particle shape. True (1967,1969) observed that a graded, angular sand showed more evidence of liquefaction than a uniform, rounded sand under shock loadings in the laboratory. Liquefaction of crushed quartz sand was observed by Studer (1978) and Studer and Prater (1977) for explosive and shock loadings. Klohn et al. (1981) were able to liquefy subangular tailings by explosions. Ivanov et al. (1981) observed that

angular to subangular cohesionless sands had a more stable structure under dynamic loadings than did rounded cohesionless sands. Based on the limited data available, it appears that it is possible to liquefy both angular and rounded cohesionless sands.

i. Dilatency

Dilatency is believed to play an important role in the early time response of explosively loaded soils having high initial densities (Drake,1978; Gilbert,1976; Lyakhov,1961; Seed,1979; Seed and Lundgren,1954; Studer and Kok,1980). In medium dense and dense sands the dilatent nature of these states tends to inhibit the onset of liquefaction. As shearing occurs in the soil mass, the grains slide over and past one another causing a volume expansion of the soil skeleton (Lambe and Whitman,1969). The rearrangement of the soil skeleton results causes an increase in void sizes that dissipates the residual excess porewater pressures and increases the effective stress. In loose soils there is a tendency for a volume decrease to occur in the soil skeleton as the soil grains try to rearrange themselves into a denser packing arrangement. This rearrangement reduces the void sizes which causes the residual excess porewater pressure to increase and the effective stress to decrease. Casagrande (1936) described this behavior and attempted to quantify it by noting that there is a 'critical density' at which no volume change will occur.

j. Local Geology

The presence and location of the groundwater table, along with geologic interfaces including underlying bedrock, often produce

secondary oscillatory shear, tensile, compressive and surface waves that may influence and enhance the possibility of liquefaction under explosive loadings. Stiff, dense soils and rock transmit high frequency and high amplitude ground motions. The magnitude of these ground motions depends on the proximity of the soil and rock to the explosive detonation point (Drake and Ingram,1981; Ivanov,1967; Oriard, 1976; Sanders,1982).

k. Soil-Rock Material Hysteresis

When material damping is high, the attenuation of explosively generated stress wave energy is greater and the extent of the liquefied zone is reduced. Damping is a function of frequency, compressibility, strain amplitude and material properties. The denser and stiffer the soil or rock the higher the frequency and amplitude of the transmitted explosive-induced ground motions (Oriard,1976; Richart et al.,1970; Rinehart, 1975). Dynamic tests of dry granular soils show that they exhibit an 'S'-shaped stress-strain curve and a locking phenomenon. It is believed that this may have a significant effect on the rise time of explosive-induced stresses, involving a strain rate soil strength dependency (Jackson et al.,1980; Whitman,1957; Whitman and Healy,1962; Whitman et al.,1964).

2. Explosive Loading Parameters

a. Load Intensity

The potential for liquefaction is strongly influenced by the magnitude of the applied stress and resulting strains. Larger intensity charges are necessary to induce liquefaction with increasing

depth and initial density. A series of consecutive explosions are usually more effective due to the superposition of applied stresses. These observations have been made by a number of investigators (Damitio,1978a; Florin and Ivanov,1961; Hall,1962; Ivanov,1967; Klohn et al.,1981; Mitchell and Katti,1981; Studer and Prater,1977; Yamamura and Koga,1974; Yang,1973).

b. Depth of Burial of Charge

A contained explosive charge is more effective in producing liquefaction than a surface charge of comparable weight and density since more of the explosive energy is transmitted to the soil. Explosives are most effective in producing liquefaction when placed at a depth of about two thirds the stratum thickness of the potentially liquefiable soil deposit (Damitio,1978a; Hall,1962; Mitchell,1970; Mitchell and Katti,1981; Prugh,1963).

Under given circumstances (i.e., loose, saturated, cohesionless soil within the influence of a sufficiently intense explosive loading), the energy released from a surface or near surface explosion of sufficient intensity can produce liquefaction (Charlie,1978b; Benson,1983; Blouin,1978; Blouin and Kim,1983; Damitio,1978a,b; Gilbert,1976; Ivanov,1967; Yang,1973). It is also feasible that a surface and a buried charge can be scaled accordingly to produce the same depth of liquefaction. Using the empirical relationships presented in the later part of this chapter, the required surface charge is estimated at about 10 times that required for a buried charge to obtain the same depth of liquefied soil.

c. Charge Density and Shape

As the density of a charge or series of charges increases, the ability to induce liquefaction also increases since a load of greater intensity will be produced. Experience has shown that the most efficient charge shape is a sphere. However, since the weight must increase with depth of burial to be effective, cylindrical charges having a height of about three to four times the diameter are generally used (Damitio,1978a; Ivanov,1967; Oriard,1976).

d. Charge Weight

In general, ground shock amplitude increases, frequency decreases and the extent of the liquefied zone increases with increasing charge weight. Repeated loadings with small, properly sequenced charges, are the most effective in producing liquefaction. However, single large charges of sufficient intensity are also capable producing liquefaction (Charlie,1978b; Benson,1983; Blouin,1978; Blouin and Kim,1983; Damitio,1978a,b; Gilbert,1976; Hall,1962, Ivanov,1967; Lyakhov,1961; Oriard,1976; Yang,1973).

e. Delay Times, Charge Patterns and Number of Cycles

Experience has shown that properly sequenced, successive explosions are more effective in producing liquefaction than a single, large explosion. The time delayed loadings take advantage of the superposition of applied stresses and the effects of repeated loadings (Damitio,1978a; Hall,1962; Ivanov,1967; Kummeneje and Eide,1961; Oriard,1976).

For explosive loadings, the duration of the applied compressive stress wave the superposition of stresses from consecutive delayed detonations can induce liquefaction. If the porewater pressures are allowed to dissipate between detonations, the soil can stabilize and may become more resistant to further liquefaction. These observations have been made by a number of investigators (Damitio,1978a,b; Florin and Ivanov,1961; Ivanov,1967; Kummeneje and Eide,1961; Oriard,1976; True,1967,1969).

The geometrical attenuation of stress waves propagated during an explosive event can be altered by the proper selection of delay times and charge patterns to produce stress distributions that can induce liquefaction. Superimposed shock waves from simultaneous explosions can increase the extent of the liquefied zone. However, the appropriate sequencing of delay times presents a complicated problem. If the delay times between successive charge detonations is too short, then incomplete liquefaction occurs. If the delay times are too long, then the soil is allowed to drain and stabilize before being fully liquefied and may in fact become more resistive to liquefaction. These observations have been made by a number of investigators (Damitio,1978a,b; Hall,1962; Ivanov,1967; Klohn et al.,1981; Kummeneje and Eide,1961; Oriard,1976; Mitchell,1981; Prugh,1963).

The number of cycles and the period of application are significant factors in producing liquefaction for seismic loading. For example, if the duration of the 1964 Alaskan earthquake had been shorter, liquefaction would not have occurred over such an extensive area (Seed and Idriss,1971). The superposition of successive explosive detonations also produces a series of stress wave 'cycles' that can

cause liquefaction if the residual excess porewater pressure is not allowed to dissipate between charge delays (Damitio 1978a).

f. Geometric Attenuation

The attenuation of the applied compressive stress wave depends on many factors including the stiffness and density of the soil or rock, soil saturation, soil compressibility, charge geometry, load intensity and duration of the applied load. The geometric spreading of stress waves accounts for a major portion of the attenuation with distance. Cylindrically shaped charges generate stress waves that propagate from the source in a cylindrically diverging pattern. Spherically shaped charges generate stress waves that propagate from the source in a spherically diverging pattern. Both charge geometries attenuate the stress wave in an ever expanding radial manner. The amount of attenuation generally tends to increase with depth and distance away from the detonation point. These observations have been made by a number of investigators (Drake and Ingram,1981; Klohn et al.,1981; Lyakhov,1961; Melzer,1978b; Oriard,1976; Rinehart,1975; Rischbieter et al.,1977; Sanders,1982; True,1967,1969).

3. Summary

As can be seen by the number of parameters that influence the occurrence of liquefaction, a complete characterization of a given site becomes extremely difficult and complex. Evaluating each parameter is a cumbersome task with much uncertainty. There is some control that can be exercised in connection with the selection, location and detonation of the explosive charge, but this is limited in terms of

site response. Under such circumstances, it is necessary to treat these factors in a general manner with a number of simplifying assumptions so that this information can be applied to a variety of sites. Obviously this limits the applicability of general trends observed to different soil types. However, for any particular case, it should be emphasized that site specific conditions must be thoroughly investigated and incorporated into a comprehensive analysis and evaluation.

D. Field Experience

1. Military High Explosive Events

The detonation of high yield explosives by the military has been done primarily to investigate structural response and crater formation processes (Crawford et al., 1974). Considerable attention has also been given to evaluating the dynamic in situ properties of various geologic materials. However, little consideration has been given to evaluating the liquefaction phenomenon for these events. Available data on porewater pressure response are limited at best and are often sketchy and incomplete. Indirect observations of liquefaction have been made at some sites and do provide some useful information. At sites having cohesionless soils where the groundwater table is near the surface, the craters are typically broad and flat in shape. In areas where the groundwater table is not within the depth of influence of the explosion, craters generally assume a deep bowl shaped form. Such observations have only recently caused a re-evaluation of past events where unusual cratering phenomena have been noted and it is believed this could possibly be explained in terms of liquefaction.

At the Pacific Proving Grounds, possible indicators of explosive-induced liquefaction include broad, flat craters, sand cones, sink holes and other collapse features beyond the crater rim (Blouin,1978; Blouin and Kim,1983; Couch et al.,1975; Ristvet et al.,1978). The SNOWBALL event also had a broad, flat crater with water, sand and silt flowing into the area after the explosion (Gilbert,1976; Jones,1976; Roddy,1976a,b). Similar trends were observed at the PRAIRIE FLAT event, including sand boils, water spouts and ground subsidence (Melzer,1978a; Roddy,1976b). Piezometers installed at the DIAL PACK event test site indicated that residual excess porewater pressures existed for some time after the explosives were detonated (Charlie,1978a, Langley et al.,1972). The PRE-DICE THROW II event exhibited similar behavior. Springs flowed for several hours after the explosion and the resulting crater depth was about half that predicted (Melzer,1978a). The DISTANT RUNNER II field test formed a large, deep, bowl shaped crater initially, with water later flowing in and nearly filling it. The DISTANT RUNNER III event produced a wide, flat crater that filled with water and sand immediately after the explosion. The DISTANT RUNNER events occurred about 350 meters apart in similar geologic materials, but had markedly different cratering characteristics. The differences in the resulting crater formations is believed to be due to variations in the soil profiles and liquefaction effects at these two sites (Benson,1983).

All these events took place in loose, saturated soils where the groundwater table was shallow relative to the depth of influence of the explosion. It should be noted that except for the DIAL PACK event, there is virtually no data available from these sites for any direct

measurements of porewater pressure response. Considering that soil and groundwater conditions for the occurrence of liquefaction exist in many areas of the world, particularly when subjected to explosive loadings, this lack of data is unfortunate.

2. Construction Blasting

Much of the field experience in explosive-induced liquefaction has come from the practical application of explosives to engineering problems. As early as 1932, explosives were used to compact fill in the United States (Engineering News Record,1932). Since that time, there have been many reports of field blasting programs involving the densification of loose sand deposits, stabilization of submerged slopes and site preparation (Abelev and Askalonov,1957; Ivanov,1967; Hall,1962; Kummeneje and Eide,1961; Klohn et al.,1981; Kok,1978c; Long et al.,1981; Lyman,1942; Mitchell and Katti,1981; Mueller,1971; Obermeyer,1980; Prakash and Gupta,1970; Prugh,1963; Quieroz et al.,1967; Sanders,1982; Solymar,1984; Solymar et al.,1984; Terzaghi,1956; Wild and Haslam,1962). During these events, care is often taken to monitor the porewater pressure response and settlements and to tailor the field blasting program to minimize the potential for liquefaction. These operations have provided some data and practical observations of soil and porewater pressure response under field explosive loadings.

3. Small Scale Field Experiments

Some work has been done with field experiments specifically designed to investigate soil liquefaction and compaction. Russian and

European researchers have performed tests in saturated, sandy soils to investigate the effect of charge weight, location, patterns and delay times on liquefaction (Ivanov,1967; Kok,1977,1978a,b; Lyakhov,1961; Puchkov,1962; Rischbieter,1978; Schaepermeier,1978b,c; Studer et al.,1978; Trense,1977). These investigations have led to the development of empirical equations that can be used to estimate the extent of liquefaction at a site in terms of explosive charge parameters. Similar investigations have been conducted by researchers in Japan (Yamamura and Koga,1974) and India (Arya et al.,1978; Prakash and Gupta,1970). The U.S. Army Corps of Engineers Waterways Experiment Station has conducted field explosive tests at several locations to investigate the influence of charge location relative to the groundwater table (Drake,1978; Carnes, 1976; Perry,1972). Evidence of liquefaction was not observed where dense, coarse or very fine sands existed or where conditions of saturation were not evident. It has been noted that where broad, shallow craters were produced in these small scale tests, loose, saturated soils were within the depth of influence of the explosion. Conversely, where deep bowl shaped craters were formed this was not the case. These observations are consistent with experience gained in military high explosive events.

E. Laboratory Experience

1. Small Scale Explosive Tests

A limited amount of tests have been conducted using small scale explosive events in the laboratory. The Russians have investigated the effects of surface, buried and underwater explosions in loose, saturated, sandy soils. These soils were tested in metallic tanks and

reinforced concrete trays (Ivanov,1967). Soil stress and porewater pressure measurements were made and the influence of successive detonations and delays was examined. Buried charges and appropriately sequenced delays were found to be the most effective in producing liquefaction. This is consistent with results obtained in small scale field tests. Laboratory tests have also been conducted to evaluate the effect of charge placement on cratering in loose, saturated, sandy soils (Piekutowski,1976; Vesic et al.,1967).

Attempts have been made to use the centrifuge to model field explosion conditions (Al-Hussani,1976; Fragaszy et al.,1983; James,1978; Schmidt,1976; Schmidt et al.,1981). This laboratory technique involves the subscale modeling of prototype stress levels where small explosive charges are detonated under the influence of an acceleration field. Results have indicated that it is possible to induce liquefaction by this method. Some measurements have been made of soil and porewater pressure response. Cratering observations have generally been consistent with field experience. Fragaszy et al. (1983) have presented their findings in terms of a porewater pressure ratio (the ratio of the residual excess porewater pressure to the initial effective stress) as a function of charge weight and this relationship is presented in Figure 2.1.

2. Shock Loading

Experiments have been performed using air shock loadings to develop compressive stresses on the order of 0.20 MPa with millisecond rise times. A direct stress loading (Van der Kogel et al.,1981) and an air overpressure loading that passes over the soil have been used

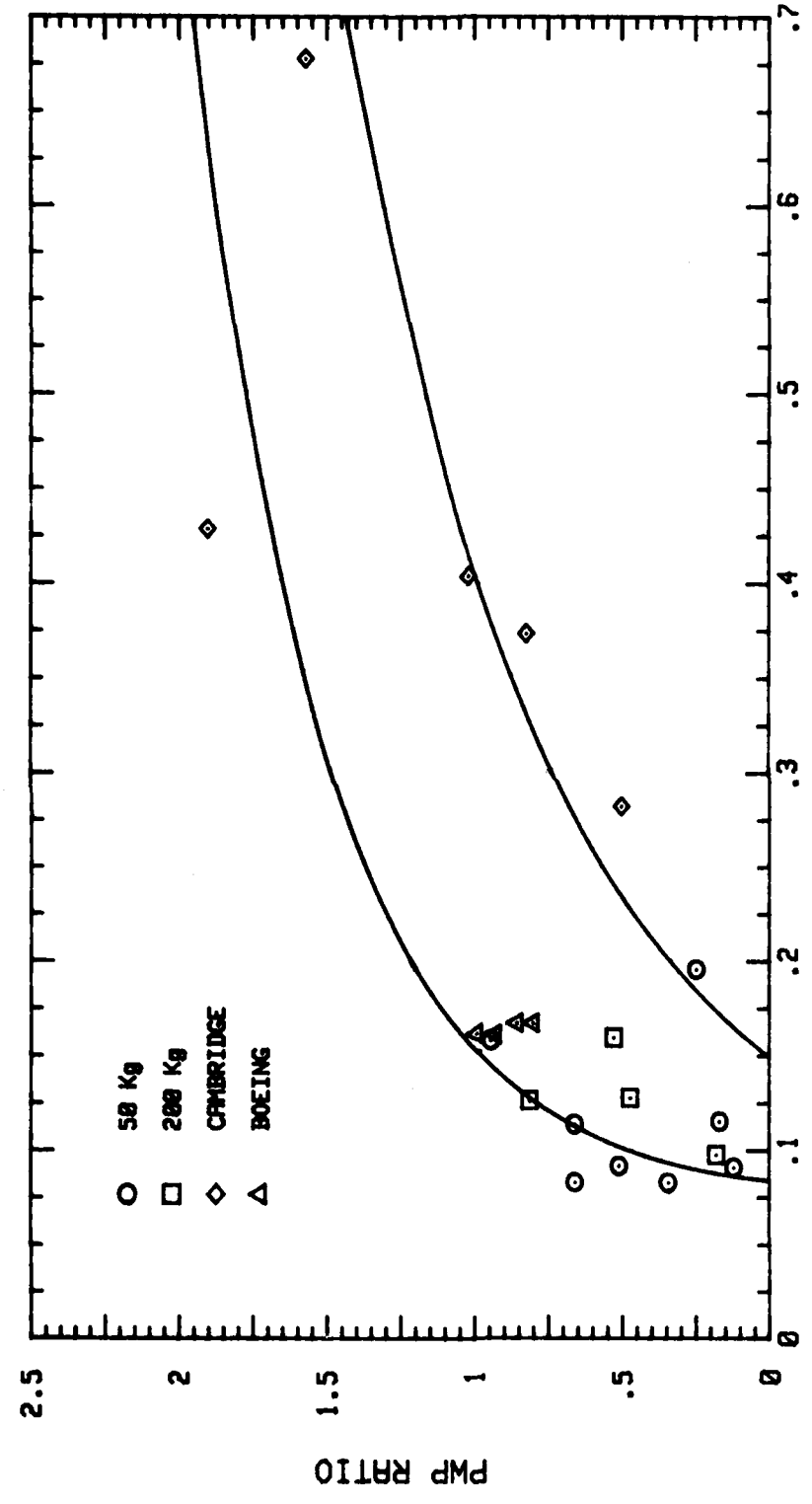

Figure 2.1 Porewater Pressure Ratio as a Function of Charge Weight and Distance from Explosive Centrifuge Modeling Experiments (Fragaszy et al.,1983)

(Studer,1978; Studer and Prater,1977; Quaak,1978). The direct loading tests were done on dry and partially saturated sands. Test results indicated that rise times for porewater pressure response decreased with increasing degrees of saturation. The air overpressure loadings were done on loose, saturated sands. Liquefaction was observed as a result of residual excess porewater pressures remaining after the stress wave was passed over the samples. Perry (1972) investigated the effects of density and moisture content on the liquefaction potential of loose sands using an explosive overpressure simulation device. Liquefaction was evaluated by monitoring the relative movements of a number of variable density inclusions in the sand after loading. In a few cases liquefaction was observed at low relative densities and high moisture contents.

Impact loading tests of saturated and nearly saturated sands have also been done. Tanimoto (1967) used a swinging pendulum to impact the side of a vertical column of loose, saturated sand. Measurements were made of porewater pressure increases and settlements caused by liquefaction. Greater settlement occurred with greater increases in porewater pressure. Kok (1977) also used a pendulum to apply a horizontal impact to a vertical column in order to observe the effect of applied stress intensity on the gradient across the soil. The more intense the applied load, the larger the gradient across the sample. Ruygrok and Van der Kogel (1980) used a free falling weight system to simulate the loading applied by ocean waves on covered, loose, nearly saturated sand and were able to obtain liquefaction in a number of tests. Allen (1975) and Allen et al.(1980) investigated the effects of

saturation and relative density on stress wave propagation velocity, observing higher velocities for dense, saturated soils.

Dynamic ram loading systems have been developed at the Waterways Experiment Station (Jackson,1978; Jackson et al.,1980; Seaman,1983). These devices are capable of generating shock loads of up to 400 MPa with millisecond rise times on uniaxial and triaxial test specimens. Dynamic compressibility, vertical stress and deformation can be measured. Based on an analysis of test data, it has been shown that strain rate effects become significant for submillisecond rise times in dry and partially saturated soils. Plans are being made at this time to incorporate a dynamic porewater pressure measurement system.

3. Quasi-Static Loading

Experiments using quasi-static, isotropic compressive loadings have been performed to investigate the liquefaction susceptability of saturated coral sands and saturated quartz sands (Fragaszy and Voss,1981; Fragaszy et al.,1983). The coral sand was obtained from the Eniwetok Atoll in the south Pacific which was the site of nuclear explosive detonations in the 1950's (Couch et al., 1975; Ristvet et al., 1978). A complete loading cycle was applied in one to two minutes and applied stresses were on the order of 35 MPa. Both drained and undrained behavior were examined and some evidence of liquefaction was observed in a few tests during unloading. Results indicate that grain fracturing may be a significant factor in liquefying coral sands and that it is possible to induce liquefaction by applying an isotropic compressive loading. Although porewater pressure increases were observed in the quartz sand, liquefaction did not occur.

F. Empirical Relationships

The empirical relationships that are available have been developed from field experience using buried charges in loose, saturated, granular soils. They are useful approximations that can be applied in a general manner to a variety of soils in field blasting programs where buried charges are used. However, they should be used with appropriate judgement and consideration for particular site specific conditions.

1. Explosive Charge

Based on field experience and observations, several empirical relationships have been developed to estimate the extent of the liquefied zone and the radius of influence of contained charges. These equations were obtained using buried, contained explosions unless otherwise indicated.

The required charge weight, W, in kilograms per delay to insure a contained explosion, is given by (Ivanov,1967; Damitio,1978b):

$$W = (0.55)\, d^3 \qquad \text{(Eq. 2.3)}$$

where, d is the buried charge depth in meters.

The depth of the liquefied soil, h_b, in meters for the charge weight, W, in kilograms per delay given in Equation 2.3, is given by (Ivanov, 1967; Damitio,1978b):

$$h_b = (1.5)\, d \qquad \text{(Eq. 2.4)}$$

where, d corresponds to that used in Equation 2.3.

The optimum placement depth, h_o , in meters for a charge weight, W, in kilograms per delay to obtain the largest radius of liquefaction at the ground surface, is given by (Lyakhov,1961):

$$h_o = (2.5)\ W^{1/3} \qquad \text{(Eq. 2.5).}$$

The maximum radius of the liquefied region, R_{max} , in meters, for the optimum placement depth, h_o , in meters from Equation 2.5, is given by (Lyakhov,1961):

$$R_{max} = (b)\ W^{1/3} \qquad \text{(Eq. 2.6)}$$

where, W is the charge weight in kilograms per delay and b is a coefficient based on the charge weight and scaled depth of burst, $d/W^{1/3}$, given in Figure 2.2.

The maximum radius of the liquefied region, R_{max} , in meters for the charge placement depth used in Equation 2.3, is given by (Ivanov,1967; Damitio,1978b):

$$R_{max} = k_3\ W^{1/3} \qquad \text{(Eq. 2.7)}$$

where, k_3 is an empirical factor based on relative density and grain size, having values given in Table 2.1.

The effective radius of influence of a buried charge, R_{eff} , in meters, is given by (Ivanov,1967; Damitio,1978b):

$$R_{eff} = k_4\ W^{1/3} \qquad \text{(Eq. 2.8)}$$

where, k_4 is an empirical factor based on relative density and grain

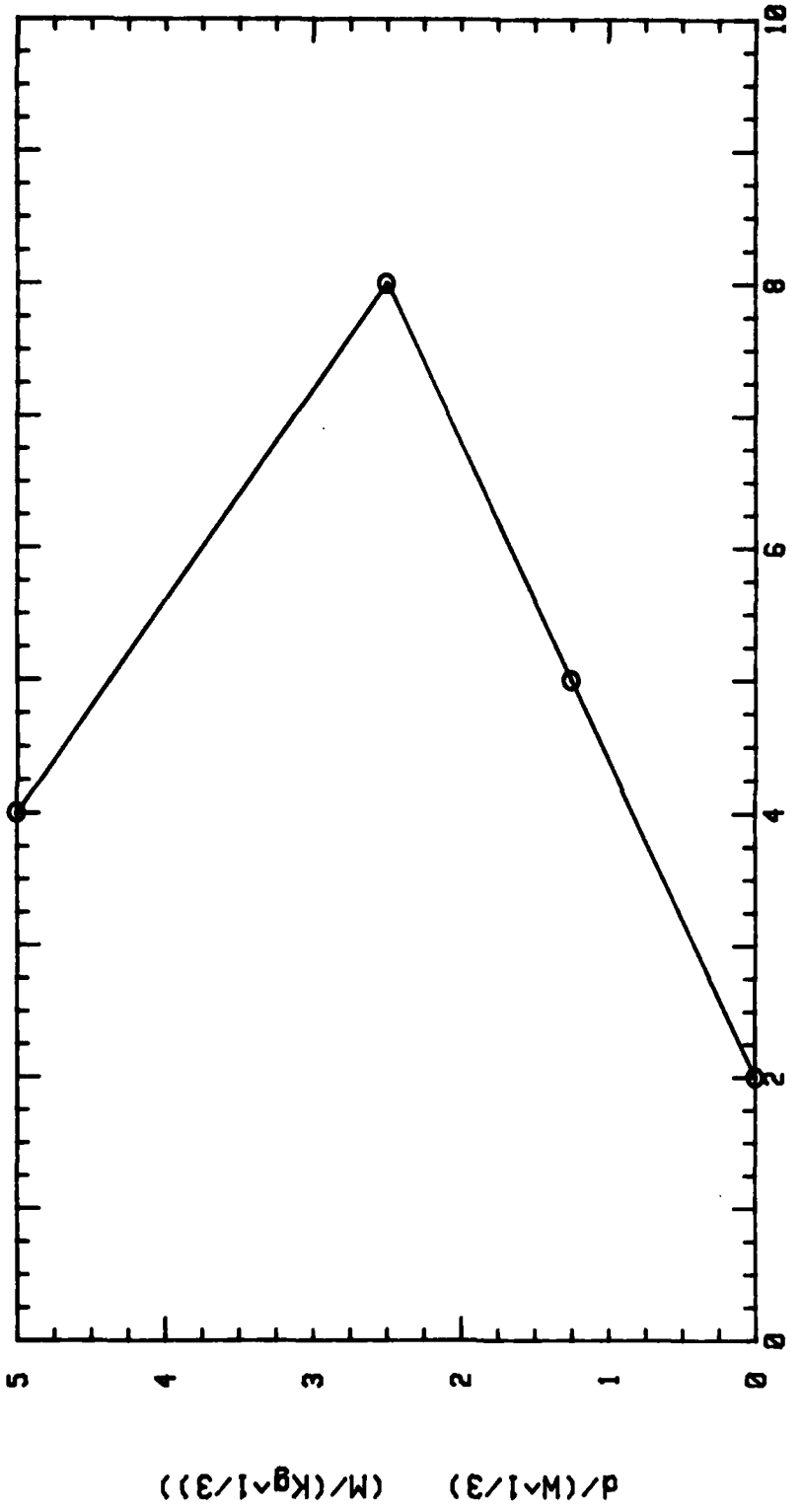

Figure 2.2 Empirical Scaling Coefficient, b, for Use in Equation 2.6 (Lyakhov,1961)

Table 2.1 Empirical Scaling Factors, k_3 and k_4, for Use for Use in Equations 2.7 and 2.8 (Ivanov,1967; Damitio,1978b)

Type of Soil	Relative Density	k_3	k_4
Fine Sand	0.0 - 0.2	25 - 15	5 - 4
Fine Sand	0.3 - 0.4	9 - 8	3
Fine Sand	> 0.4	< 7	< 2.5
Medium Sand	0.3 - 0.4	8 - 7	3 - 2.5
Medium Sand	> 0.4	< 6	< 2.5

size, having values given in Table 2.1. In-plane charge spacings should be limited to two times the effective radius of influence for maximum effectiveness.

An estimate of the maximum depth of liquefaction, h_s, in meters, was determined from tests using surface detonations of explosives and is expressed by Equation 2.9. Due to the lower ground shock energy transmission from surface explosions, the extent of the liquefied zone is less than for buried charges (Ivanov,1967; Damitio,1978b):

$$h_s = (1.2)\ W^{1/3} \qquad \text{(Eq. 2.9)}.$$

2. Compressive Stress

Several empirical relationships have also been developed to estimate peak compressive stresses developed in the soil as a function of charge weight and distance from the detonation point. The equation for the peak compressive stress, σ_{pk}, in MPa, has the following form:

$$\sigma_{pk} = K\ (\frac{R}{W^m})^{-n} \qquad \text{(Eq. 2.10)}$$

where, R is the radial distance from the charge in meters, W is the charge weight in kilograms per delay, K is a ground transmission constant based on charge confinement conditions and local geology, and n and m are empirical exponents. When m is taken as one half, the equation is referred to as 'square root scaling' and generally matches results from row, line and near surface charges. When m is taken as one third, the equation is referred to as 'cube-root scaling' and generally matches results from deeply buried point charges (Ambraseys

and Hendron,1968; Dowding,1985; Drake and Ingram,1981). In the field the actual propagation relationships should be established by small scale in situ explosive tests.

For a saturated soil, the peak compressive stress, σ_{pk} , in MPa, from contained point charges, is given by (Lyakhov,1961):

$$\sigma_{pk} = (58.9) \left(\frac{R}{W^{1/3}}\right)^{-1.05} \qquad \text{(Eq. 2.11)}.$$

The peak compressive stress, σ_{pk} , in MPa, from concentrated charges detonated in water, is given by (Cole,1948):

$$\sigma_{pk} = (54.9) \left(\frac{R}{W^{1/3}}\right)^{-1.13} \qquad \text{(Eq. 2.12)}.$$

In comparing Equations 2.11 and 2.12, it can be seen that they differ only slightly in their constants which indicates that the peak compressive stress developed in a saturated soil is very near to that developed in water. However, since a saturated soil is a two-phase medium, different behavior can be expected under explosive loadings.

The peak compressive stress, σ_{pk} , in MPa, from concentrated charges detonated in a saturated sandy soils, is given by (Drake and Little,1983):

$$\sigma_{pk} = (5.6 \times 10^{-6}) \, (f) \, (\rho_t \, V_c) \left(\frac{R}{W^{1/3}}\right)^{-2.35} \qquad \text{(Eq. 2.13)}$$

where, f is a ground shock coupling factor found in Figure 2.3 , ρ_t is the total mass density in kilograms per cubic meter and V_c is the compressive stress wave propagation velocity in meters per second. The

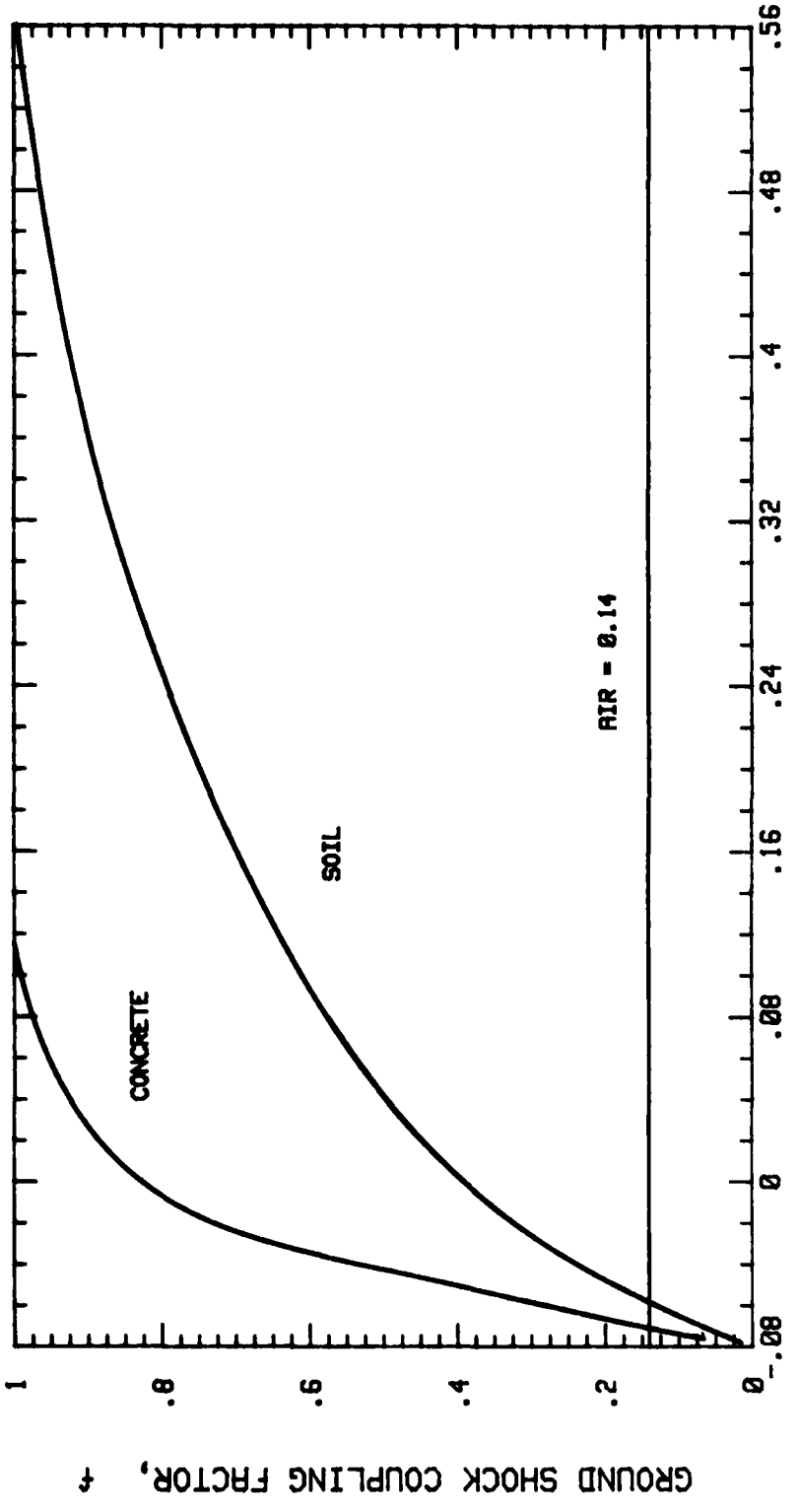

Figure 2.3 Groundshock Coupling Factor, f, For Use in Equations 2.13 and 2.18 (Drake and Little,1983)

quantity '$\rho_t V_c$' is commonly referred to as the acoustic impedance or specific acoustic resistance of the medium.

3. Particle Velocity

A widely used scaling law for peak particle velocities, V_{pk}, in meters per second, as a function of charge weight and distance from detonation point, has the following form:

$$V_{pk} = K \left(\frac{R}{W^m}\right)^{-n} \qquad \text{(Eq. 2.14)}$$

where, R is the radial distance from the charge in meters, W is the charge weight in kilograms per delay, K is a ground transmission constant based on charge confinement conditions and local geology and n and m are empirical exponents. When m is taken as one half, the equation is referred to as 'square root scaling' and generally matches results from row, line and near surface charges. When m is taken as one third, the equation is referred to as 'cube-root scaling' and generally matches results from deeply buried point charges (Ambraseys and Hendron,1968; Dowding,1985; Drake and Ingram,1981). In the field the actual propagation relationships should be established by small scale in situ explosive tests.

For large explosions in deep soil deposits, Drake and Ingram (1981) suggest that the following equations be used to estimate the peak particle velocity, V_{pk}, in meters per second, for row charge explosive configurations:

$$V_{pk} = (7.2) \left(\frac{R}{W^{1/3}}\right)^{-1.15} \qquad \text{(Eq. 2.15)}$$

where, W is the charge weight in kilograms per delay per meter of charge row length, and for point charge explosive sources:

$$V_{pk} = (8.0) \left(\frac{R}{W^{1/2}}\right)^{-2.3} \qquad \text{(Eq. 2.16)}$$

where, W is the charge weight in kilograms per delay.

The peak particle velocity, V_{pk}, in meters per second, from small buried charges in saturated sands, is given by (Long et al., 1981):

$$V_{pk} = (0.6) \left(\frac{R}{W^{1/2}}\right)^{-1.35} \qquad \text{(Eq. 2.17).}$$

Drake and Little (1983) recommend the following equation for the peak particle velocity, V_{pk}, in meters per second, for contained point charges in loose, saturated sands:

$$V_{pk} = (5.6)\ (f)\ \left(\frac{R}{W^{1/3}}\right)^{-2.35} \qquad \text{(Eq. 2.18)}$$

where, f is a ground shock coupling factor found in Figure 2.3.

4. Liquefaction Coefficient

Based on a series of tests using buried, contained, point charges in loose, saturated sand, Kok (1977,1978b) and Studer and Kok (1980) developed an empirical relationship for estimating residual excess porewater pressure increases in the field. The relationship is expressed in nondimensionalized form as a function of charge weight and radial distance from the charge:

$$L_c = \frac{u_r}{\sigma'_o} = 1.65 + 0.64 \ln \left(\frac{W^{1/3}}{R}\right) \qquad \text{(Eq. 2.19)}$$

where, L_c is the liquefaction coefficient, u_r is the residual excess porewater pressure, σ'_o is the initial effective stress, R is the radial distance from the charge in meters and W is the charge weight in kilograms per delay. The relationship given by Equation 2.19 is presented in Figure 2.4 for various porewater pressure ratios. Field explosive test results are shown in Figure 2.5.

G. One-Dimensional Stress Wave Propagation

Two useful equations have been developed from the theory of elasticity and the theory of stress wave propagation in a linear elastic, isotropic, homogeneous medium. The equations were derived considering a planar, longitudinal, compressive stress wave propagating along a medium. In general, these equations are only approximations for soils based on the assumptions in their derivations and can only be applied for small strain conditions. However, in a saturated soil with undrained loading conditions, the response is primarily governed by the water phase, making the assumptions reasonable and justifying the use of these equations. Rinehart (1975) indicates that these relationships are valid on the wave front of any type of propagating stress wave, but are only valid for planar stress waves propagating behind a wave front.

1. Compressive Stress

A linear relationship exists between the instantaneous stress at any point in an elastic medium propagating a stress wave and the particle velocity at the same point. The equation relating the

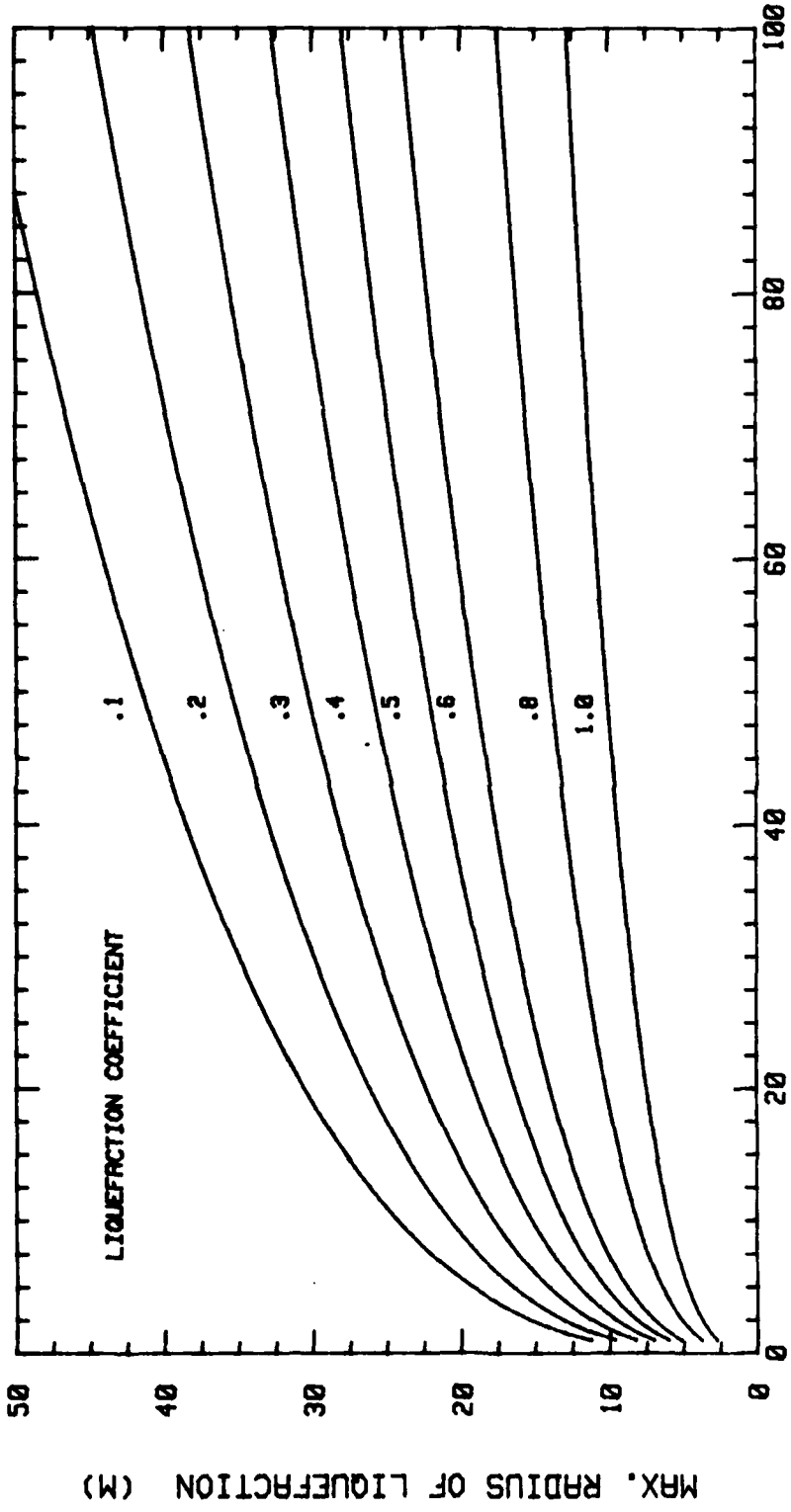

Figure 2.4 Liquefaction Coefficient as a Function of Charge Weight and Distance (Studer and Kok, 1980)

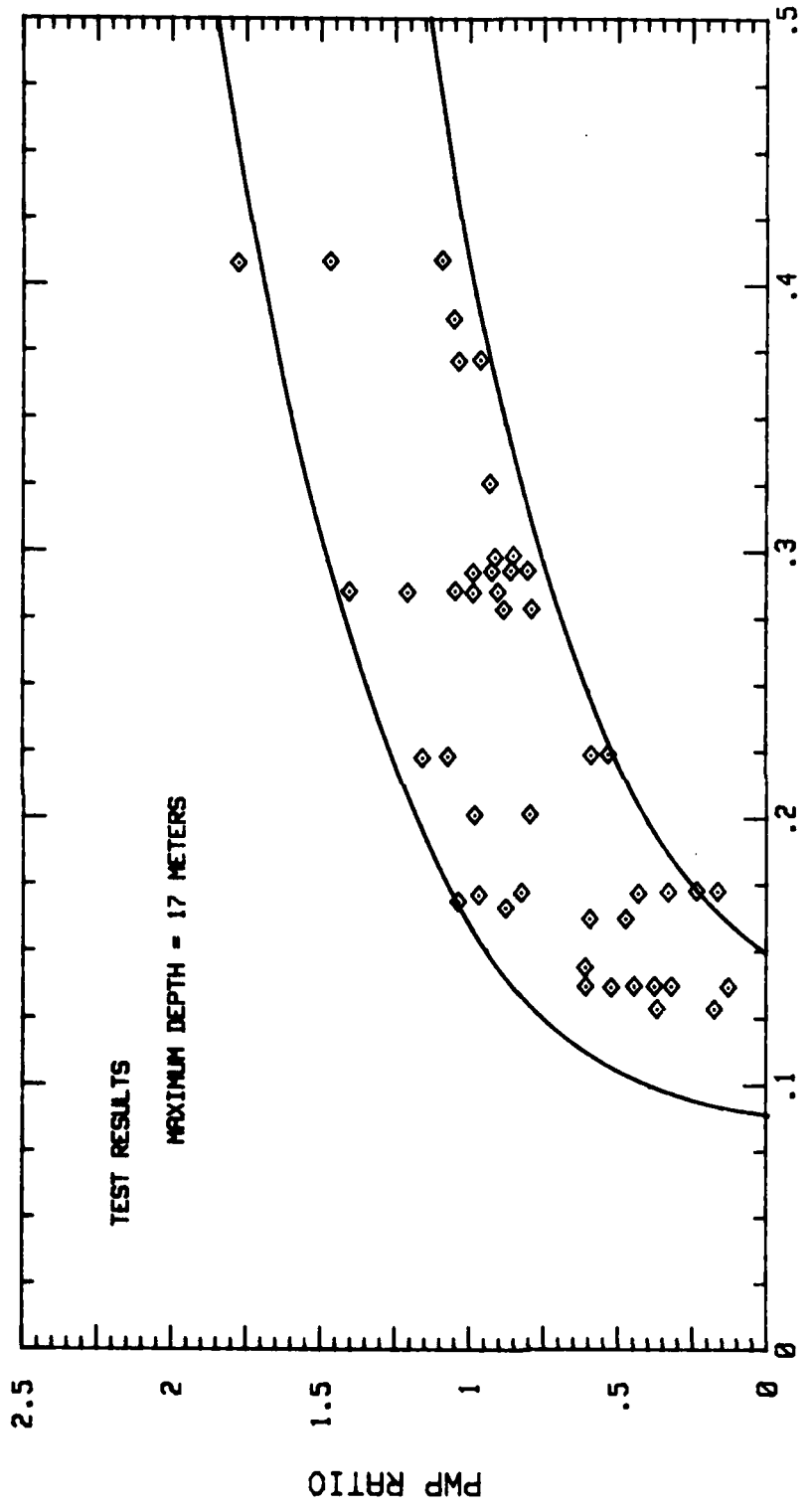

Figure 2.5 Experimental Results for the Porewater Pressure Ratio as a Function of Charge Weight and Distance Using Buried Charges (Kok,1978; Studer and Kok, 1980)

compressive stress, σ_c , and the particle velocity, V_p , is given by (Kolsky,1963; Timoshenko and Goodier,1970):

$$\sigma_c = (\rho V_c) V_p \qquad \text{(Eq. 2.20)}$$

where, ρ is the mass density and V_c is the compressive stress wave propagation velocity through the medium. The quantity 'ρV_c' is commonly referred to as the acoustic impedance or specific acoustic resistance of the medium.

2. Compressive Strain

The compressive strain, ε_c , developed in the medium can be determined form the following equation (Kolsky,1963; Timoshenko and Goodier,1970):

$$\varepsilon_c = \frac{V_p}{V_c} \qquad \text{(Eq. 2.21).}$$

It can be seen from Equation 2.21 that the compressive strain, ε_c , is only a function of the compressive stress wave propagation velocity through the material and the particle velocity as the stress wave propagates.

III. DEVELOPMENT OF A NEW EXPERIMENTAL SOIL DYNAMICS FACILITY

A. Design of the Experimental Facility

An experimental facility was designed and constructed to investigate the transient and long-term porewater pressure response of saturated soils. Samples of saturated sand can be prepared at varying initial densities and effective stresses. The experimental boundary conditions are for one-dimensional, confined, compressive loadings without drainage. The system is capable of applying compressive shock loadings on the order of 35000 KPa having millisecond rise times to peak stress.

The experimental facility is located in the Department of Civil Engineering's Geotechnical Engineering Research Laboratory at Colorado State University. The facility is divided into two areas. One contains the electronic recording equipment and supporting devices and the other contains the experimental set-up which is located behind a concrete wall for safety. Various aspects of the system, including the design considerations and construction, will be discussed in the following sections.

B. Cannon for Shock Load Application

To simulate the compressive stress conditions associated with explosive loadings, it is necessary to apply a high amplitude stress having a millisecond rise time to peak stress. The possibility of using a compressed air shock loading system, similar to that used in typical shock tube experiments, was considered but then abandoned since

it did not meet the loading requirements of this experimental investigation. Further investigations into the literature showed that direct impact methods would be the most practical way to obtain the compressive stress pulse desired, without using explosives. A loading system using a gas powered cannon that fired a 6.80 cm diameter, 10.15 cm long stainless steel projectile was designed and constructed. The cannon operates using compressed nitrogen gas and has one internal moving part called a 'poppet valve.' The principle of operation involves applying an equal pressure on both sides of the poppet valve when preparing to fire. The release of pressure on one side of the valve to atmospheric pressure allows a rapid release of the remaining high pressure into the cannon barrel to propel the projectile. The projectile velocity was varied by using different nitrogen pressures in the cannon. The cannon design was based on a working system in the laboratory used for dynamic loading of rock core specimens. The cannon was pressurized and fired by a manually controlled mechanical valving system. Figure 3.1 shows the cannon.

C. Confining Tube

One objective of these experiments was to examine the influence of the initial effective stress on the sample's porewater pressure response. A controlled method of applying both a confining pressure and a back pressure to the sample was developed. Since a direct impact method of stress application was to be used, consideration was also given to insuring that nearly all the loading was applied to the sample and not the confining tube system.

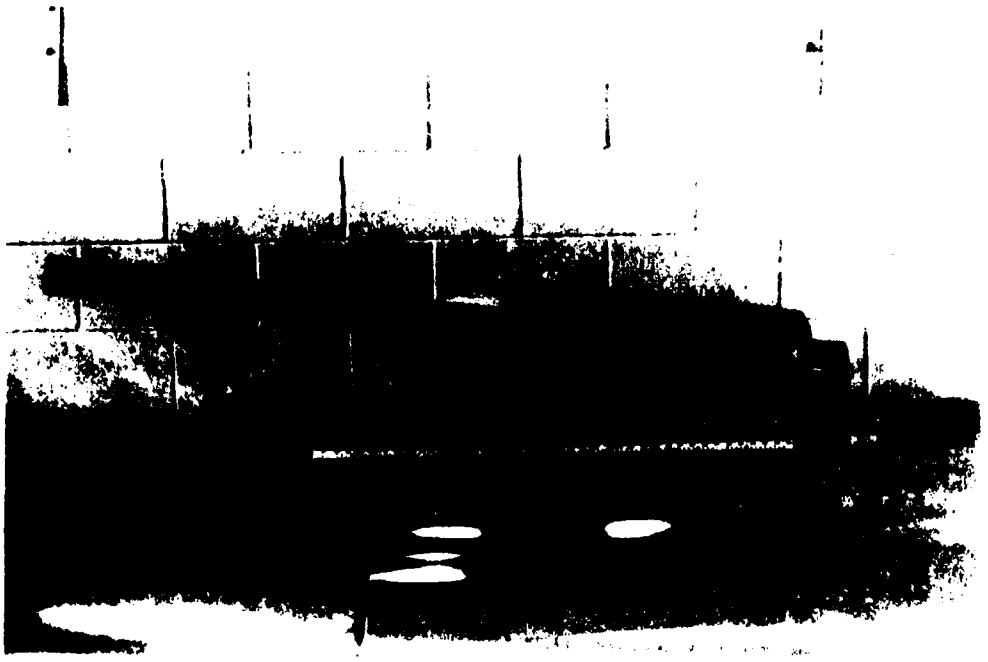

Figure 3.1 Cannon for Application of Impact Shock Loadings

The confining tube was constructed from a 122 cm long section of seamless, stainless steel pipe having a 1.27 cm wall thickness with a 8.90 cm inside diameter. Welded to each end of the confining tube was a 30.48 cm diameter, 2.54 cm thick, drilled, stainless steel flange plate used to bolt the entire system together. High strength steel bolts with lock washers were used on each flange plate. The confining tube was filled with distilled, de-aired water. A pressure line was attached to the tube at the midpoint using a high pressure, one-way quick disconnect valve in series with a high pressure plug valve. This type of connection was used to maintain undrained loading conditions. Pipe thread fittings were used in connecting the valves to the confining tube for a high pressure seal. The confining tube was pressurized by a small hydraulic pressure vessel filled with distilled, de-aired water and connected to a high pressure air line. The pressure vessel was used to maintain an interface between the air pressure and the water. The distilled, de-aired water in the confining tube and the pressure vessel was periodically replaced. Based on the effective stress required, the line air pressure would be increased to the correct confining pressure which then applied pressure to the confining tube through the interface vessel. The interface pressure vessel is shown in Figure 3.2.

The porewater pressure transducer where the measured pressure would be the impact stress applied to the sample. The transducer was located as near to the sample as possible in the confining tube. The transducer was flush mounted with the inside of the confining tube wall and a high pressure seal was obtained according to the manufacturer's specifications.

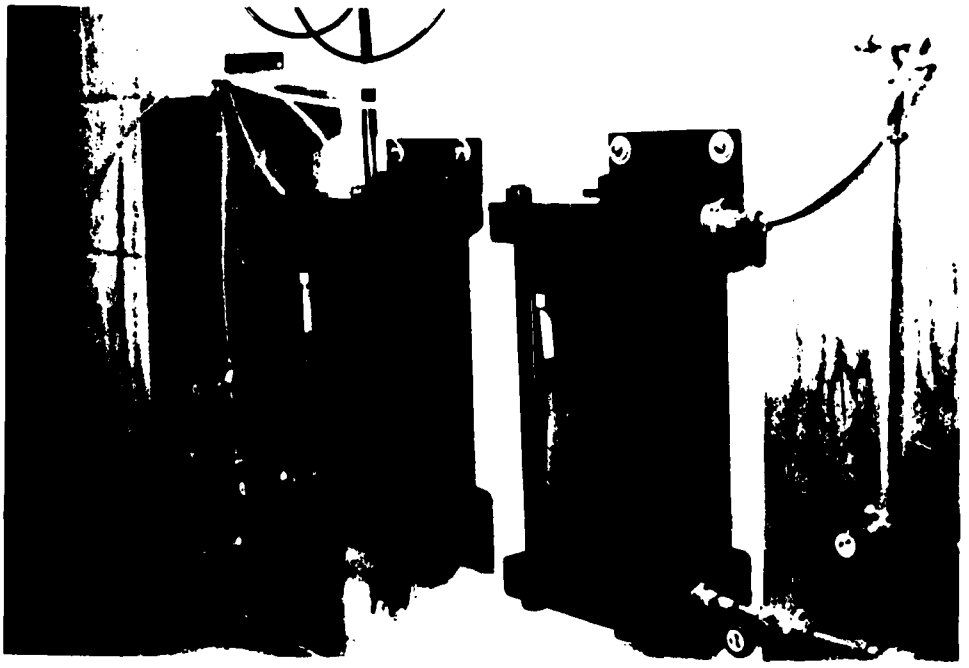

Figure 3.2 Interface Pressure Vessels Used in Pressurizing the Confining Pressure Tube and the Sample Container

The end of the confining tube impacted by the projectile, was required to effectively transmit the impact stress to the confining pressure. This could not be accomplished with a stiff, rigidly fixed loading plate since under such conditions the applied stress would be transmitted to the confining tube. In meeting this requirement, a stainless steel impact piston was designed that was not directly attached to the tube. The piston was allowed to move under the applied load. One end of the piston was machined to fit within the end of the confining tube and was equipped with five high pressure O-ring seals. The other end of the piston was machined to the projectile diameter with a bevelled edge for placing a brass loading cap. The loading cap was used to prevent excessive deformations of the exposed end of the piston from repeated impacts.

A 2.54 cm thick, 30.48 cm diameter stainless steel plate was bolted on the impact end to hold the piston in place. The plate was fitted with a high pressure O-ring seal that came in contact with the end face of the confining tube. The hole in the plate for the piston contained two teflon rings to minimize friction between the piston and the end plate. Details of the impact piston, the confining tube and the porewater pressure transducer location are shown in Figure 3.3.

D. Sample Container

An important requirement in the design of the sample container was to have undrained, one-dimensional, confined compressive loading conditions. To accomplish this, the design used a rigid sample container to minimize system strain effects on the soil sample. It was also necessary to be able to apply a back pressure within the sample

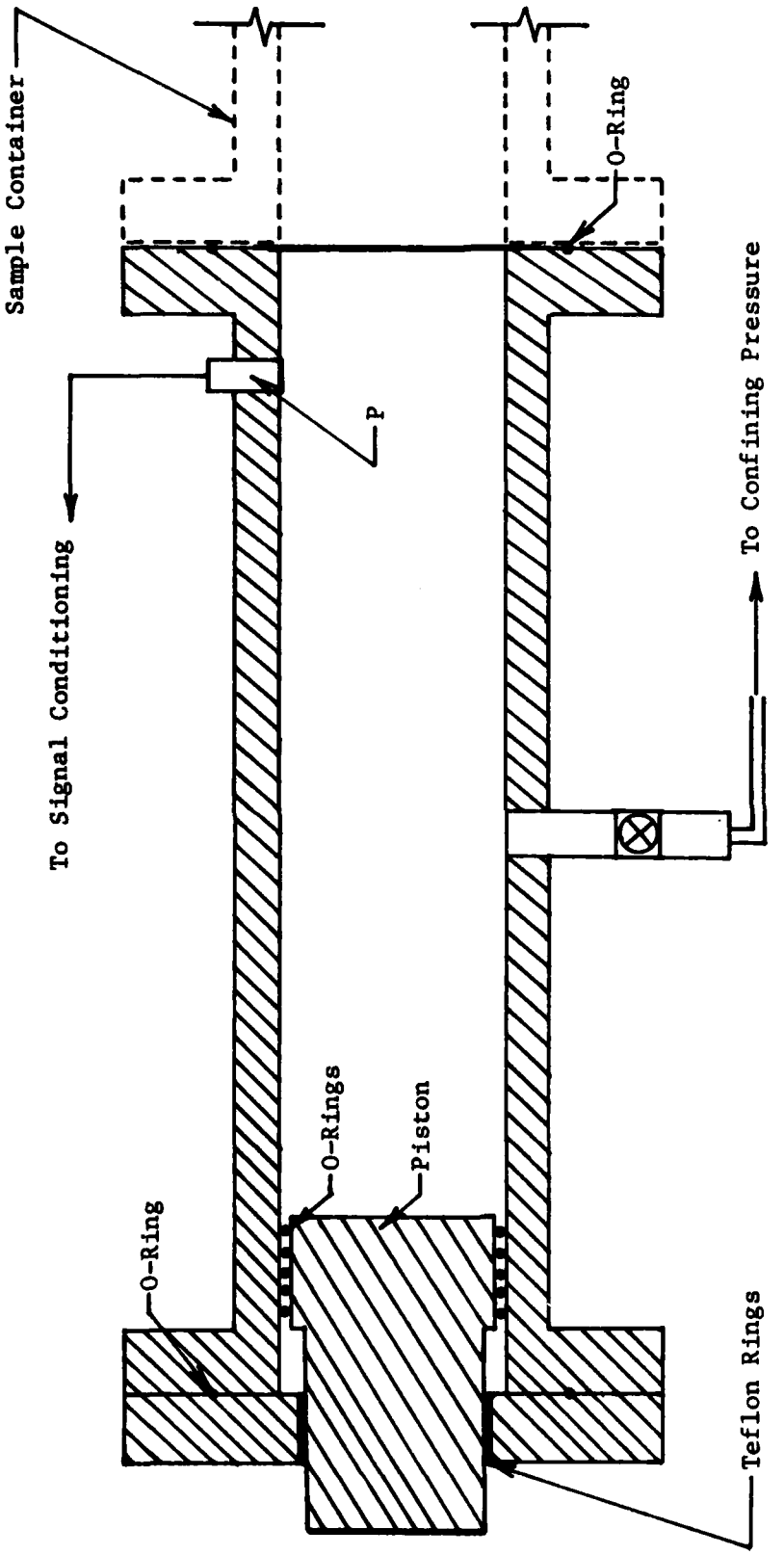

P = Porewater Pressure Transducer (Not To Scale)

Figure 3.3 Cross Sectional View of the Confining Pressure Tube

and have a large aspect ratio for the sample (i.e. thin sample) to minimize any inertia effects that might occur with the passage of the stress wave.

The sample container was constructed from of a 15.25 cm long section of seamless, stainless steel pipe having a 1.27 cm wall thickness with an 8.90 cm inside diameter. Welded to each end was a 30.48 cm diameter, 2.54 cm thick, drilled, stainless steel flange plate used to bolt the entire system together. High strength steel bolts with lock washers were used on each flange plate. Two pressure lines were attached to the container at the midpoint using a high pressure, one-way quick disconnect valve in line with a high pressure plug valve on each. The lines were located 180 degrees apart and used in preparing and saturating the sample. This type of connection was used to maintain undrained loading conditions. Pipe thread fittings were used in connecting the valves to the sample container for a high pressure seal.

In pressurizing the sample container, it was necessary to prevent any soil grains in the sample from moving out into the two pressure lines. A modified fitting with a recessed internal slot was used. A small porous stone was sized to fit snugly in the recess of the two fittings. Each stone was securely glued in place with a silicone adhesive.

Since air bubbles in the sample could not be tolerated, it was necessary to flush and back pressure the sample container using distilled, de-aired water. The sample was back pressured using a small hydraulic pressure vessel filled with distilled, de-aired water and connected to a high pressure air line. Figure 3.2 shows the pressure

vessel which was the same design as that used for the confining tube. The pressure vessel was used to maintain an interface between the air pressure and the water. The distilled, de-aired water in the pressure vessel was periodically replaced. A 0.033 cm thick latex rubber membrane was placed between the sample container and the confining tube before bolting them together. The line air pressure was increased to 345 KPa which then applied the back pressure to the sample container through the interface vessel.

The porewater pressure transducer was located where an average sample porewater pressure would be measured. The transducer was placed at the midpoint of the sample container. The transducer was flush mounted with the inside of the sample container wall and a high pressure seal was obtained according to the manufacturer's specifications. Although the transducer was not located in the center of the sample, results from its position would be indicative of the average applied compressive stress amplitude. The porewater pressure transducers in the confining tube and the sample container were aligned and positioned on the same side and in the same plane.

The end of the sample container that attached to the confining tube was machined smooth to seal with the high pressure O-ring on the adjoining face. A 2.54 cm thick, 30.48 cm diameter stainless steel plate was attached to the other end of the sample container and was fitted with two concentric high pressure O-ring seals. The steel plate was bolted securely in place with high strength steel bolts and lock washers. Details of the sample container and porewater pressure transducer location are shown in Figure 3.4.

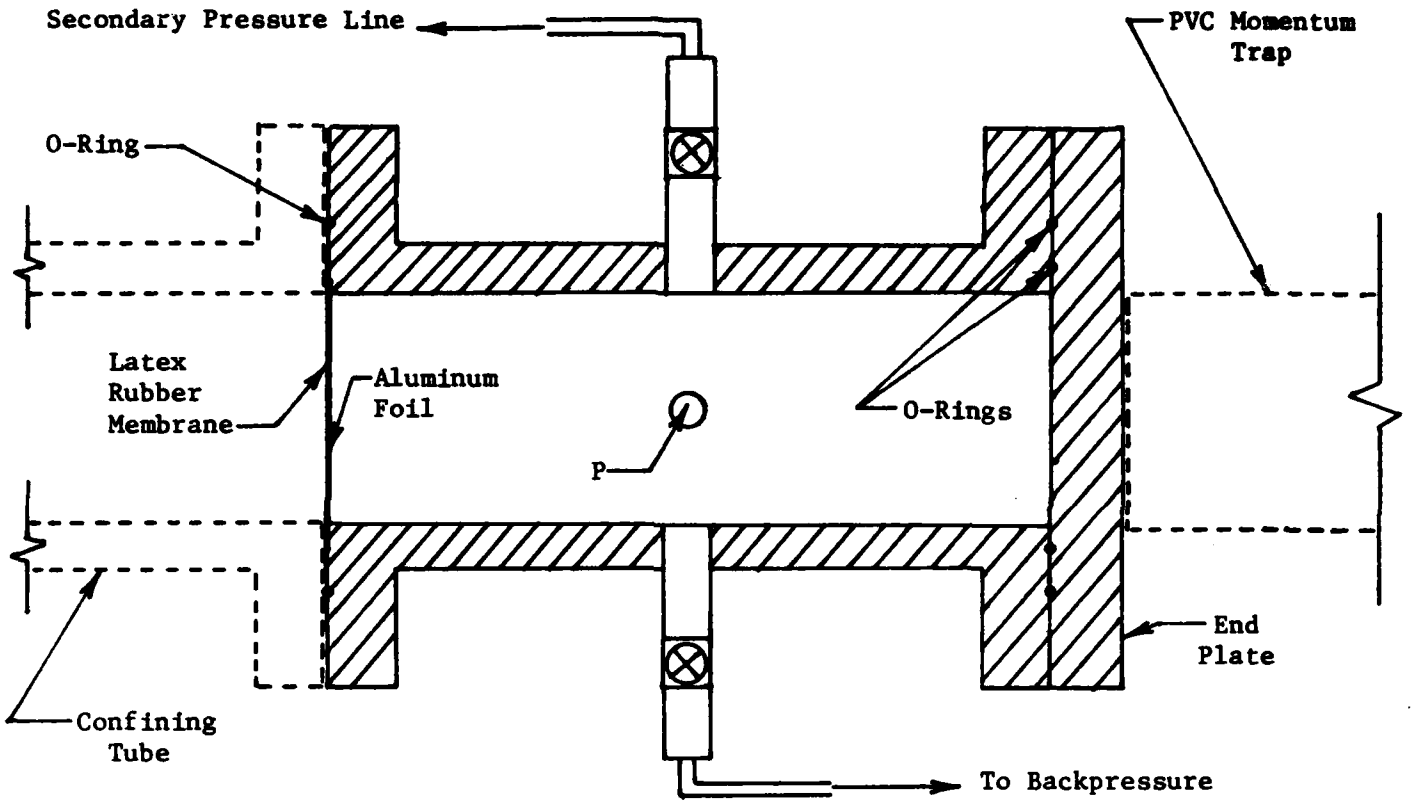

Figure 3.4 Cross Sectional View of the Sample Container

E. Momentum Trap

To effectively apply a single compressive loading to the soil, stress wave reflections from the end of the sample container needed to be minimized. The momentum trap system used in this investigation typically reduced reflected stress waves to less than about 50 percent of the applied compressive stress.

Based on these observations and an investigation of the phenomenon of stress wave propagation through materials, several criteria were established to aid in finding an efficient method of stress wave energy dissipation:

- the material should have an acoustic impedance close to that of water or the soil-water mixture. The better the acoustic impedance match the better the stress wave transmission between mediums,

- the material should be long enough to capture the stress wave,

- the material should have a larger contact area than the sphere, being at least the same size as the sample cross sectional area to be the most effective, and

- the material should be free to move away from the sample container end plate as the stress wave passes through it. This would require a low friction support mechanism and would allow the stress wave to dissipate its energy within the material apart from the sample. The material also must not be allowed to rebound back towards its original position where it could impart a stress wave due to its own motion.

An investigation of commercially available materials to satisfy the first requirement led to the selection of a solid polyvinylchloride (PVC) rod. PVC has an acoustic impedance just above that of water. Two 92 cm long sections of 9 cm diameter PVC rod were obtained in

accordance with the second requirement. To satisfy the third requirement, the ends of the rods were machined and trued to be flush with each other and the steel end plate.

In satisfying the fourth requirement, a low friction, free moving support system was designed. A 305 cm long section of 15 cm diameter thin walled PVC pipe was selected. The pipe was attached to a 305 cm long section of 8 cm wide steel channel section which was fixed to and supported by two heavy duty, adjustable surveying tripods. The solid PVC rods were placed inside the pipe and the unit was aligned with the sample container. This arrangement provided a stationary support system that allowed the rods to move freely as the compressive stress wave passed through them.

F. Instrumentation

1. Porewater Pressure Transducers

To simulate the type of loading encountered with an explosion, it is necessary to apply a compressive stress pulse of a sufficient magnitude with millisecond rise time to peak stress. The measurement of porewater pressures associated with this type of loading places specific requirements on the transducers, amplifiers and signal conditioners necessary to accurately monitor the pressure changes over the time domain of the loading. Considering the type of loading to be applied in the laboratory and the specific requirements of this research program, a number of criteria were established to evaluate commercially available transducers and supporting equipment. The requirements included the following:

- the transducer must be able to measure the porewater pressure response of the soil sample independent of the soil skeleton stress,

- the transducer must have a linear response to pressures of up to 35 MPa, having millisecond rise times,

- the transducer must have a resonant frequency greater than the shock facility system where it is used,

- the transducer must be ale to survive repeated shock loadings,

- the transducer must have minimal acceleration sensitivity,

- the transducer must be able to survive some amount of overpressure and still have a linear response,

- the transducer must able to survive electronically in water for at least several days,

- the transducer must have a minimum sensitivity of less than seven KPa at Full Scale Output voltage,

- the transducer must be able to measure both the transient and long-term porewater pressure responses,

- the transducer must be able to consistently reproduce pressure responses under loading conditions,

- the transducer must be flush mountable in the steel walls of the confining tube and sample container, having a high pressure seal of at least 17 MPa, and

- the transducer must be small in size due to physical space limitations and soil sample size.

A review of many instrumentation companies' products led to the selection of a porewater pressure transducer manufactured by ENDEVCO, Inc., of San Juan Capistrano, California. The ENDEVCO Model 8511a-5kM1

met the above requirements. It is a piezoresistive, silicon diaphragm, strain gage pressure transducer. The signal conditioner units were ENDEVCO Model 4476.1a and the power supply units were ENDEVCO Model 4470 for these transducers.

The transducer was modified by the manufacturer to meet the first requirement. A one millimeter thick, stainless steel circular plate was mounted on the transducer casing over the diaphragm. The plate had several very small holes (smaller than the smallest grain size of the soil) placed in it in a star pattern. The space behind the plate was filled with silicon oil. Since the plate was not in contact with the transducer diaphragm, measured stresses would correspond to the porewater pressures only. Stresses applied by the soil skeleton would be transmitted through the points of contact between the plate and the housing. Figure 3.5 shows the modified transducer. Table 3.1 gives information on the features and characteristics of the transducer.

2. Digital Waveform Recorder

To simulate the type of loading encountered with an explosion, it is necessary to apply a compressive stress pulse of sufficient magnitude with millisecond rise time to peak stress. The recording of measured data associated with this type of loading places specific requirements on the instrumentation necessary to accurately monitor the porewater pressure transducer output over the time domain of the loading. Considering the type of loading to be applied in the laboratory and the specific requirements of this research effort, a number of criteria were established in order to evaluate commercially available waveform recorders. The requirements included the following:

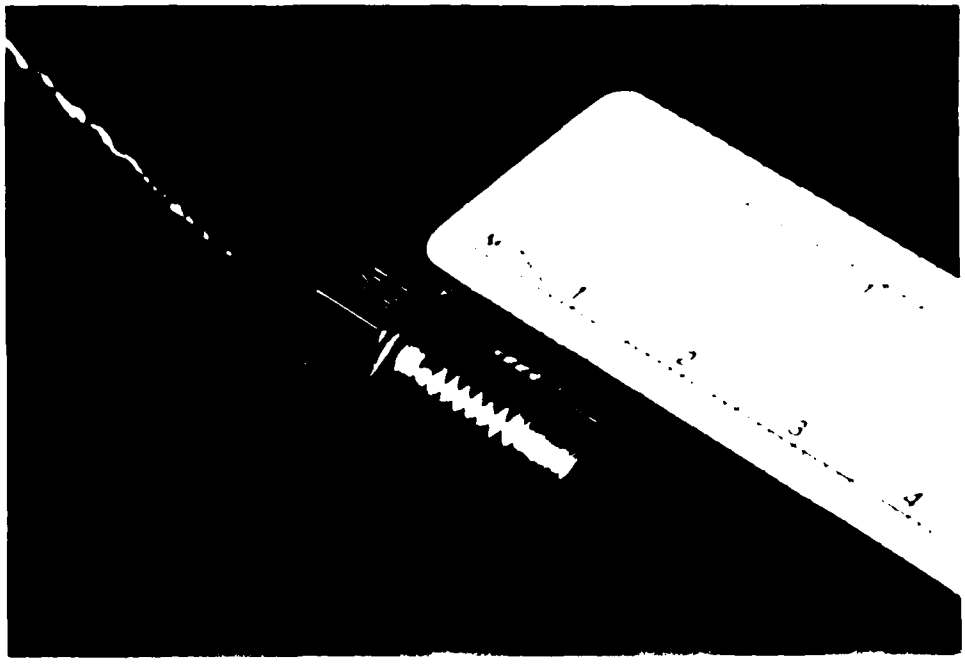

Figure 3.5 Modified Porewater Pressure Transducer Used in the Confining Pressure Tube and the Sample Container

Table 3.1 Manufacturer's (ENDEVCO) Specification Data Sheet for the Porewater Pressure Transducer

ENDEVCO® PRODUCT DATA

SERIES 8511

5 000 to 50 000 psi
High resonance frequency

PIEZORESISTIVE PRESSURE TRANSDUCERS

The Endevco Model 8511 is a rugged, piezoresistive pressure transducer for high pressures. It has a ⅜ in. mounting thread and is available in ranges from 5 000 to50 000 psig. It offers high shock resistance, high overload capability, and low photosensitivity.

Endevco pressure transducers feature a four-active arm strain gage bridge diffused into a sculptured silicon diaphragm for maximum sensitivity and wideband frequency response. Self-contained hybrid temperature compensation provides stable performance over the wide temperature range of 0 to 200°F (-18 to +93°C). Endevco transducers also feature excellent linearity (even to 3x range), high shock resistance, and high stability during temperature transients.

The Model 8511 is widely used for high pressure applications such as studies of structural loading by shock waves resulting from explosive blasts, pulsations in hydraulic systems, and combustion problems. It features an ablative coating over the diaphragm to protect against particle impingement.

SPECIFICATIONS FOR THE 8511 SERIES
(According to ANSI and ISA Standards)

PERFORMANCE	8511-5K	8511-10K	8511-20K	8511-50K
RANGE (psig) (1 psi = 6.895 kPa)	5 000	10 000	30 000	50 000
SENSITIVITY[1] (mV/psi at 10.00 Vdc)	100 ±.030	.050 ±.015	.025 ± 008	.010 ± 003
RESONANCE FREQUENCY[2] (kHz)	>500	>500	>500	>500
LINEARITY				
Independent (±__% of FSO, 0 to FSO)	0.3	0.8	0.4	0.5
Independent at 3x overrange (±__% of 3x FSO)	0.3	0.8	1.0	Note[3]
HYSTERESIS (% of FSO)	0.3	0.8	0.2	0.5
REPEATABILITY (±__% of FSO)	0.1	0.5	0.1	0.5
COMBINED LINEARITY AND HYSTERESIS (RSS maximum, % of FSO)	1.2	1.5	1.2	2.0
ZERO MEASURAND OUTPUT (±__mV)	10.0	10.0	10.0	10.0
ZERO SHIFT				
At 3x Overrange (±__% of 3x FSO)	0.1	0.2	Note[4]	Note[3]
With Mounting Torque at 15 lbf·in. (±__% of FSO)	0.1	0.1	0 1	0.1 @ 25 lbf · ft
At Maximum Temperature[5] (±__% of FSO, ref. 75°F)	3 0	3.0	3 0	3.0
SENSITIVITY SHIFT				
At Maximum Temperature[5] (±__% of FSO, ref. 75°F)	4.0	4.0	4 0	4.0
THERMAL TRANSIENT RESPONSE (psi/°F) (per ISA-S37.10, Para. 6.7, Proced. 1)	1.1	1.5	0.4	0.1
WARMUP TIME (seconds)	15	15	15	15
ACCELERATION SENSITIVITY[6]				
Longitudinal (psi/g)	0.003	0 004	0 008	0 003
Lateral (psi/g)	0.001	0.002	0 004	0.003
BURST PRESSURE				
Minimum Differential (±__psi)	20 000	30 000	40 000	75 000

[1] The unit is calibrated at 10 00 Vdc excitation. It may be operated at other voltage but the desired voltage should be specified at time of order. Endevco Model 4422, 4423 or 4470 Signal Conditioner is recommended as the excitation source.

[2] Improved performance can be obtained by removal of the ablative coating on the diaphragm.

[3] Overrange is limited to 75 000 psi. A shift in calibration may occur after exposure to pressures above 50 000 psi.

[4] Overrange is limited to 40 000 psi. Zero shift at 2x range is typically +1% of 2x FSO.

[5] Tighter specifications available on special order.

NOTE: All values are typical over the compensated temperature range except where noted.

Endevco cautions the user that this product has not been clinically tested for medical applications, and no claim has been made for sterility, nonpyrogenicity, lack of reactivity or electrical safety.

Table 3.1 (cont'd.) Manufacturer's (ENDEVCO) Specification Data Sheet for the Porewater Pressure Transducer

SPECIFICATIONS FOR MODEL 8511

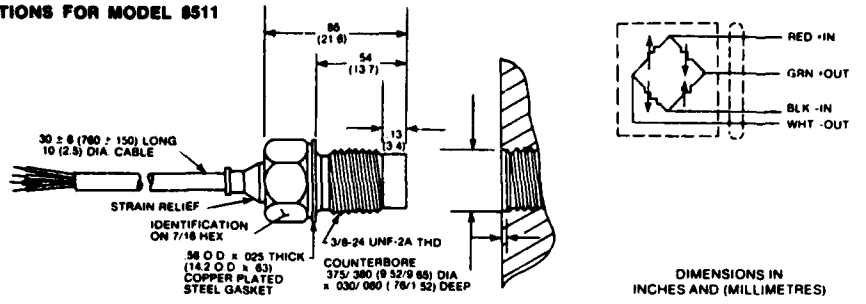

ELECTRICAL	ALL MODELS
EXCITATION	
Rated	10.00 Vdc
Maximum	18 Vdc
ELECTRICAL CONFIGURATIONS	Four-active-arm piezoresistive bridge
POLARITY	Positive output for increasing pressure
RESISTANCE	
Input	1 000 Ω
Output	1 300 Ω
Isolation (ambient conditions)	>100 MΩ at 50 V
PHYSICAL	
DEAD VOLUME	0.0003 in.³ (0.0049 cm³)
MOUNTING	Threaded case, 3/8-24 UNF-2A threaded length 0.520 in.
MOUNTING TORQUE	12 ±2 lbf·ft to 20 000 psi 25 ±2 lbf·ft above 20 000 psi 1 lbf·ft = 1.356 N·m
MATERIAL	
Case	Stainless steel
Exposed to Measured Fluid*	Case, Parylene C, epoxy, copper gasket, ablative
CABLE	Integral, 4-conductor, shielded, Teflon-insulated 32 AWG (7/40) silver plated copper conductors, gray PVC jacket, 30 in (0.76 m) long
IDENTIFICATION	8511-XX, where XX denotes rated pressure in psig
WEIGHT	0.4 oz. (11 g) less cable

ENVIRONMENTAL	
TEMPERATURE RANGE	
Compensated	0°F to 200°F (-18°C to +93°C) Can be compensated over any 200°F (110°C) span from -65°F to +225°F on special order
Maximum	-65°F to +250°F (-54°C to +121°C)
VIBRATION	1 000 g, sinusoidal
SHOCK	20 000 g, 100 μs, half-sine
HUMIDITY (per MIL-STD-202E, Method 103B, Test Condition B)	Isolation resistance greater than 100 MΩ at 50 V. External case is sealed with epoxy. Circuit within case, vented through tube, is coated with Parylene C.

*Designed for use with dry non-conductive gases. Not suitable for use with high pH or low pH liquids, long term exposure to water, or exposure to solvents which may attack epoxies.

Continued product improvement necessitates that Endevco reserve the right to modify these specifications without notice.

RELIABILITY: Endevco maintains a program of constant surveillance over all products to ensure a high level of reliability. This program includes attention to reliability factors during product design, the support of stringent Quality Control requirements, and compulsory corrective action procedures. These measures, together with conservative specifications, have made the name Endevco synonymous with reliability. Endevco's Quality and Reliability System meets the requirements of MIL-Q-9858A and MIL-STD-785A.

CALIBRATION: Each transducer is calibrated at room temperature for pressure sensitivity with 10.00 Vdc excitation. Special calibrations available—consult factory.

U.S. Patent Nos. 4 065 970 and 4 093 933 apply to this transducer.

- the waveform recorder must be able to interface with the computer system,

- the waveform recorder must provide digital output for the purpose of mass storage operations and calculations,

- the waveform recorder must be able to record data at rates up to the megahertz range, with variable sampling rates,

- the waveform recorder must be capable of recording enough data points to represent the transducer output,

- the waveform recorder must have a minimum sensitivity of 14 KPa when in line with the transducer, and

- the waveform recorder must be able to record at least four channels and be expandable for future modifications.

A comparison of similar products offered by various companies led to the selection of a digital waveform recorder (GOULD/BIOMATION Model 2805) manufactured by GOULD, Inc., Santa Clara, California that met these requirements. This recorder included features such as a dual time base for recording at two different sampling rates, the ability to select the number of data points recorded by each time base, pretrigger and delayed mode recording, and the ability to have up to 8 channels internally trigger and record at the same time, outputting digital data through a single interface port. The versatility and flexibility of this recording system proved to be extremely useful during the conduct of these experiments. Figure 3.6 shows the digital waveform recorder. Table 3.2 gives information on the features and characteristics of the waveform recorder.

Figure 3.6 Digital Wave Form Recorder, Desktop Computer and Supporting Peripheral Devices

Table 3.2 Manufacturer's (GOULD/BIOMATION) Specification Data Sheet for the Digital Wave Form Recorder

ANALOG OUTPUTS:	**Display Vertical (Y):**	D/A output reproduces complete signal in memory every 2 ms, 0.8 V fullscale, adjustable from 0.6 to 1.0 V fullscale Vertical position control allows ±1.5 V adjustment of baseline. Vertical X1 Expand allows full scale display and overlap of multichannel traces.
	Display Horizontal (X):	Repetitive 2 ms ramp synchronized with Y output. 1 V p-p amplitude. Horizontal Expand X1, X2, X5, and X10 increases ramp slope accordingly. Maximum amplitude clamped at ±1.5 V. Horizontal position control allows ±1.5 V adjustment of origin.
	Display Blanking (Z, $\bar{Z}$):	Repetitive 4 μs pulses synchronized with X ramp retrace. Z signal is nominally a 0 to +5 V pulse. $\bar{Z}$ is nominally a +5 to 0 V pulse. Also usable as trigger signals to synchronize the internal sweep of an oscilloscope
	Plot Output:	Front panel pushbutton initiated analog output whenever in Display mode. Duration is 200 s for entire memory contents, 0-1 V p-p amplitude, adjustable from 0.8 to 1.2 V p-p. Reverts to Display output after single plot. LED "Ready" indicator lit when unit is in the Plot mode.
DIGITAL INTERFACE:	**Data Output:**	8 bits parallel, TTL levels positive true, word serial asynchronous data transfer under control of Flag and Command signals. 1 μs to 500 μs/address, 2 ms latency for asynchronous rates slower than 500 μs/point
	Flag Output:	Positive TTL transition indicates data word on output lines can be read. Minimum pulse width 0.2 μs.
	Command Input:	Negative TTL transition requests next data word. Minimum pulse width 0.1 μs.
	Output Request:	Input of TTL zero (or ground connection) requests initiation of digital output mode. LED "Ready" indicator lit when unit is in Digital output.
	Output Status:	Output of nominally +3 V level indicates unit is in the digital output mode
	Record:	Output of nominally +3 V level indicates unit is recording.
	Time Base Control:	Ten parallel lines, nine lines normally TTL high when "EXT" selected on front panel Time Base A control. Input of TTL zero (or ground connection) on any one line selects time base in conjunction with high (open) or low (ground) on tenth line to select μs or ms modifier.
SYSTEM CONSIDERATIONS	**Channels:**	Each system consists of a single master control unit and up to three slave units for a total of eight channels. The necessary rear panel cables and connectors will be provided
	Trigger:	A Trigger can be derived from any of the eight signals
	Output Control:	An Output Control switch (for Digital or Plot) is provided concentric with each vertical position control. Pulling the switch out disables the output for display, Digital or Plot. Only one channel at a time can be available for Digital or Plot outputs. All eight channels can be displayed simultaneously for comparison.
MISCELLANEOUS	**Operating Temp. Range:**	0–50°C
	Power:	100, 120, 220, or 240 VAC ±10%, approx. 75 W, 50–400 Hz.
	Size:	Height; 5.25" (13.4 cm). Width; 12.75" (32.4 cm). Depth; 19" (48.3 cm).
	Weight:	Approx. 25 lbs. (11.3 kg)
	Warranty:	All Biomation products are warranted against defects in materials and workmanship for one year from date of delivery
	Accessories:	Each unit is supplied with a line cord and a copy of the Operating and Service Manual

Table 3.2 (cont'd.) Manufacturer's (GOULD/BIOMATION) Specification Data Sheet for the Digital Wave Form Recorder

ANALOG INPUT CHARACTERISTICS EACH CHANNEL:	**Analog Impedance:**	1 MΩ//25 pF.
	Input Voltage Range:	100 mV to 50 V selectabe 9 ranges in 1-2-5 sequence
	Maximum Input Voltage:	100 V peak, 35 V rms
	Input Coupling:	Selectable DC or AC (low frequency cutoff is 2 Hz).
	Input Connection:	Selectable Input, Ground, Record or Hold.
	Input Offset:	Adjustable ±1 x fullscale input sensitivity range
	Offscale Indicators:	Two LEDs indicate when input signal level exceeds + or - the full scale input range.
	Input Bandwidth:	DC to 1.25 MHz on all sample rates.
ANALOG-TO-DIGITAL CONVERTER:	**Resolution:**	8 bits (1 part in 256) at all sample rates.
	Aperture:	The Track-and-Hold Circuit exhibits less than 1 ns aperture uncertainty.
	Maximum Conversion Rate:	5 MHz
TIME BASE MEMORY:	**Sample Interval:**	Internal. Single or dual record rates with independently selectable sample intervals from 0.2 μs to 100 ms in a 1-2-5 sequence.
		External. Selectable for input of sample pulses of nominally +5 V to 0 V with risetime <100 ns. Rate continuously variable from 0.2 μs to 500 μs per address. If delay of more than 500 μs occurs between advance pulses, all further pulses will have 2 ms latency.
	Memory size:	8 bits x 2048 words per channel.
	Total Record Time:	2048 x Sample Interval, varies from 0.4 ms to 200 s when using Internal sample interval selection.
RECORD MODES:	**Normal:**	Recording begins at (delayed) Trigger event. Recording stops after 2048 samples are stored
	Pretrigger:	Recording is continuous after Arm event until Trigger is received, which starts selected delay count. End of delay stops recording process. Delay selection allows a desired portion of the data recorded prior to the Trigger event to be retained in memory.
	Dual Time Base:	Usable in either Normal or Pretrigger operation with Internal Time Base only. Time Base A is used for initial part of recording. Switch to Time Base B after selected Trigger Delay.
	Hold:	Either channel may be held while the other channel is updated.
TRIGGER CHARACTERISTICS:	**Trigger Modes:**	Auto. Recording automatically initiated after each display output sweep (USEFUL PRIMARILY DURING SETUP)
		Normal. Internal or External trigger event accepted during any display or record sweep depending on Record Mode selected
		Single. Trigger event accepted only after Arm function
	Trigger Source:	Internal. Trigger event detected from either signal input
		External. Trigger event detected from front panel EXT input, impedance 1 MΩ//15 pF, minimum pulse width 100 ns, minimum amplitude 400 mV
	Trigger Slope:	Selectable + or -
	Trigger Level:	Adjustable ±1 x fullscale input (±3 V External)
	Trigger Coupling:	Selectable AC or DC
	Trigger Delay:	Proportional to Sample Interval selected or input. Selectable via three front panel decade switches from 0 to 9990 sample intervals in increments of 10 sample intervals.
	Arm Function:	Initiated by front panel momentary pushbutton or via rear panel TTL level pulse input. LED "Ready" indicator lit when unit is Armed and ready to be triggered

3. Computer

A key component of the laboratory instrumentation system is the computer. The computer is essential for controlling the electronic instrumentation and interpreting the recorded data. In view of the importance and central role of the computer in integrating the overall laboratory facility, a number of criteria were established to evaluate commercially available computer systems. These criteria included the following:

- the computer system must be able to interface with the other laboratory equipment, serving as a controller where necessary,
- the computer system must be able to permanently storing the recorded data on mass storage mediums,
- the computer system must be able to analyze and graphically display the stored data,
- the computer system must be able to produce hard copy output of the stored data, and
- the computer system must be expandable for future modifications.

Based on a comparison of the products offered by several companies, HEWLETT-PACKARD was chosen to supply the computer system as it best met the above requirements. The computer system originally obtained at the start of this research effort consisted of a desktop computer, Model HP-9835A with CRT display and an eight pen plotter, Model HP-9872C. The system interface directly with the digital waveform recorder and the university's main computer facility. Since the start of this research effort, a dot-matrix line printer, Model HP-82905B and a

floppy disc mass storage unit, Model HP-9885M have been added. This system has proved to be flexible and capable of handling the needs of the laboratory facility. Figure 3.6 shows the computer and supporting peripherals devices.

4. Triggering Mechanism

An external triggering mechanism was used to initiate the recording of transducer output data by the digital waveform recorder. An HP-5300A/5304A digital timer/counter unit was used to control triggering and determine the projectile impact velocity. Just before the projectile impacted the loading cap, it opened an electrical circuit that started the timer/counter. When the projectile impacted the brass loading cap, the circuit was closed, the timer/counter stopped and a dc triggering voltage was sent to the digital waveform recorder. The triggering system initiated data acquisition immediately upon the application of the compressive loading to the piston.

IV. EXPERIMENTAL INVESTIGATION

A. Description of Monterey No. 0/30 Sand

1. Source of Material

The soil used in this investigation was obtained from Lone Star Industries Inc., Oakland, California in 1982 by the United States Department of the Interior, Bureau of Reclamation in Denver, Colorado and Colorado State University. A quantity of 900 kilograms was acquired with 225 kilograms being stored at Colorado State University for these experiments. The soil is a clean, uniform, subangular fine sand processed from material dredged from the beach north of Monterey, California and is used in sand blasting operations. The company designation for the sand is 'Monterey No. 0/30' which is based on gradation requirements and this term will be used throughout the text in reference to the sand. A detailed description of the sand and its behavior under cyclic loading is given by Muzzy (1983) and Charlie et al. (1984).

2. Preparation of the Bulk Sample

Five 45 kilogram bags were chosen at random from the lot and transported from the Bureau of Reclamation to the Department of Civil Engineering's Geotechnical Engineering Research Laboratory at Colorado State University. The sand was thoroughly mixed to insure a uniform distribution of material so that samples used in the experiments would be representative of the bulk quantity. After mixing, the sand was

divided into 23 kilogram quantities and stored in canvas bags with plastic liners. Random samples were chosen to be used in analyzing the physical properties of the sand.

3. Physical Properties of Monterey No. 0/30 Sand

Several tests were performed to investigate various physical properties of the Monterey No. 0/30 sand. All tests were conducted according to the American Society for Testing and Materials (ASTM) standard laboratory procedures where applicable and include the following:

- grain size analysis (ASTM D422),
- classification (Unified Soil Classification System, ASTM D2487),
- specific gravity (ASTM D854),
- relative density determination (ASTM D2049),
- photomicrograph (Bureau of Reclamation),
- spectrographic analysis (Bureau of Reclamation) and
- skeleton stress-strain curves (Hendron,1963; Whitman et al. 1964).

Selected test results and analysis are given in Chapter V.

B. Variation of Parameters

In considering the number of factors observed to influence liquefaction presented in Chapter II, it was necessary to limit variables to be investigated during this research effort. Three important and significant parameters that could be varied in a controlled manner in the laboratory were selected for study:

- the initial packed relative density of air dry samples,
- the initial effective stress on the samples, and
- the number and intensity of applied compressive shock loads.

The initial relative densities of the samples used in this experimental investigation were approximately 0, 20, 40, 60 and 80 percent. Each of these five relative densities were subjected to four different initial effective stresses, which were 86 KPa, 172 KPa, 345 KPa and 690 KPa. For each sample the back pressure was maintained at 345 KPa with the confining pressure adjusted according to the required effective stress. The first series of samples was loaded by four 'high' stress impacts (between 2.6 MPa and 8.5 MPa per impact) and the second series of samples was loaded by six 'low' stress impacts (between 0.10 MPa and 4.2 MPa per impact).

C. Sample Preparation

The preparation of each sample used in the experiments followed a prescribed method of placement to insure uniformity and consistency throughout the course of the research. Each sample was randomly taken from the 23 kilogram bags in which the bulk of the material was stored. All samples were placed in the sample container at the air dry moisture content of less than 0.10 percent.

1. Placement Methods

In preparing samples, two methods of placing the sand were used to meet the relative density requirements. One method used a funnel while the other involved a combination of funnel placement and

controlled, layered compaction. Before placing sand in the sample container, carbon dioxide gas was flushed through both of the pressure valving systems and the sample container. Then the placement of the sand began with the carbon dioxide gas continually flowing until the sample was completed. The vacuum line was attached to the remaining inlet valve which was kept closed until the sample placement was completed and the membrane was in place.

a. Funnel Placement

To obtain a very low density sample, near zero relative density, the sand was placed using an 18 cm diameter metal funnel with a 1.27 cm diameter by 23 cm long spout. The larger part of the funnel held about one half the amount of sand required to fill the sample container.

The empty funnel was placed in the sample container with the bottom of the spout held against the container bottom. Then about half of the sand was poured in. The funnel was slowly lifted upward and simultaneously rotated inside the sample container while keeping the spout about 1.27 cm or less above the placed material. During this motion additional sand was placed in the funnel for continuous sample placement.

b. Undercompaction

The preparation of samples at relative densities greater than zero percent was accomplished using a method presented by Ladd (1978) called weight. Each layer was placed using the funnel approach described previously. The layers were individually compacted to

successively higher percentages of the final sample density, varying linearly by layer. When the final layer was placed, the entire sample was at the required density. Based on Ladd's (1978) findings it, was decided that ten layers of soil would be used and that the first layer would be five percent undercompacted. The undercompaction method provided a uniform density across the extent of the sample. The tools and equipment used are shown in Figure 4.1.

2. Membrane Placement

When all the sand had been poured, the top of the sample was leveled. Loose sand grains on the flange plate were placed into the sample container and the top releveled. Then a piece of 0.00254 cm thick aluminum foil about 10 cm in diameter was centered over the sample and held in place with a small amount of vacuum grease where it contacted the flange plate. The aluminum foil was used to provide a buffer between the sand and the membrane reducing membrane penetration effects and protecting the membrane from puncture. After the foil was in position, a thin layer of vacuum grease was placed on the flange plate where the rubber membrane would be located. The vacuum grease was evenly distributed and then a 16 cm diameter, 0.033 cm thick circular latex rubber membrane was centered over the sample. The membrane was flattened by carefully working around its circumference until there was about 1.27 cm left to seal. A final check for sand particles on the flange plate was made and the last section of the membrane was pressed down and sealed. The vacuum line was then opened to draw down the membrane into final position while the carbon dioxide gas continued to flow through the sample container. With the sample

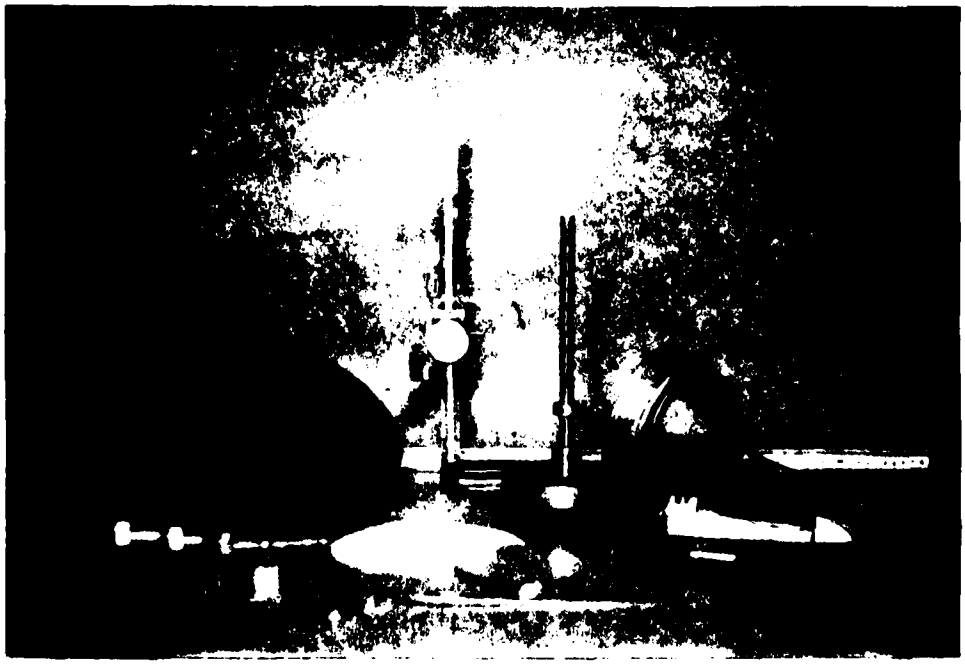

Figure 4.1 Equipment Used in Preparing a Sample by the Undercompaction Method

under vacuum (35 KPa), several measurements across the membrane were made to determine the placed dry density of the sample.

D. System Assembly

Once the sample container was prepared, the next step was to assemble the entire system as a unit. The O-ring seal on the confining tube flange plate was lightly coated with vacuum grease and the tube was filled with distilled, de-aired water. The sample container was then lifted using a chain falls suspended from the overhead roller support system to a point above the confining tube, then aligned and slowly lowered. When the sample container was about 2.54 cm above the flange plate, the space between the flange and membrane was filled with distilled, de-aired water and then the sample container was lowered to its final position. Before bolting and sealing the flange plate connection, an alignment check of flange plate bolt holes was made. The bolts were tightened in a specified pattern until the lock washers were moderately compressed. Then the bolts were tightened to their final position. These steps were taken so that the high pressure O-ring seal would seat evenly about the flange plate.

With the sample container and confining tube bolted together, another chain falls was attached to the opposite end of the confining tube. By alternately raising and lowering the two ends of the unit, the entire system aligned horizontally with the cannon barrel. Two pipe hangers, suspended from the overhead roller support system, were positioned at each end of the assembly. The hangers were attached to the confining tube and both chain falls removed. The confining tube and sample container were then supported by the pipe hangers and free

moving roller support system. The assembled system, ready for loading, is shown in Figures 4.2 and 4.3.

E. Sample Saturation and Effective Stress Application

A pressure line was attached to the confining tube, 35 KPa pressure was introduced into the line, and the plug valve opened. The carbon dioxide pressure line was connected to the bottom of the sample container and a line open to the atmosphere was connected to the top of the sample container. The valves on both sides were closed at this time. The carbon dioxide line was opened under a controlled flow rate at a low pressure for about 15 seconds. Then the line connected to the top of the sample container was opened to the atmosphere and the carbon dioxide gas continued to flow across the sample for 30 minutes.

After 30 minutes, the carbon dioxide pressure line was removed and the plug valve closed. The valving system attached to the interface pressure vessel was then purged of any air bubbles using a distilled, de-aired water supply suspended about 70 cm above the sample container. Then the back pressure line was connected to the bottom of the sample container, the plug valve opened and distilled, de-aired water was flushed through the sample. The line coming out of the top of the sample container was put into a 1000 milliliter graduated cylinder to collect the outflow. After about three pore volumes of distilled, de-aired water had passed through the sample, the top and bottom plug valves were closed and the top line removed. The confining pressure and the back pressure were incrementally increased to obtain the required effective stress. The sample was allowed to saturate and consolidate for a minimum of 6 hours.

AD-A173 137 BLAST INDUCED LIQUEFACTION POTENTIAL AND TRANSIENT POREWATER PRESSURE RES (U) COLORADO STATE UNIV FORT COLLINS DEPT OF CIVIL ENGINEERING W A CHARLIE ET AL 2/3

UNCLASSIFIED 15 OCT 85 AFOSR-TR-86-0946 AFOSR-80-0260 F/G 8/13 NL

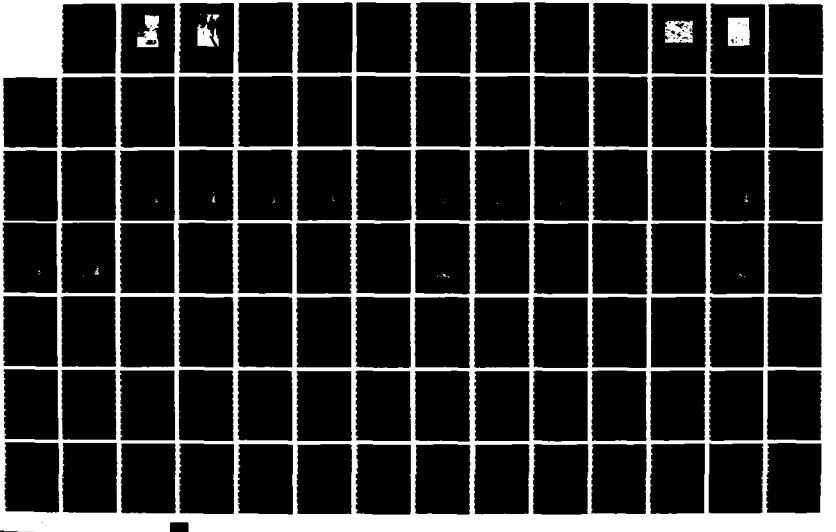

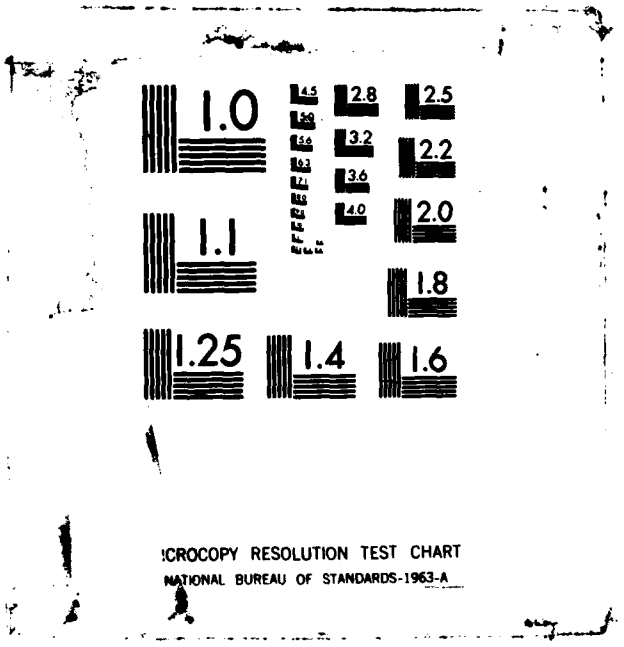
1.0
1.1
1.25
1.4
1.6
1.8
2.0
2.2
2.5
2.8
3.2
3.6
4.0
4.5
5.0
5.6
6.3
7.1
8.0
MICROCOPY RESOLUTION TEST CHART
NATIONAL BUREAU OF STANDARDS-1963-A

Figure 4.2 Experimental Shock Facility Prepared for Loading (View from Cannon)

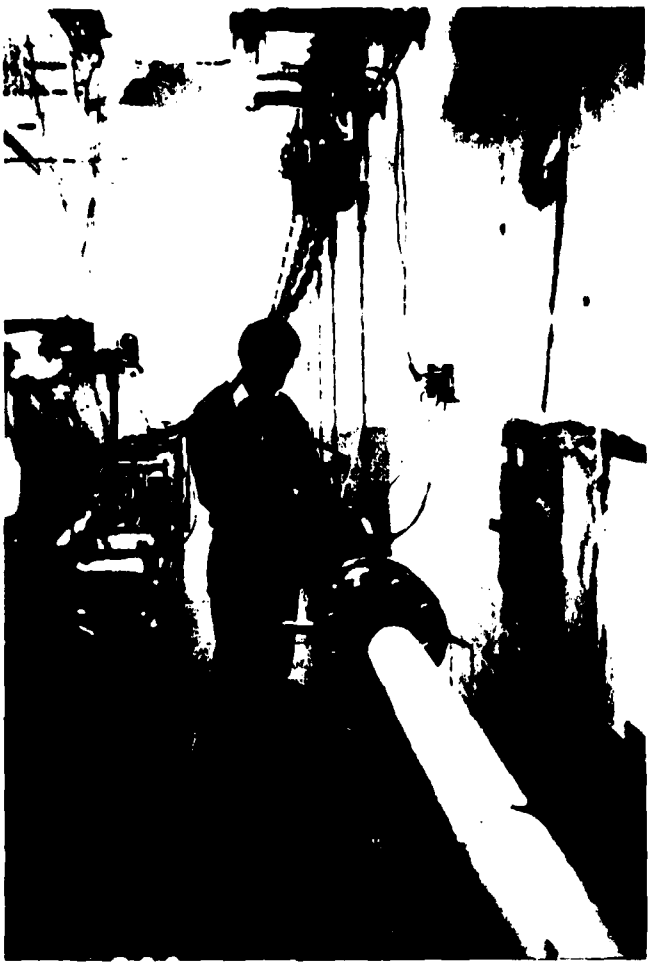

Figure 4.3 Experimental Shock Facility Prepared for Loading (View from Momentum Trap)

Once the saturation period was completed, it was then necessary to check the sample's porewater pressure response and determine the degree of saturation. The porewater pressure transducers were connected to the signal conditioner panel and the excitation voltage, amplifier zero and bridge balance were checked and adjusted. The back pressure was increased about 35 KPa and the inlet valve closed. An output voltage was recorded for each transducer.

The confining pressure was incrementally increased to the required effective stress, and the output voltage of each transducer was noted. The degree of saturation was determined by comparing the sample's porewater pressure response to the increase in confining pressure. If the ratio of these two values was unity, corresponding to a 100 percent porewater pressure response, then the sample was considered saturated. In this investigation it was not always possible to obtain a porewater pressure ratio equal to one even though the same saturation procedure was consistently used for each sample. However, measured compressive stress wave propagation velocities through the samples showed they were saturated. It was observed that the porewater pressure response varied in a predictable manner with increasing sample density and effective stress. A presentation and discussion of this observation is given in Chapter V.

F. Final Preparations and Experimental Procedure

When the confining pressure and the back pressure were restored to their desired values, the two plug valves (one on the confining tube and one on the sample container) were closed to prevent drainage through the pressure lines. The valves were left closed throughout the

loading sequence for each experimental run, to maintain undrained loading conditions.

The confining tube and sample container assembly were aligned with the cannon barrel and leveled. The brass loading cap was placed on the impact piston. The triggering mechanism was set, its operation checked and the timer/counter was reset. The PVC rods in the momentum trap assembly were aligned with and centered on the steel end plate on the sample container and the tripods leveled. A final check of the entire system alignment was made.

The output of the two transducers was adjusted to a value of zero volts to gain maximum benefit of the digital waveform recorder's range. The controls on the waveform recorder were set and adjusted and then verified by the computer. The computer then initiated a program sequence to handle the data transfer from the digital waveform recorder for each impact and store the output on a mass storage medium. A final check of all system components was made before the loading phase.

The next step was to load the sample. With the projectile inserted in the cannon barrel, the cannon was pressurized and the reservoir pressure was verified with a gage separate from the nitrogen supply bottle. Then the pressure behind the poppet valve was reduced to the atmospheric, which opened the poppet valve, releasing the high pressure into the cannon barrel to propel the projectile. The value on the timer/counter was recorded and the computer initiated the data transfer and storage. The time recorded from the timer/counter was used to determine the impact velocity of the projectile. This sequence was repeated for each impact loading.

When an experimental run was completed, the entire system was disassembled in reverse order. A vacuum was applied to the sample container to drain the pore fluid. With the sample container suspended from the chain falls, the membrane and foil paper were removed, the soil sample removed, and the sample container thoroughly cleaned and dried. Each of the porous stones were subjected to a vacuum to remove water. The next sample was prepared and loaded according to the procedure previously described.

V. EXPERIMENTAL RESULTS

A. Physical Properties of Monterey No. 0/30 Sand

Basic physical and index properties for Monterey No. 0/30 sand were evaluated according to accepted standard laboratory testing procedures set forth by the American Society for Testing and Materials (ASTM). A summary of the tests performed is presented given in Table 5.1. Details of the grain size analysis, classification and relative density tests are given by Muzzy (1983) and Charlie et al. (1984).

1. Grain Size Analysis

A grain size distribution analysis (ASTM D422) was performed. The results obtained indicate a fine, uniform, poorly graded sand with less than one percent of the material being finer than 0.150 mm in size. The D_{50} particle size for this material is 0.45 mm. A grain size curve showing the distribution of the particle sizes is shown in Figure 5.1.

2. Classification

From the results of the grain size analysis the uniformity coefficient, C_u , was determined to be 1.65 and the coefficient of curvature, C_c , was determined to be 1.00. Based on these results and the grain size curve, the soil was classified as an SP material (sand, poorly graded with little or no fines) according to the Unified Soil

Table 5.1 Physical Properties of Monterey No. 0/30 Sand (Muzzy,1983; Charlie et al.,1984)

USCS Classification		SP
Specific Gravity		2.65
Particle Size Data:		
	D_{10}	0.29 mm
	D_{30}	0.38 mm
	D_{50}	0.45 mm
	C_u (1)	1.65
	C_c (2)	1.00
% Passing #100 Sieve (3)		0.05 %
Relative Density Test Data:		
Dry Unit Weight:		
	Maximum	1700 Kg/M^3
	Minimum	1470 Kg/M^3
Void Ratio:		
	Maximum	0.803
	Minimum	0.563

Note: (1) C_u = coefficient of uniformity

(2) C_c = coefficient of curvature

(3) U.S. Standard Sieve Size

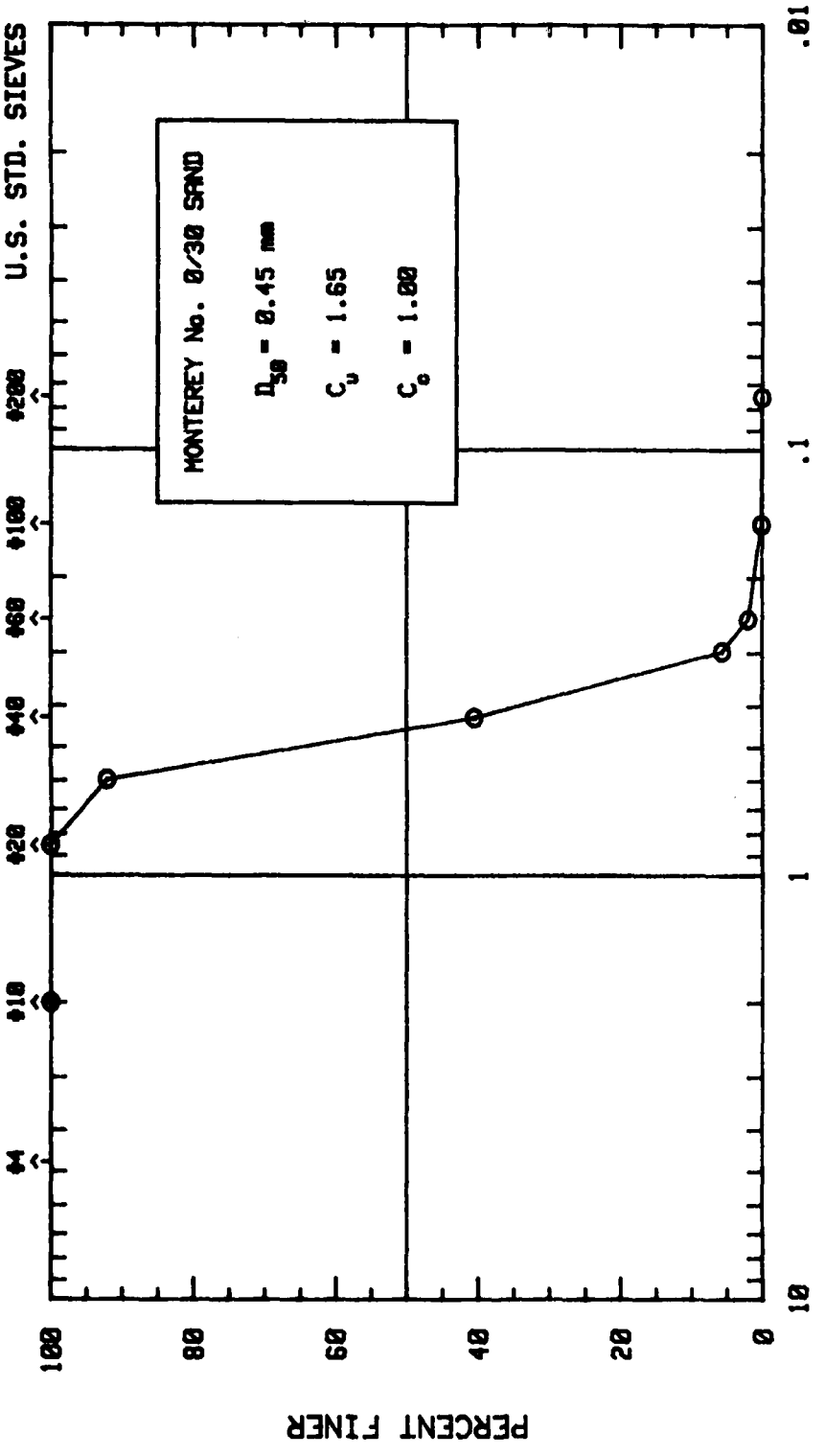

Figure 5.1 Grain Size Distribution for Monterey No. 0/30 Sand (Muzzy,1983; Charlie et al.,1984)

Classification System (ASTM 2487). From the results of a specific gravity test (ASTM D854), a value of 2.65 was determined for the sand.

3. Relative Density

A relative density test (ASTM D2049) was performed to determine the minimum and maximum dry density limits for the sand. This test was performed at the Bureau of Reclamation Soil Mechanics Laboratory in Denver, Colorado, using a calibrated shaker table. As is shown in Table 5.1, the range of dry densities varied by 230 Kg/M^3.

4. Photomicrograph and Spectrographic Analysis

Figure 5.2 shows a photomicrograph of the sand made with a scanning electron microscope at the Bureau of Reclamation Soil Mechanics Laboratory in Denver, Colorado. The soil grains are uniform in size and are subangular to subrounded in shape. Figure 5.3 shows a spectrographic analysis performed at the same laboratory facility to investigate the mineralogic content of the sand. The predominant mineral constituent present is silicon with several others existing in substantially smaller amounts.

5. Skeleton Stress-Strain Curves

Static one-dimensional, confined, compression tests (Hendron,1963; Whitman et al.,1964) were performed on air dry samples of Monterey No. 0/30 sand. The results of tests were used to obtain stress-strain information for the soil skeleton and to determine the constrained modulus of the skeleton to be used in the finite difference approximation presented in Chapter VI. To simulate the initial stress

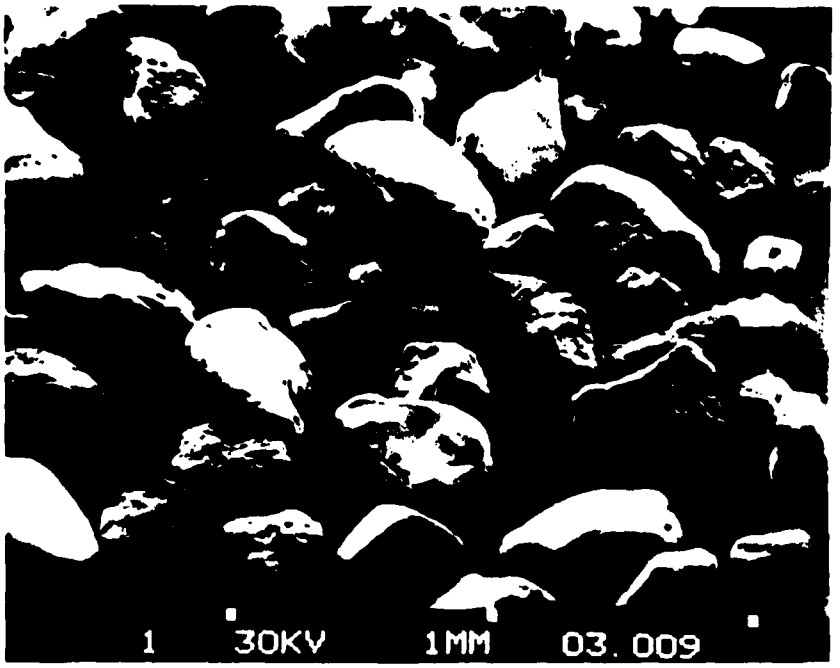

Figure 5.2 Photomicrograph of Monterey No. 0/30 Sand (Muzzy,1983; Charlie et al.,1984)

Figure 5.3 Spectrographic Analysis Results for Monterey No. 0/30 Sand (Muzzy, 1983; Charlie et al.,1984)

conditions in the experimental investigation, a corresponding initial effective stress was applied to each sample. The compressive strain values were referenced to the initial applied stress. Each sample was loaded and unloaded in increments two times to develop the stress-strain relationship for the soil skeleton. From these results, a constrained modulus for loading and unloading was determined.

Two sets of tests were run for comparative purposes. Samples tested had relative densities of 40 and 80 percent. Each sample was tested at initial effective stresses of 86 KPa and 690 KPa. The data obtained for the relative densities and effective stresses examined provides practical limits for analysis. The skeleton stress-strain curves for Monterey No. 0/30 sand are shown in Figures 5.4, 5.5, 5.6 and 5.7 and a summary of the numerical results is given in Table 5.2. The results show that the soil skeleton stiffness increases with increasing initial effective stress and density. Hysteresis between the loading and unloading curves decreases with increasing initial effective stress and density.

B. Static C-Parameter Response

Before loading of each sample the porewater pressure response was checked to determine the degree of saturation. This was done by increasing the confining pressure on the sample and monitoring the sample's porewater pressure response without drainage. The ratio of the sample porewater pressure response to the increase in confining pressure is termed the 'C-parameter' (Lambe and Whitman, 1969) for a one-dimensional confined, compressive loading of a saturated soil with undrained conditions. A ratio of one indicates a saturated sample and

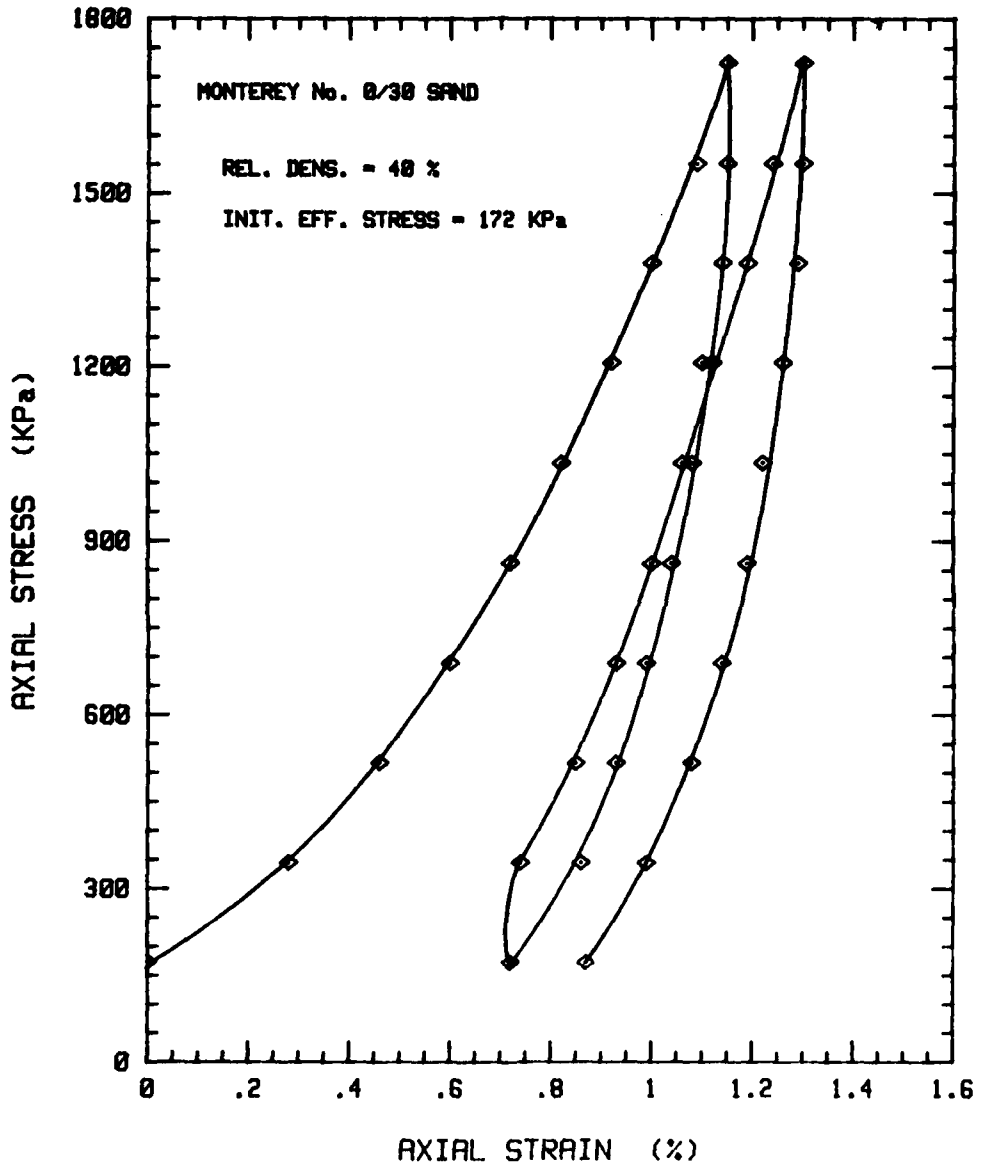

Figure 5.4 Skeleton Stress-Strain Curve for Monterey No. 0/30 Sand at D_r = 40% and σ_o' = 172 KPa

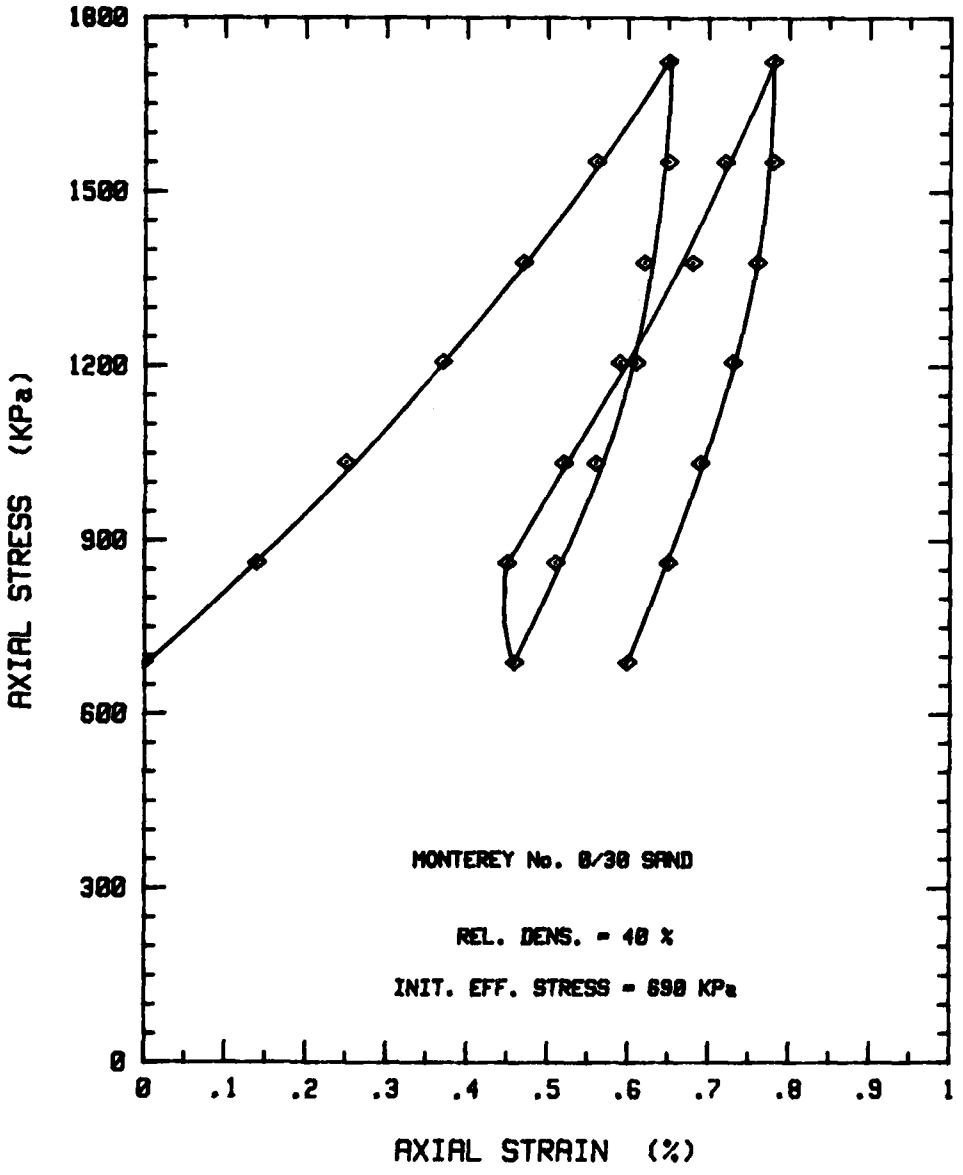

Figure 5.5 Skeleton Stress-Strain Curve for Monterey No. 0/30 Sand at D_r = 40% and σ'_o = 690 KPa

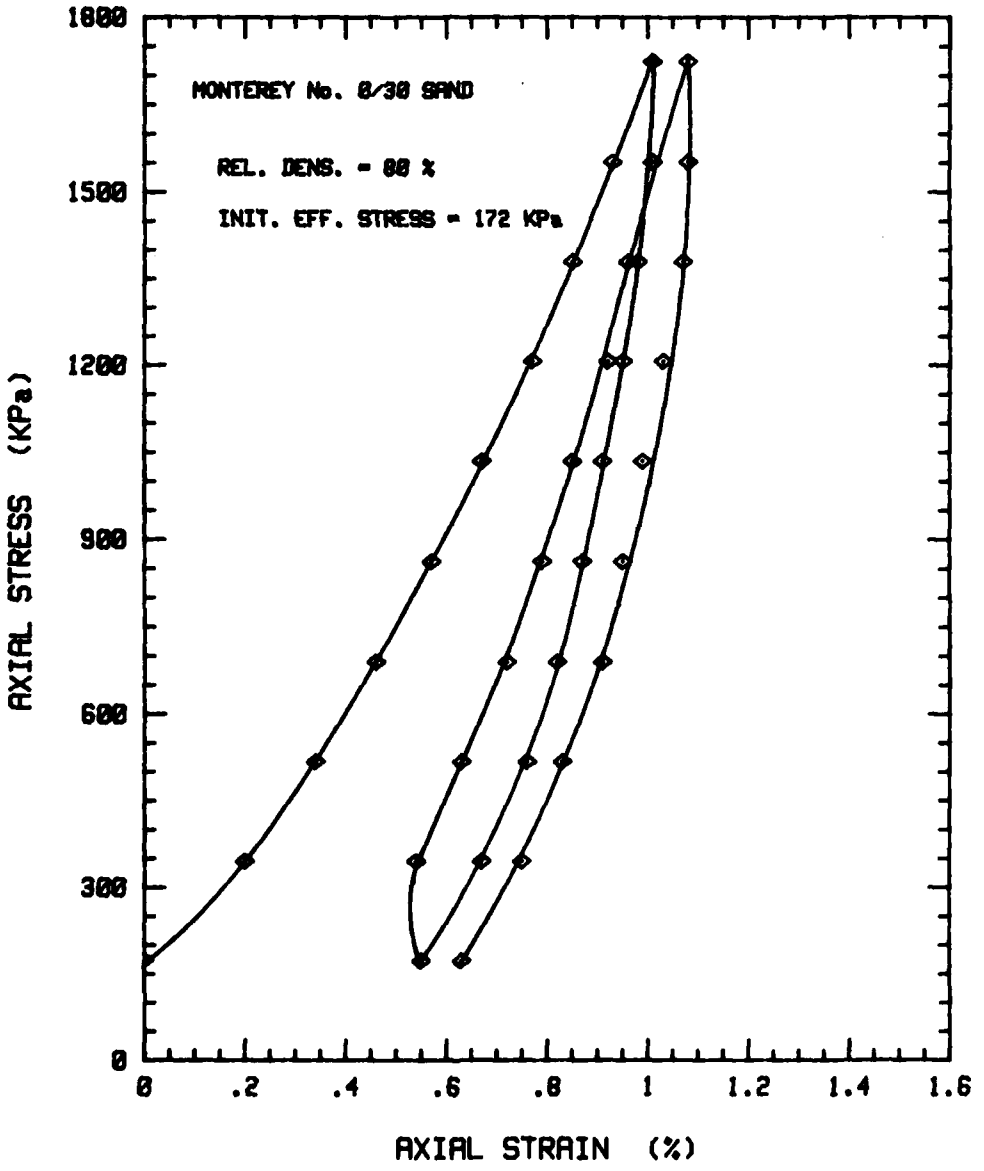

Figure 5.6 Skeleton Stress-Strain Curve for Monterey No. 0/30 Sand at D_r = 80% and σ_o' = 172 KPa

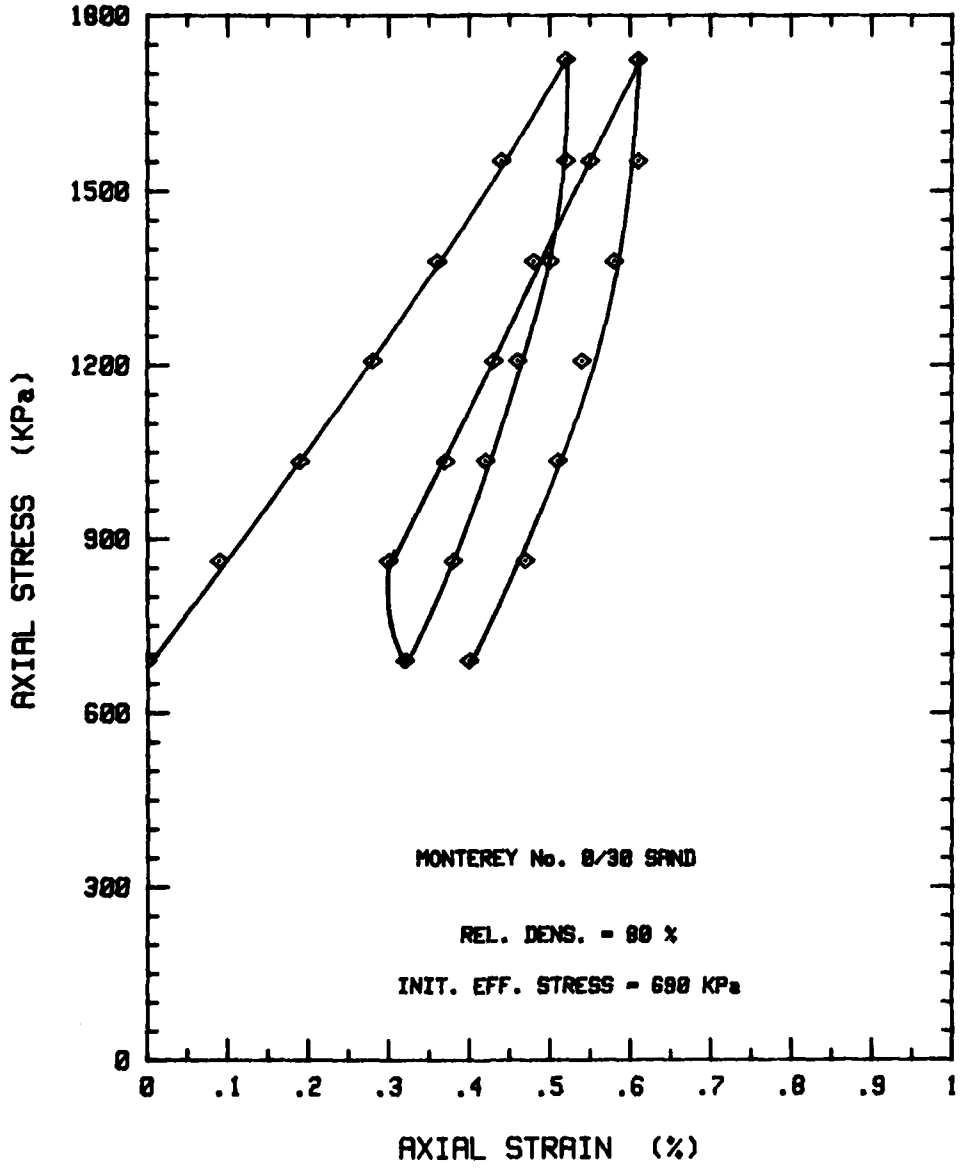

Figure 5.7 Skeleton Stress-Strain Curve for Monterey No. 0/30 Sand at D_r = 80% and σ_o' = 690 KPa

Table 5.2 Constrained Loading and Unloading Modulus for Static, One-Dimensional, Confined Compression Tests on Dry Monterey No. 0/30 Sand

D_r (%)	σ_o (KPa)	D_l (1) (KPa)	D_u (2) (KPa)
40	172	61500	307500
40	690	156700	617000
80	172	86190	431000
80	690	191700	958500

Note: (1) Constrained modulus for loading
(2) Constrained modulus for unloading taken as 5 times constrained modulus for loading in finite difference analysis

values less than one indicates that the sample is not saturated or has a very stiff soil skeleton. For an initial effective stress of 86 KPa, a ratio of one was consistently obtained. However, a C-parameter of one was not obtained for higher initial effective stresses. Since the preparation and saturation process was identical for each sample, it was assumed that the porewater pressure ratios obtained indicated of a saturated condition. An examination of the compressive stress wave propagation velocity through samples verified this assumption. The calculated compressive stress wave velocities were close to 1500 meters per second in all samples investigated. This is the value that would be expected for saturated conditions.

Throughout the experimental investigation it was noted that the porewater pressure ratio varied in a predictable manner with variations in effective stress and relative density (Figure 5.8). In considering this observation and those previously discussed, it is believed that the porewater pressure ratio response noted can be attributed to changes in the soil skeleton stiffness which increases with increasing initial relative density and effective stress. Accordingly, all samples were considered to be saturated.

C. Pressure-Time Histories

The pressure-time histories represent the porewater pressure transducer responses to applied shock loadings as function of time. They include both the peak and long-term response for the confining pressure and the sample porewater pressure. Selected pressure-time histories, representative of the behavior observed in this experimental investigation, are shown in Figures 5.9 through 5.28. A summary of

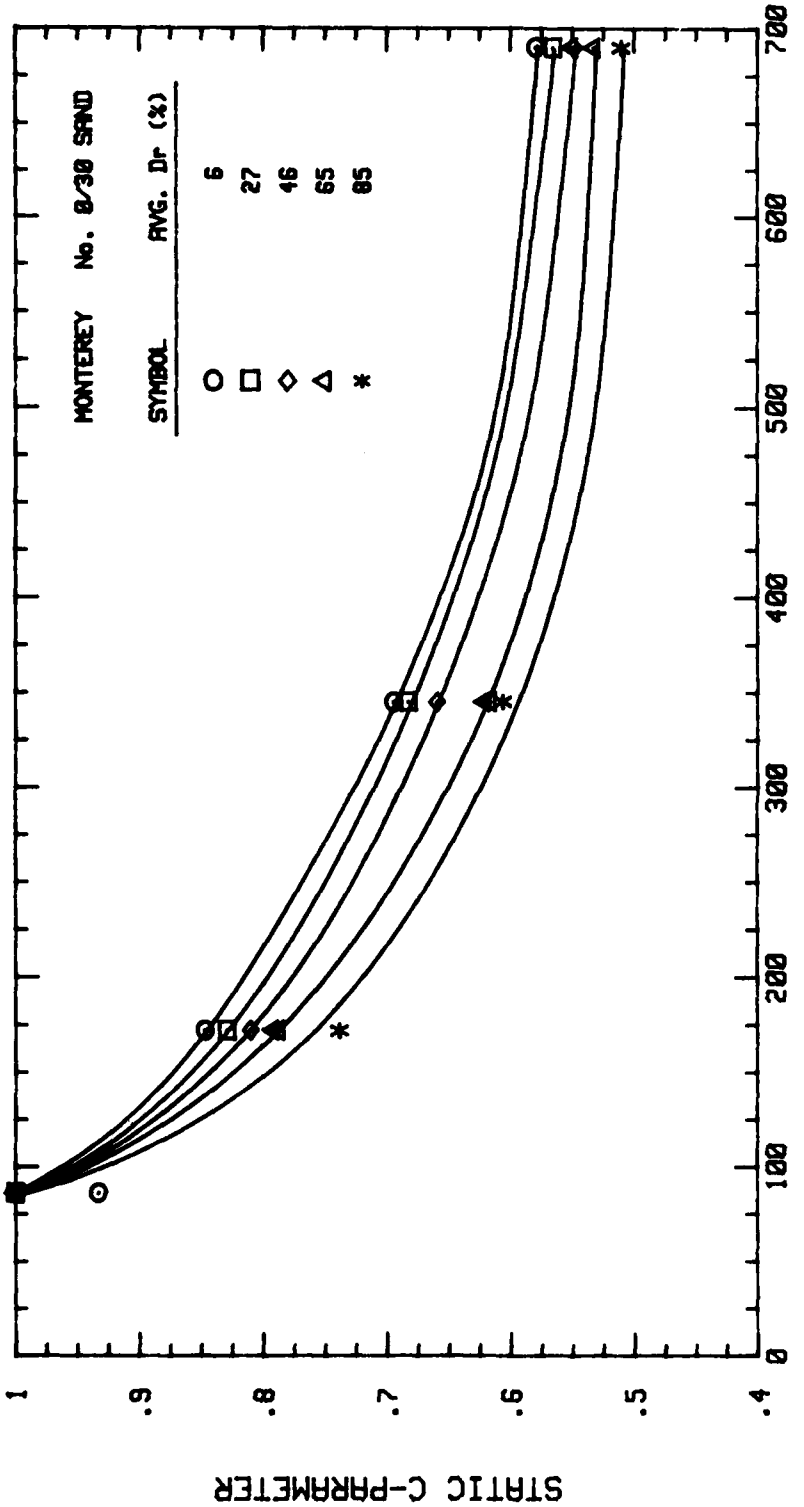

Figure 5.8 Static C-Parameter Response as a Function of Effective Stress for Monterey No. 0/30 Sand

numerical results from the pressure-time histories of all samples investigated is given in Chapter VI, Tables 6.2 through 6.12.

Figures 5.9 through 5.18 show the experimental results for the '40%' relative density series at an effective stress of 172 KPa. Figures 5.19 through 5.28 show the experimental results for the '80%' relative density series at an effective stress of 172 KPa. The confining pressure and sample porewater pressure responses have been plotted together on each figure. The 'series' designation for relative density has been used to group together data having approximately the same relative density. The designations include data that is within 10 percent greater than the series number (including the series number). For example, a '40%' series designation would include all data for a relative density from 40 percent to 49 percent.

The pressure-time histories are indicative of the system response during and after loading. On each figure, the traces of the confining pressure and sample porewater pressure follow each other closely in their response trends. The two curves are slightly offset from one another in the time domain due to the relative locations of each transducer. The sample peak porewater pressure is greater than the applied stress peak values for each impact.

In all cases the confining pressure transducer response returned to its original baseline value once the compressive stress wave energy had dissipated. The response of the confining pressure transducer was as expected since the static confining pressure should be constant if the system is not allowed to drain. The residual excess porewater pressure indicated by the sample transducer, was above its original baseline value after each loading and continued to increase with each successive

impact. The response of the sample porewater transducer was as expected since an increase in the residual excess porewater pressure should be maintained for undrained conditions. Liquefaction occurs when the residual excess porewater equals the effective stress which is also when the back pressure plus the residual excess porewater pressure equals the confining pressure.

The information from the pressure-time history records was used in performing the data analysis presented in Chapter VI. The porewater pressure response was evaluated as a function of initial effective stress, initial sample density, peak compressive strain.

D. Composite Data Curves

Figures 5.29 through 5.33 show the porewater pressure ratio as a function of the sum of the sample peak porewater pressures grouped by initial relative density. Figure 5.34 shows the results combined on a single plot. The general trend is for the porewater pressure ratio to decrease with increasing initial relative density at a given sample peak porewater pressure.

Similarly, Figures 5.35 through 5.38 show the porewater pressure ratio as a function of the sum of the peak sample porewater pressures grouped by initial effective stress. Figure 5.39 shows the results combined together on a single plot. Here, the general trend is for the porewater pressure ratio to decrease with increasing initial effective stress at a given sample peak porewater pressure.

It is evident from Figures 5.29 through 5.39 that both the initial relative density and initial effective stress are important factors that influence porewater pressure increases in a saturated,

cohesionless soil. The analysis presented in Chapter VI develops empirical relationships that relate the porewater pressure ratio to these two parameters and the peak compressive strain.

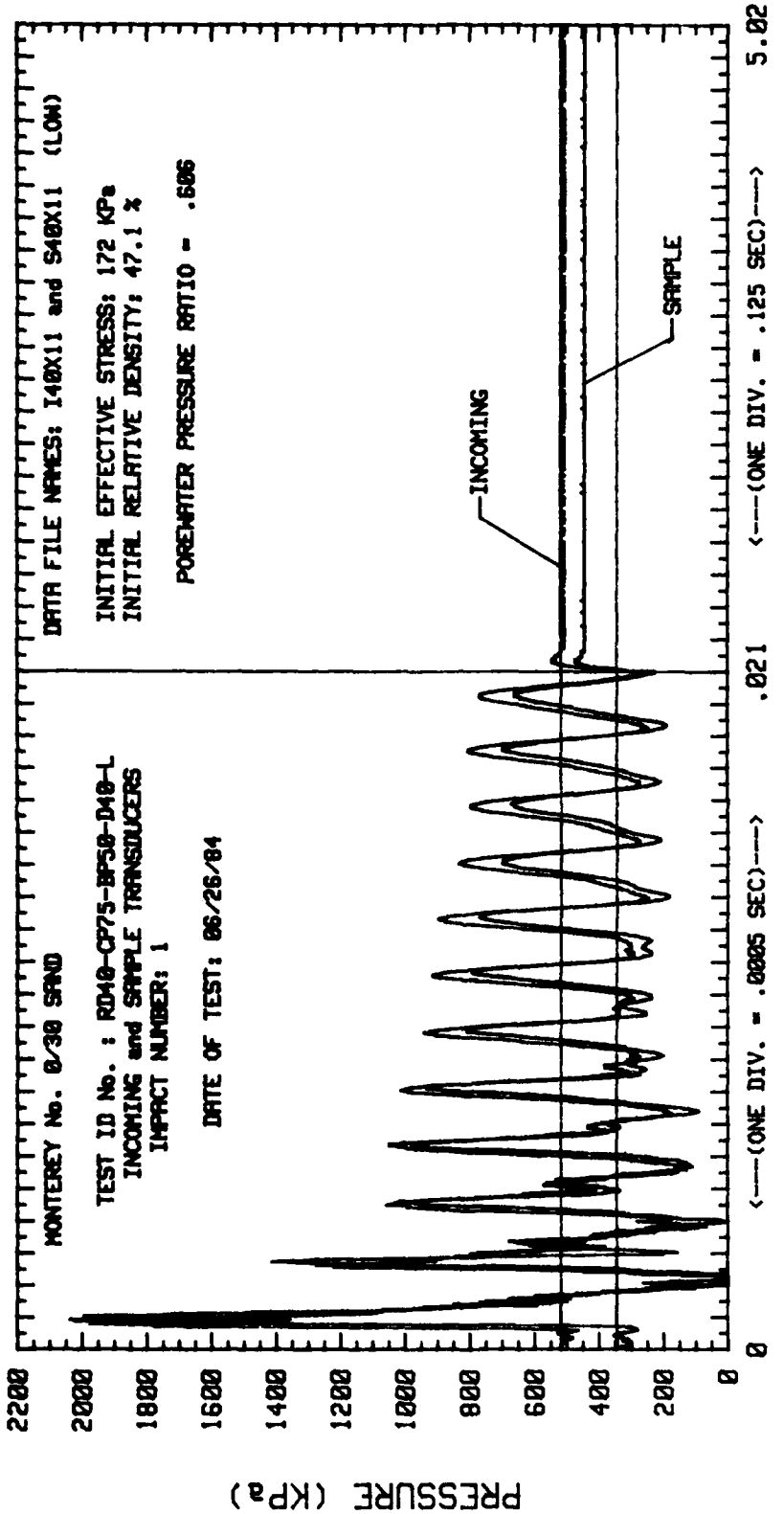

Figure 5.9 Pressure-Time Histories for D_r = '40%' Series and σ_o' = 172 KPa (Low Impact Stress-First Impact)

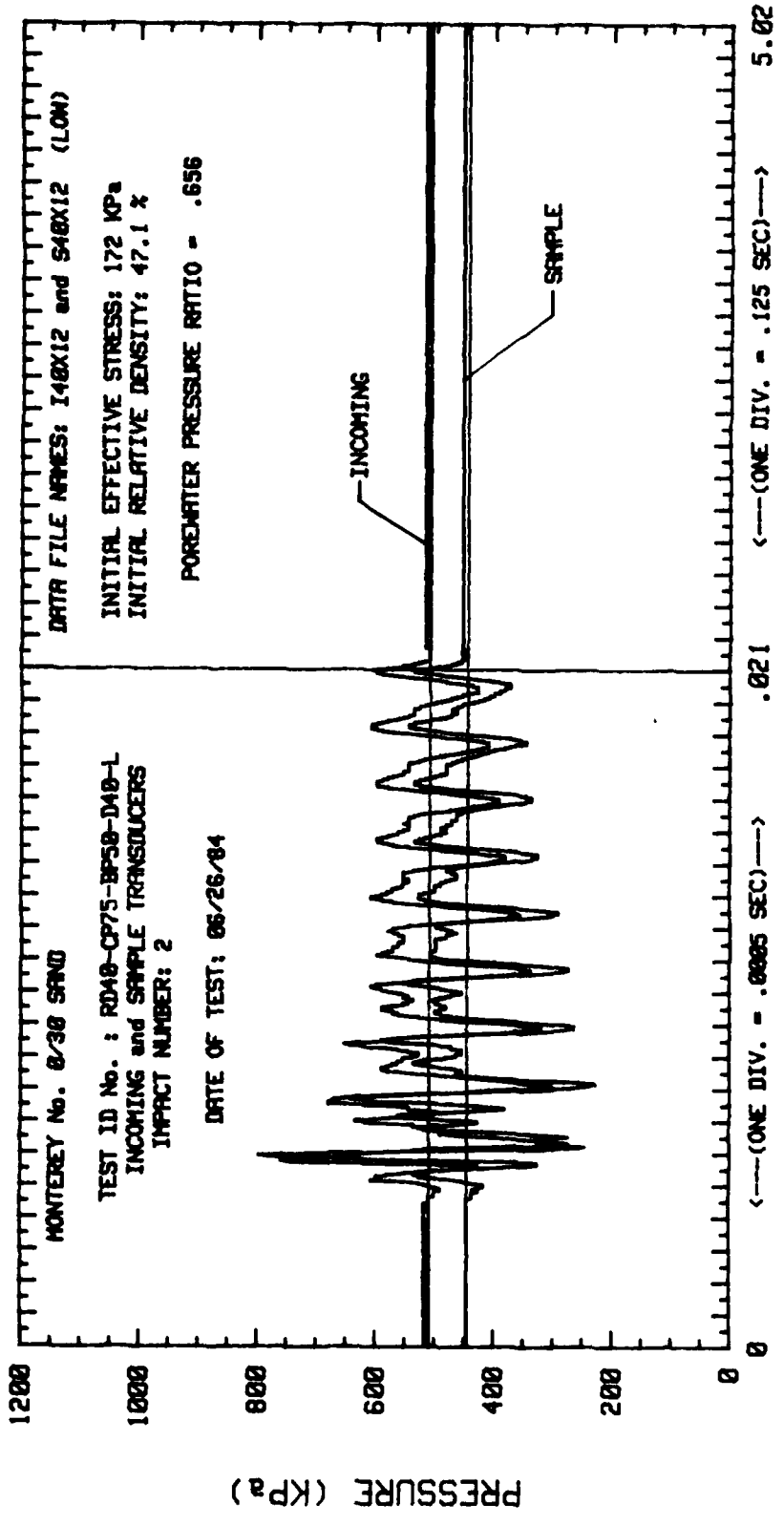

Figure 5.10 Pressure-Time Histories for D_r = '40%' Series and σ_o' = 172 KPa (Low Impact Stress-Second Impact)

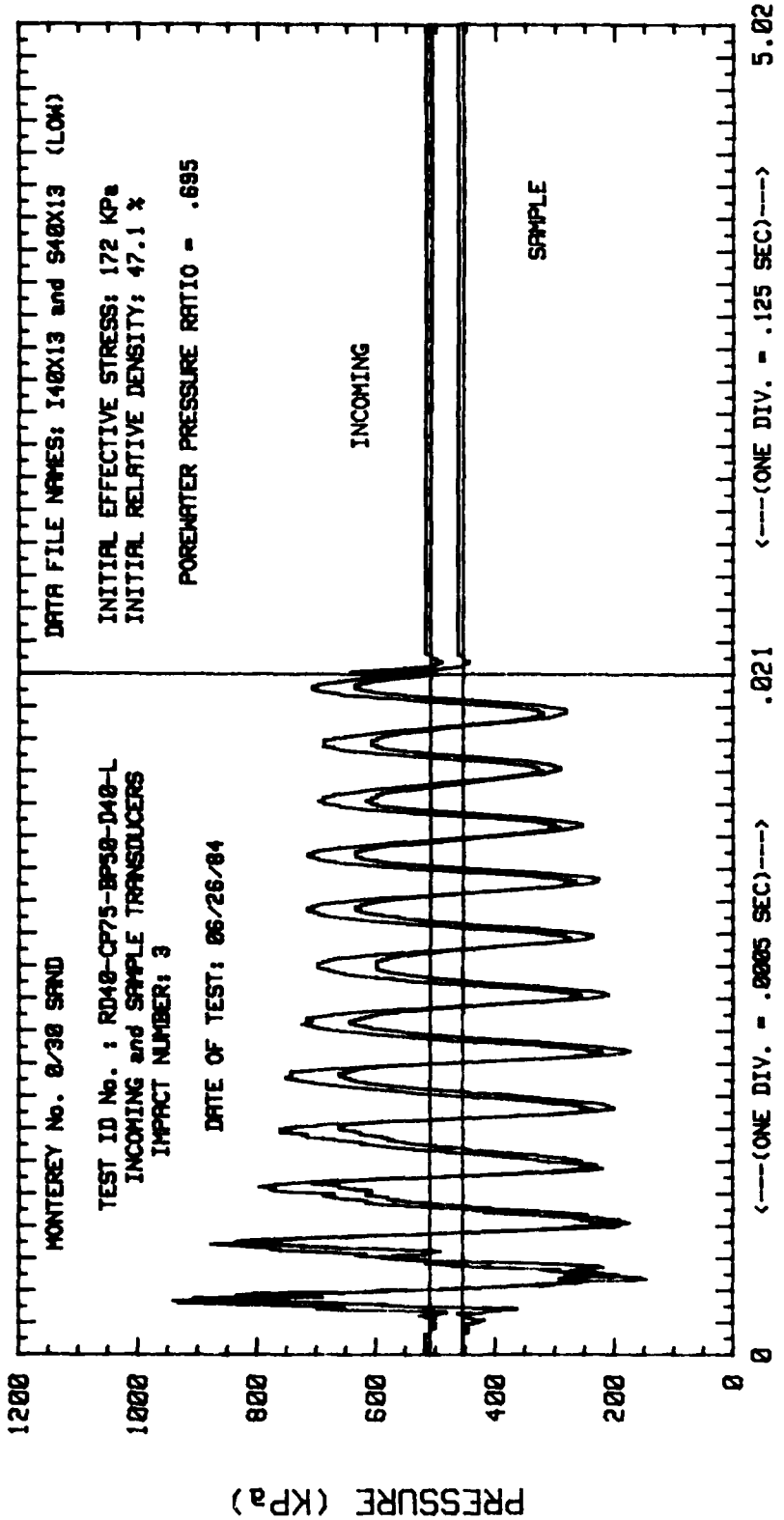

Figure 5.11 Pressure-Time Histories for D_r = '40%' Series and σ_o' = 172 KPa (Low Impact Stress-Third Impact)

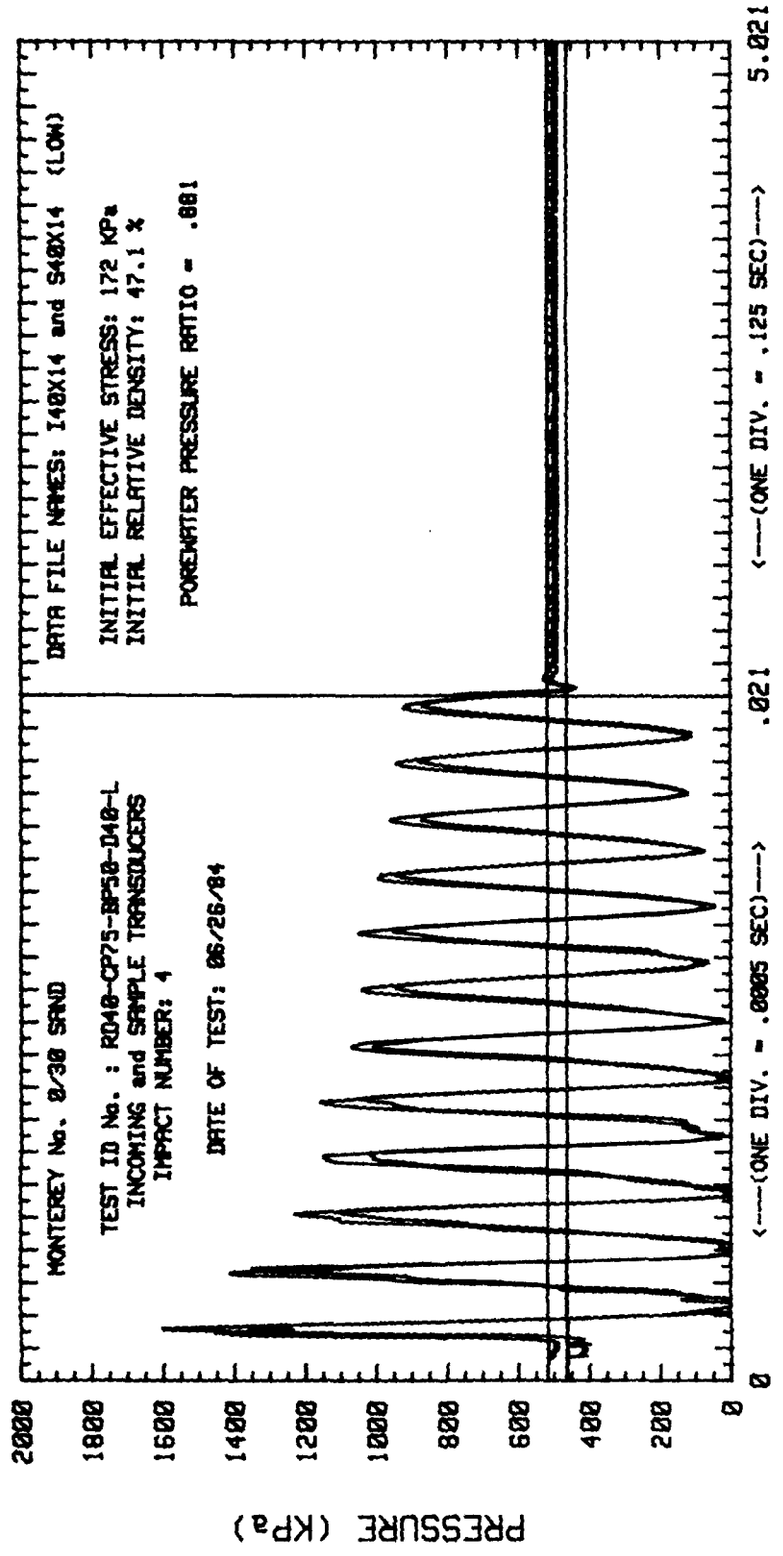

Figure 5.12 Pressure-Time Histories for D_r = '40%' Series and σ_o' = 172 KPa (Low Impact Stress-Fourth Impact)

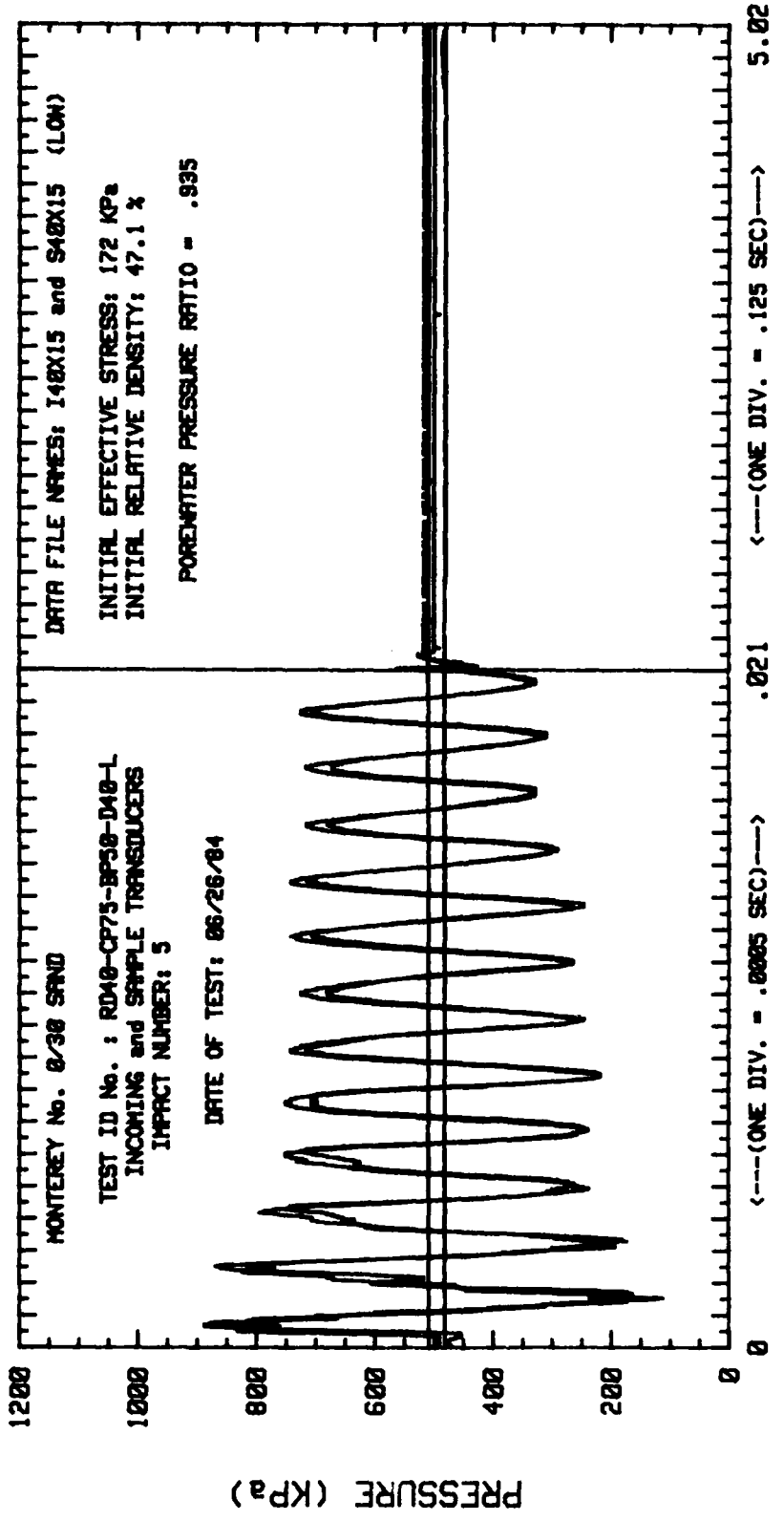

Figure 5.13 Pressure-Time Histories for D_r = '40%' Series and σ_o' = 172 KPa (Low Impact Stress-Fifth Impact)

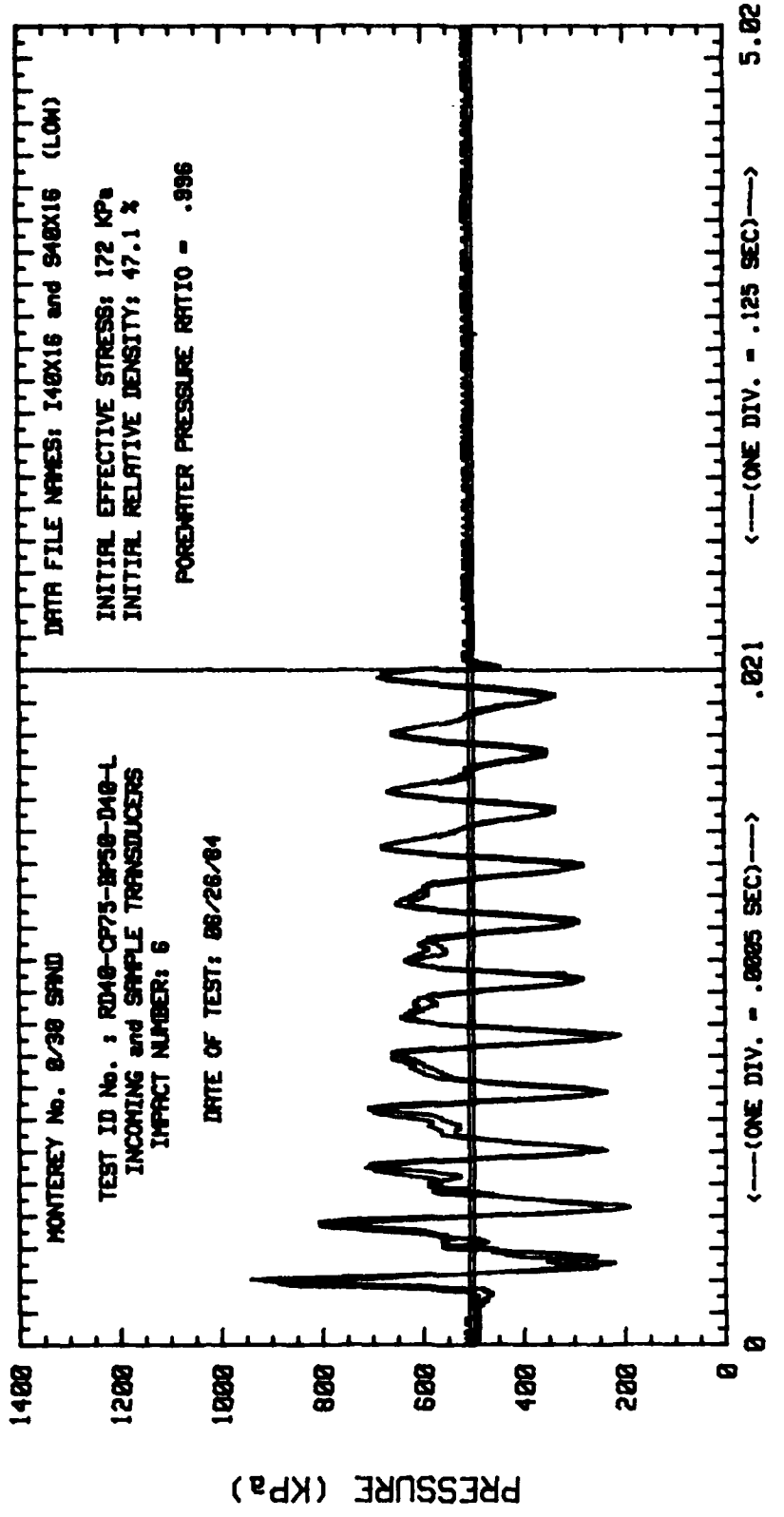

Figure 5.14 Pressure-Time Histories for D_r = '40%' Series and σ_o' = 172 KPa (Low Impact Stress-Sixth Impact)

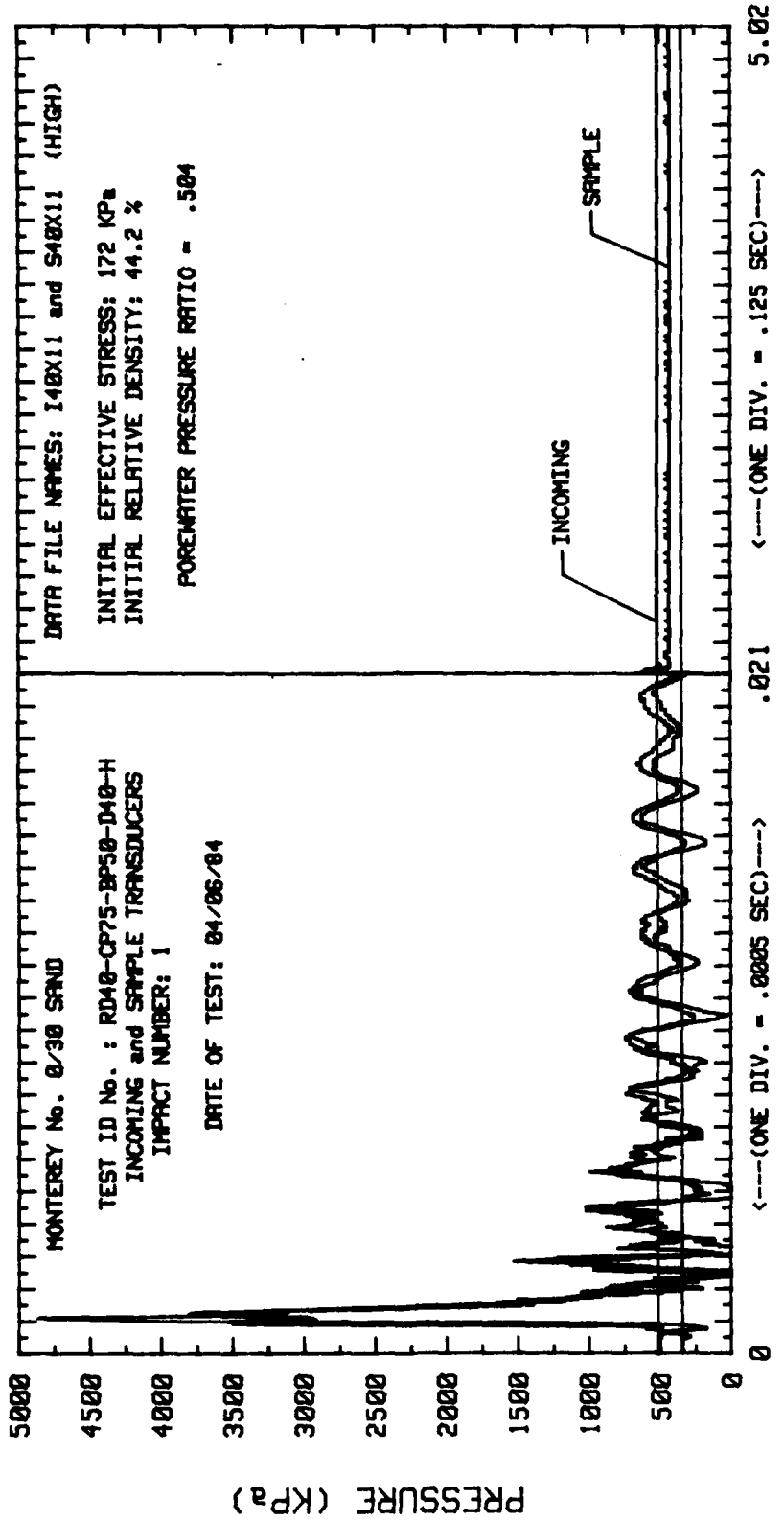

Figure 5.15 Pressure-Time Histories for D_r = '40%' Series and σ'_o = 172 KPa (High Impact Stress-First Impact)

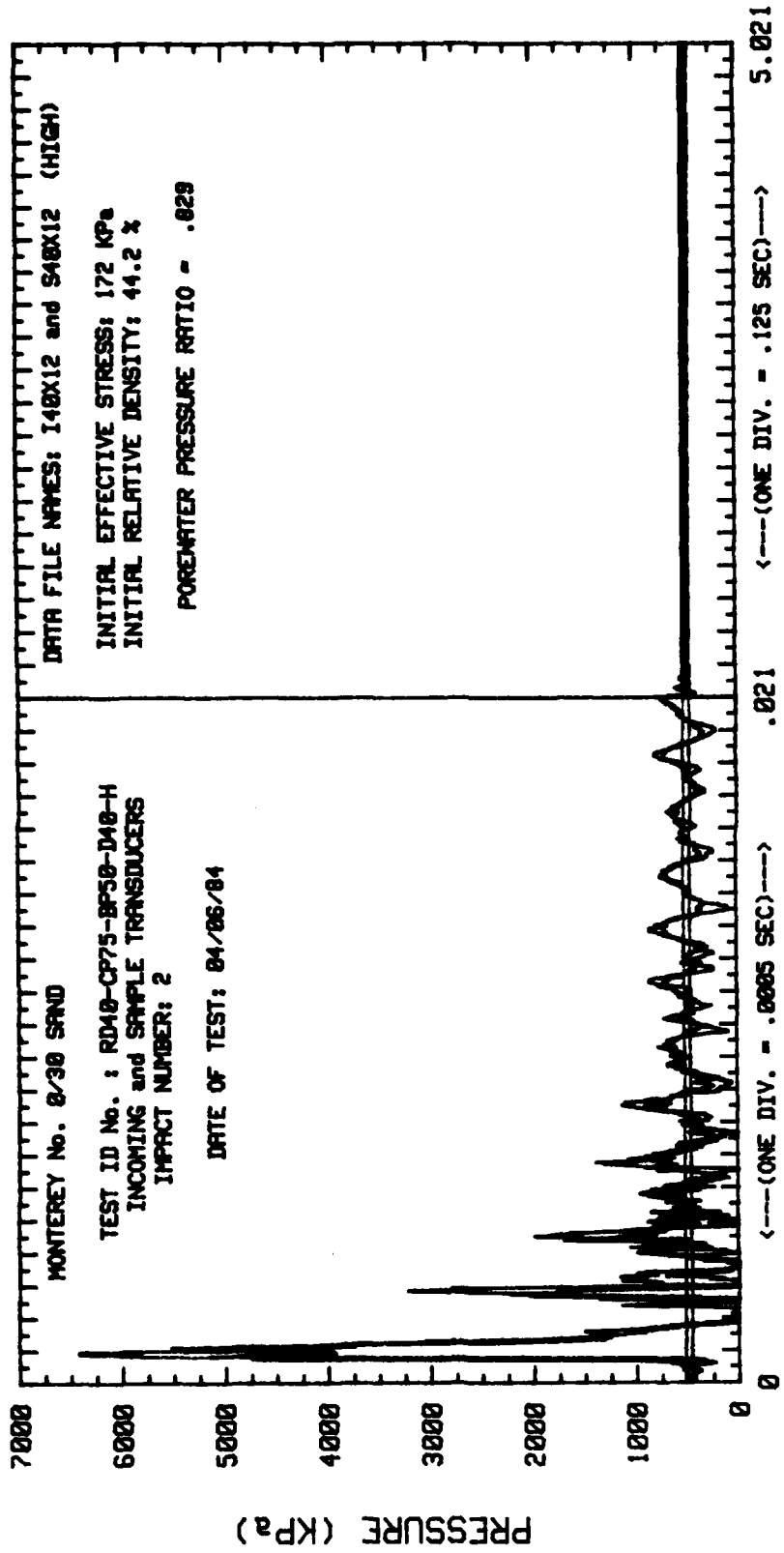

Figure 5.16 Pressure-Time Histories for D_r = '40%' Series and σ_o' = 172 KPa (High Impact Stress-Second Impact)

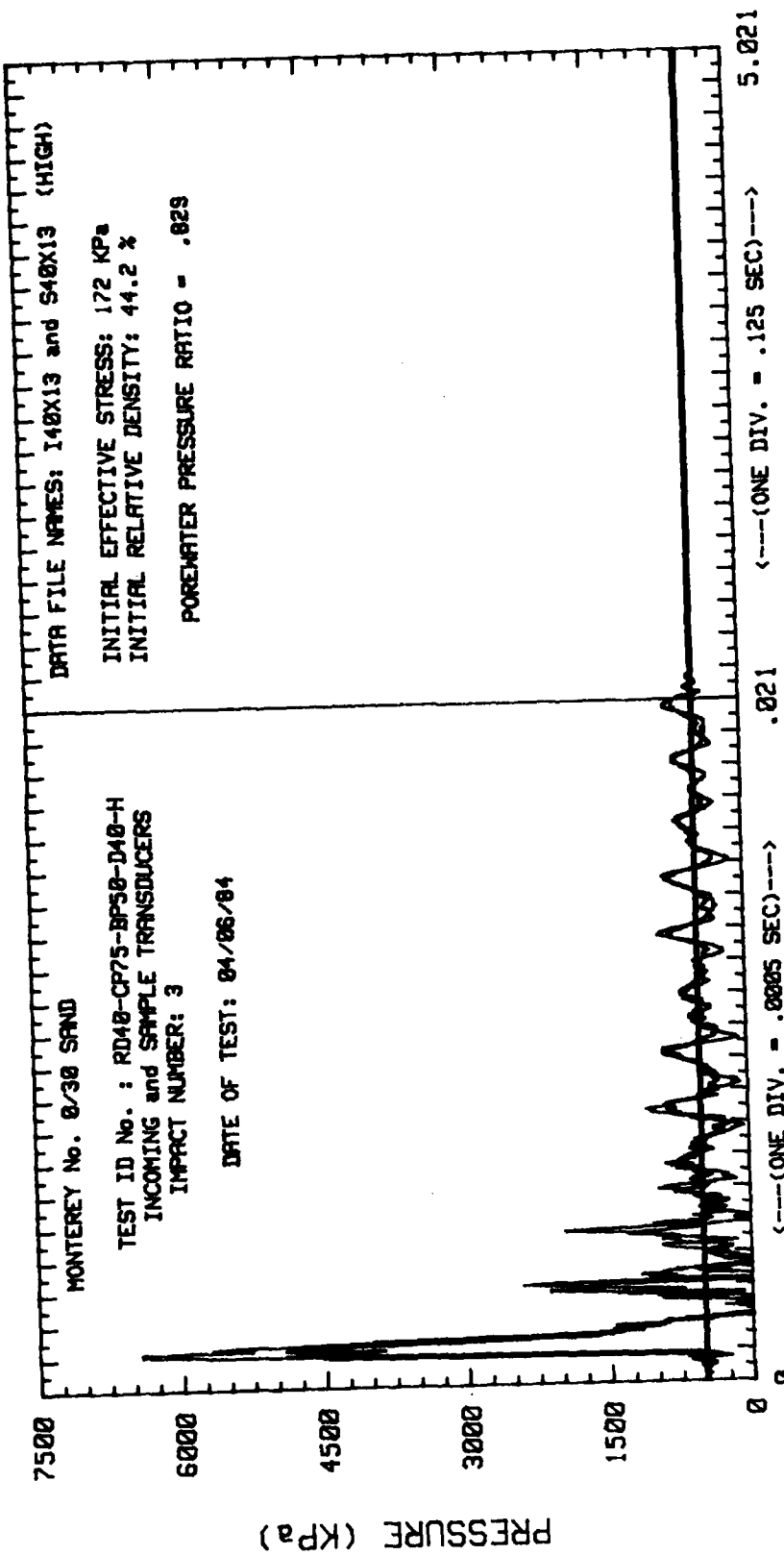

Figure 5.17 Pressure-Time Histories for D_r = '40%' Series and σ_o' = 172 KPa (High Impact Stress-Third Impact)

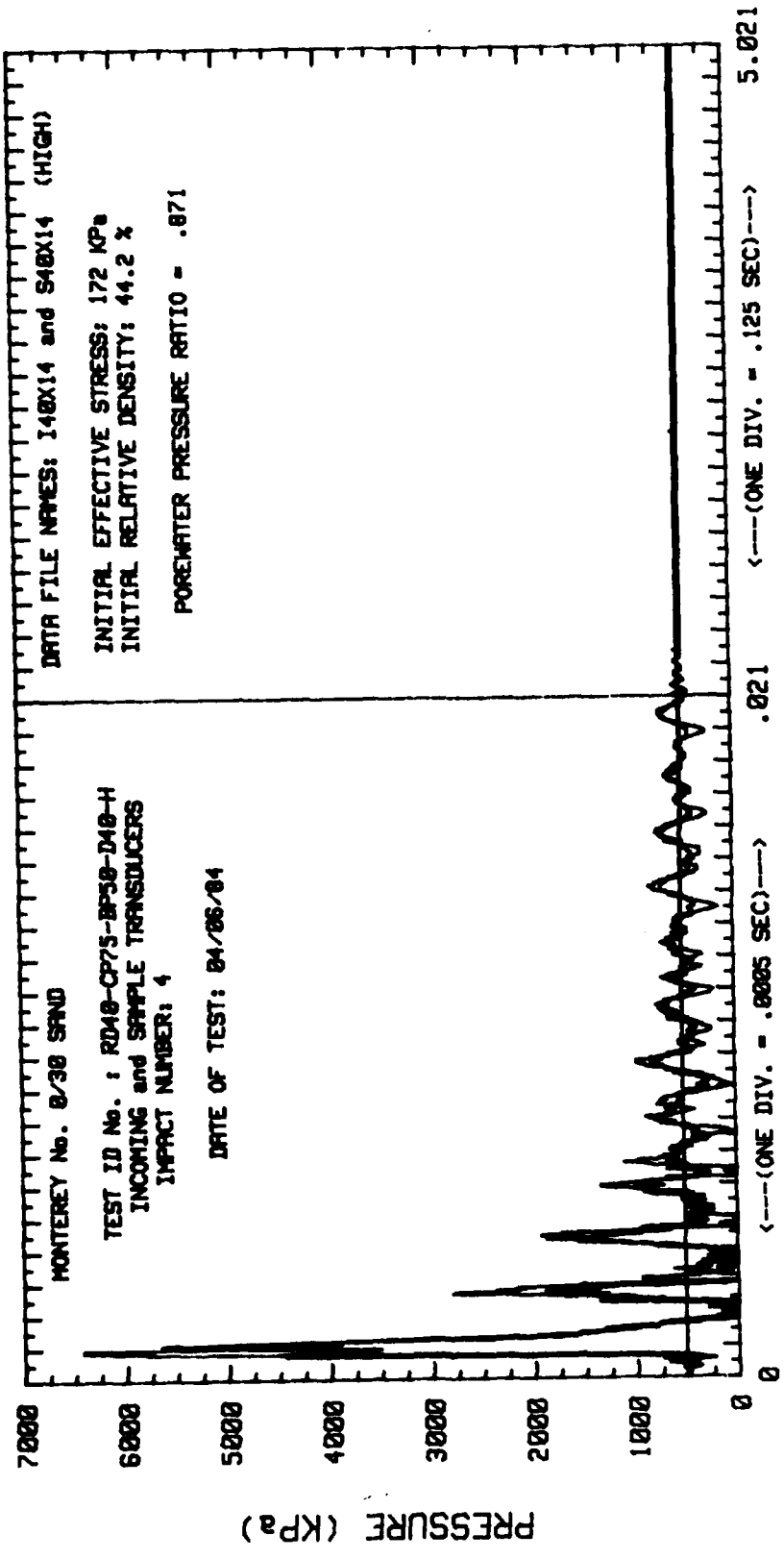

Figure 5.18 Pressure-Time Histories for D_r = '40%' Series and σ_o' = 172 KPa (High Impact Stress-Fourth Impact)

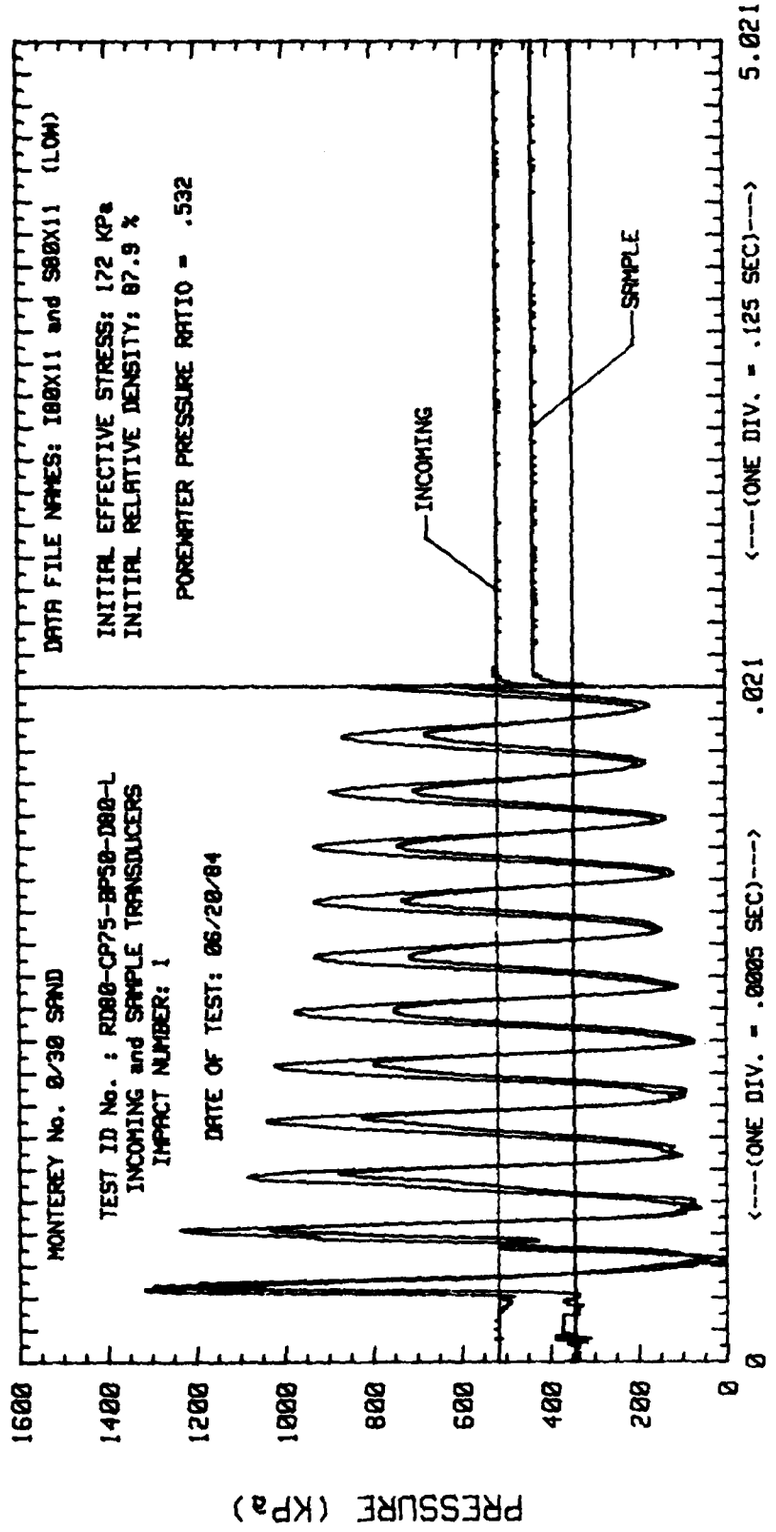

Figure 5.19 Pressure-Time Histories for D_r = '80%' Series and σ'_o = 172 KPa (Low Impact Stress-First Impact)

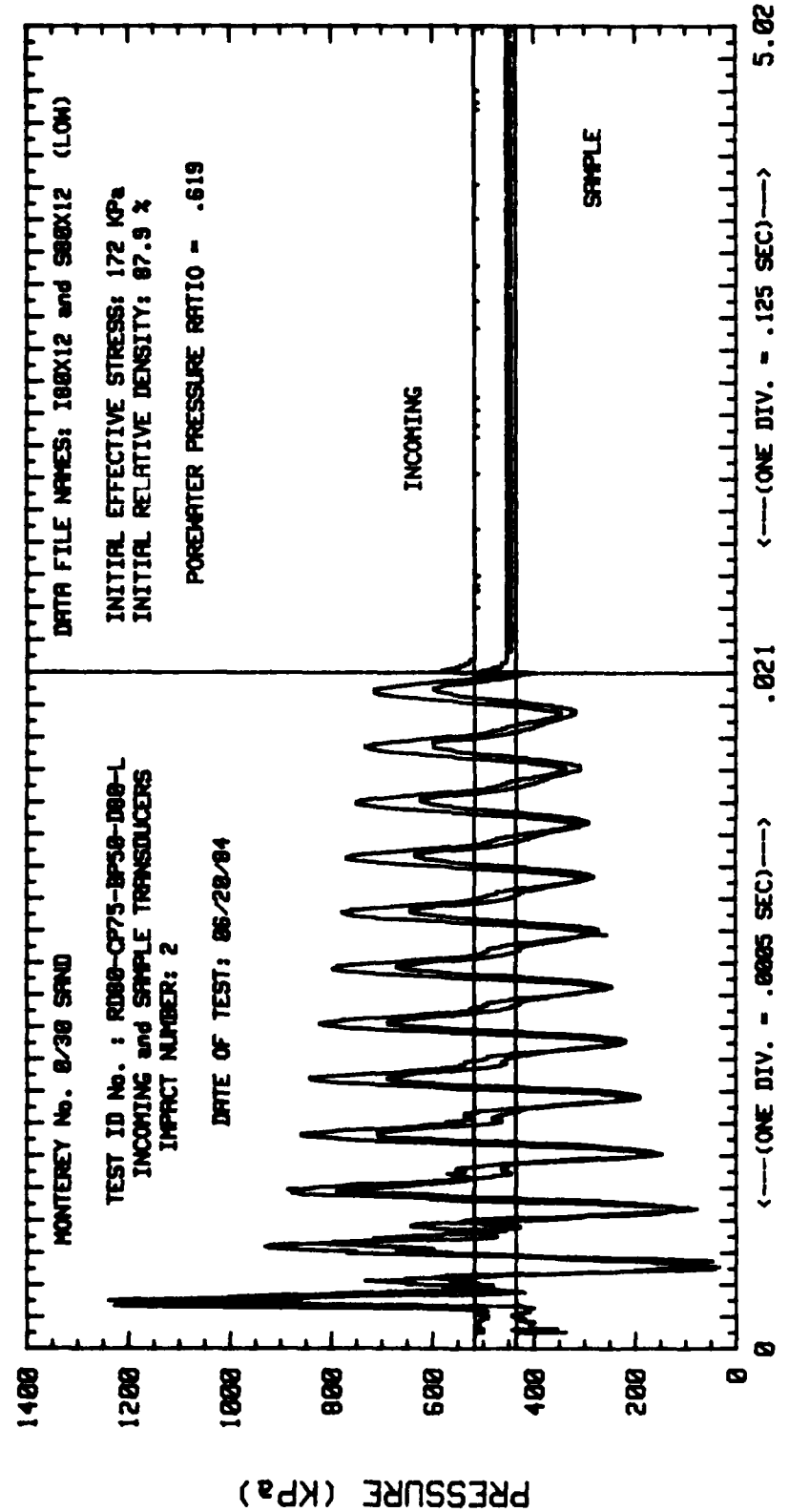

Figure 5.20 Pressure-Time Histories for D_r = '80%' Series and σ_o' = 172 KPa (Low Impact Stress-Second Impact)

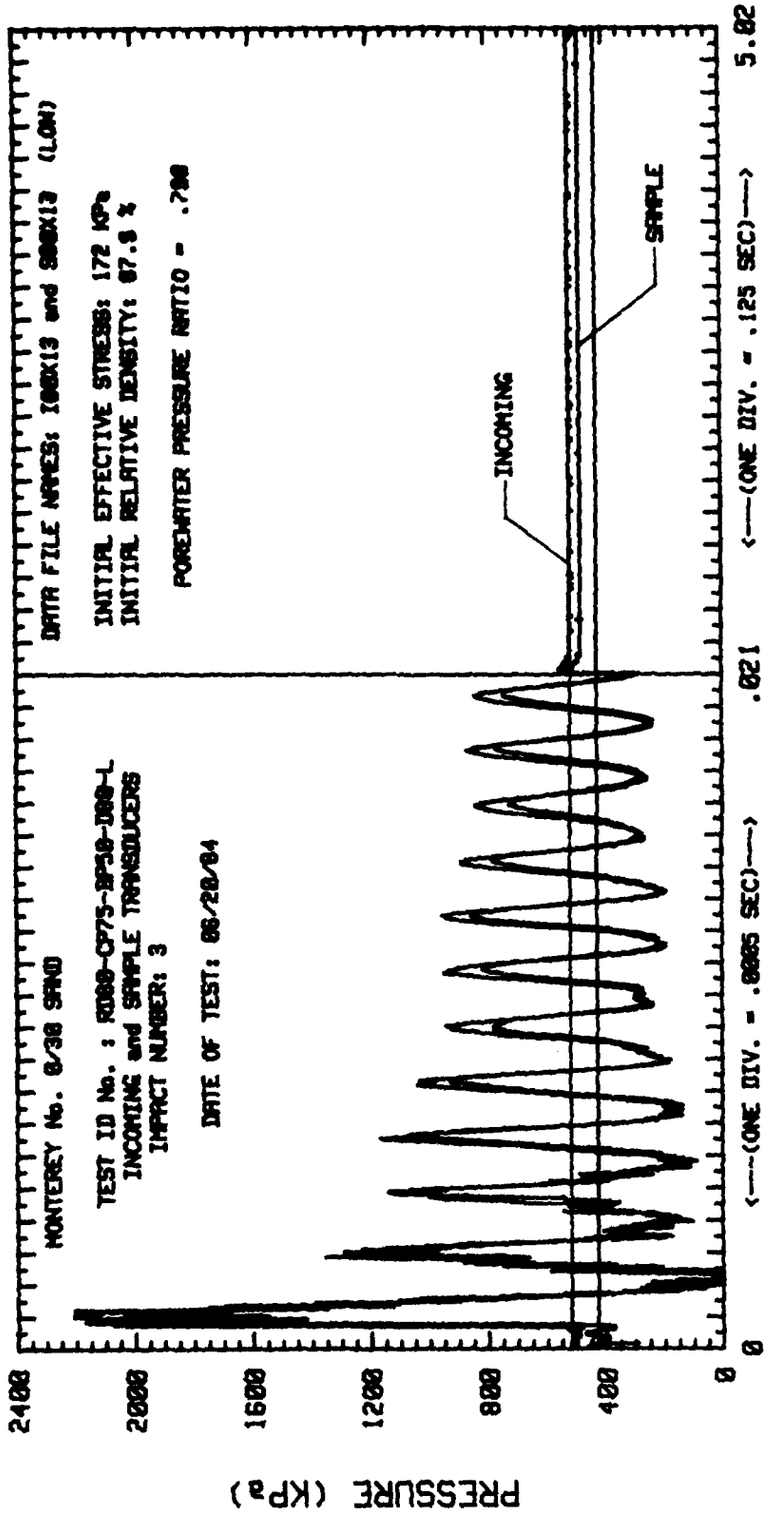

Figure 5.21 Pressure-Time Histories for D_r = '80%' Series and σ_o' = 172 KPa (Low Impact Stress-Third Impact)

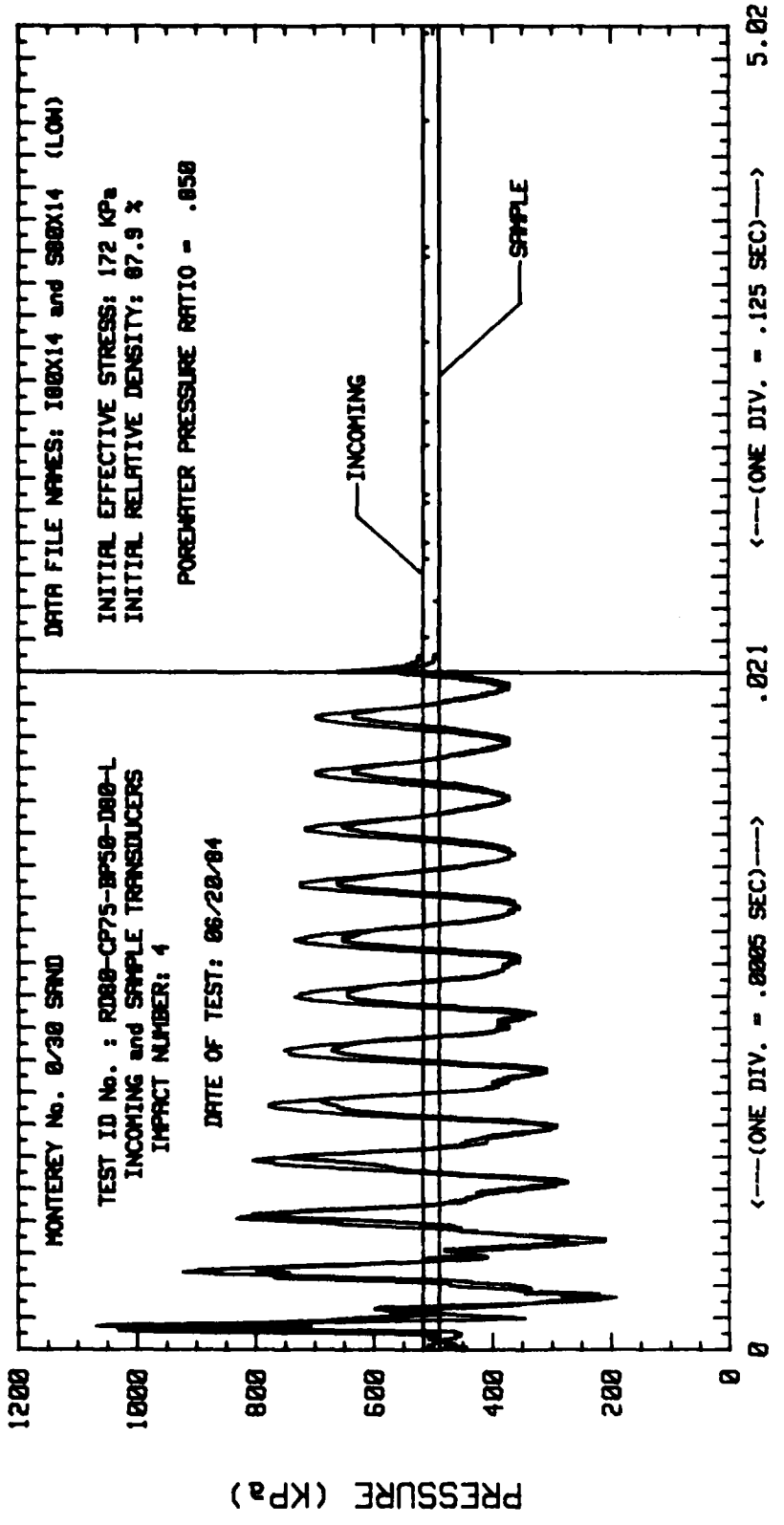

Figure 5.22 Pressure-Time Histories for D_r = '80%' Series and σ_o' = 172 KPa (Low Impact Stress-Fourth Impact)

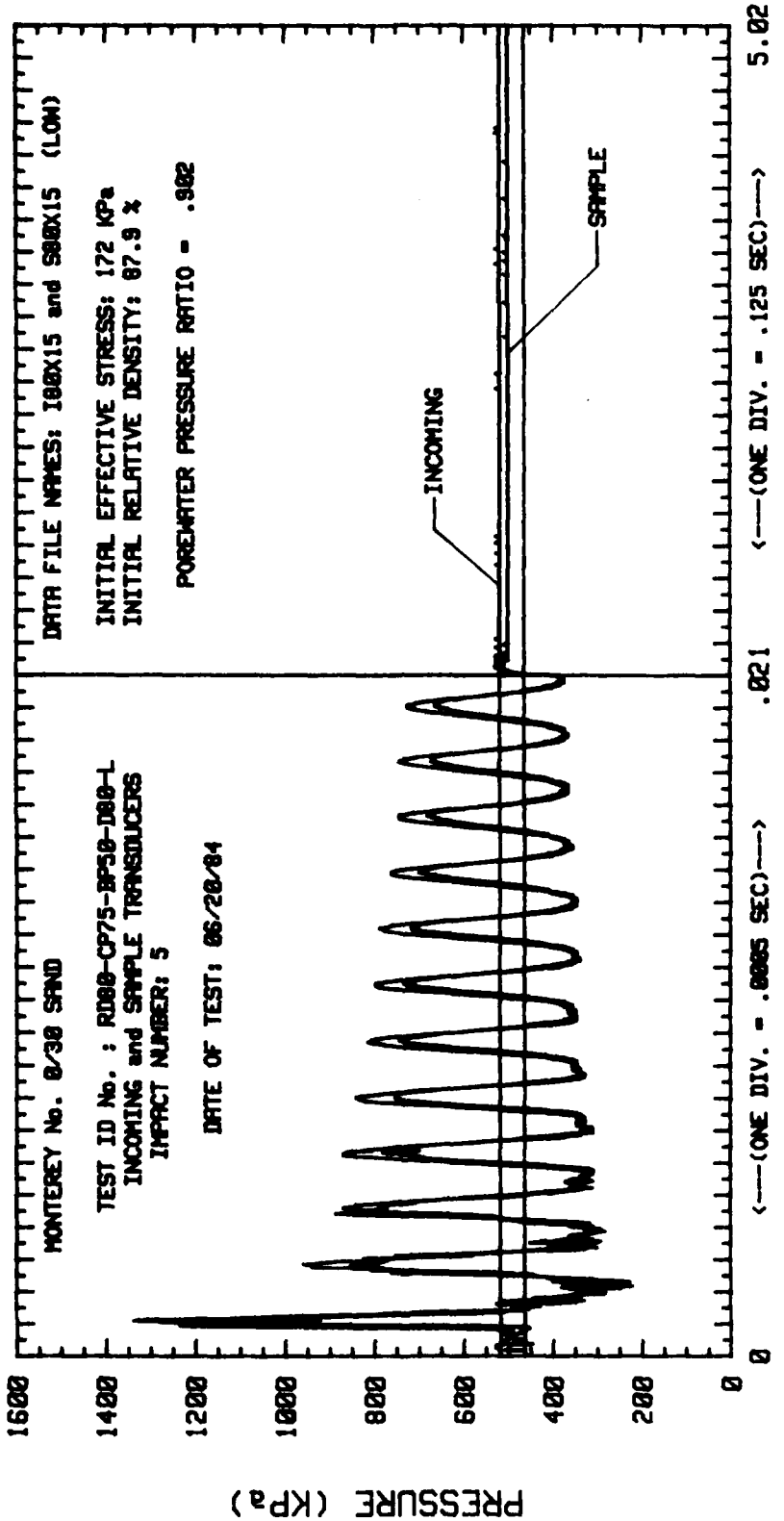

Figure 5.23 Pressure-Time Histories for D_r = '80%' Series and σ'_o = 172 KPa (Low Impact Stress-Fifth Impact)

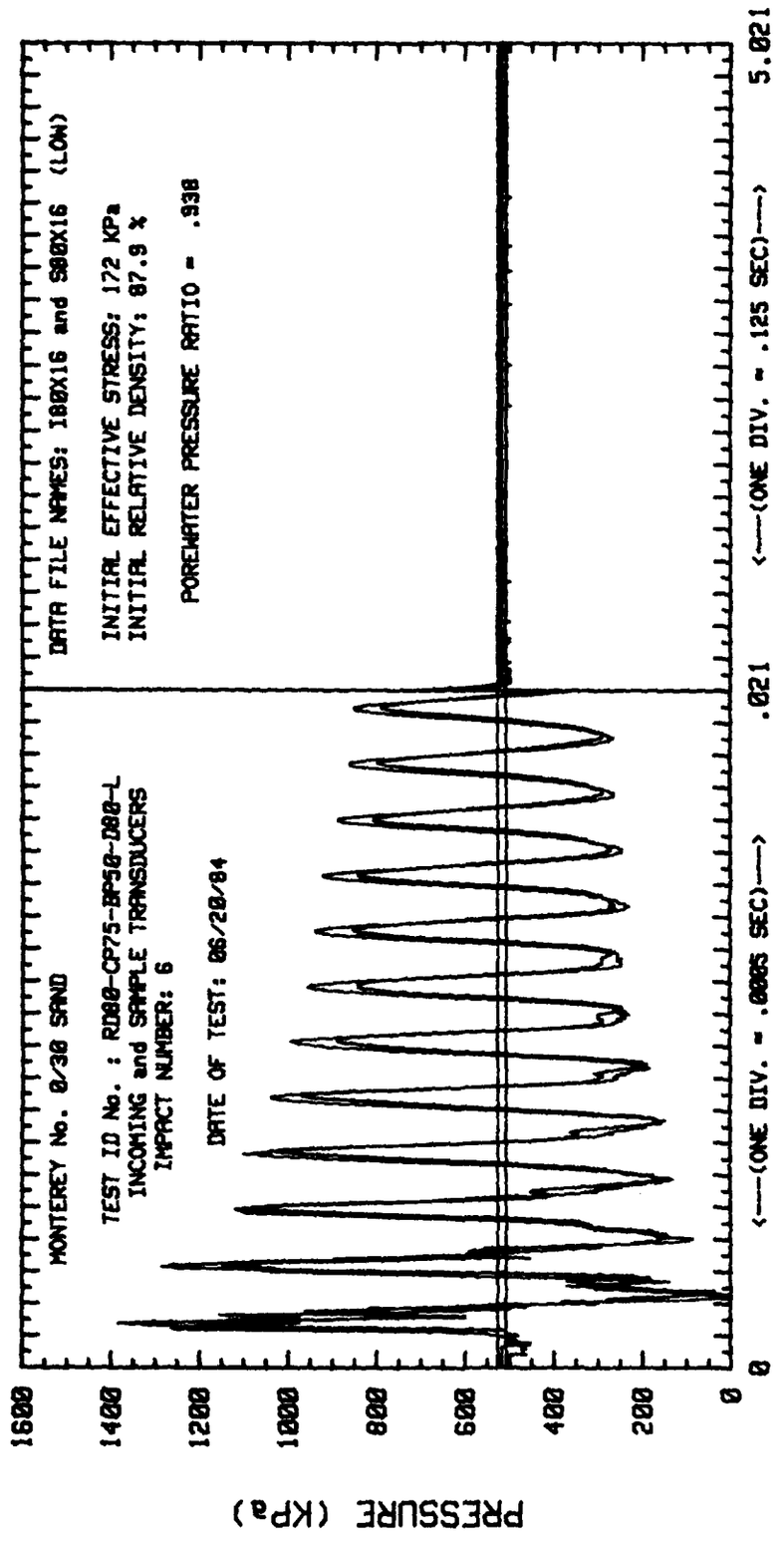

Figure 5.24 Pressure-Time Histories for D_r = '80%' Series and σ'_o = 172 KPa (Low Impact Stress-Sixth Impact)

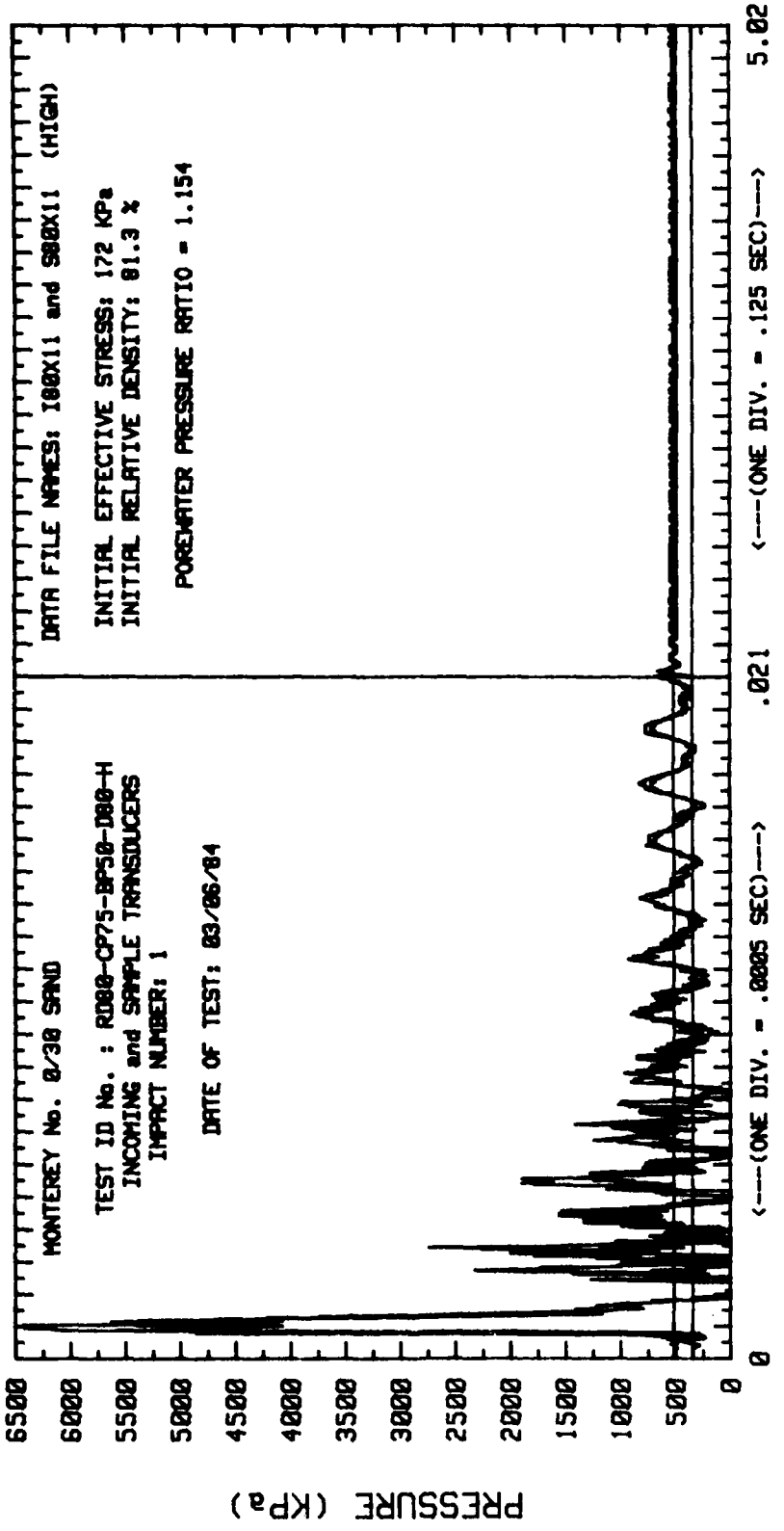

Figure 5.25 Pressure-Time Histories for D_r = '80%' Series and σ'_o = 172 KPa (High Impact Stress-First Impact)

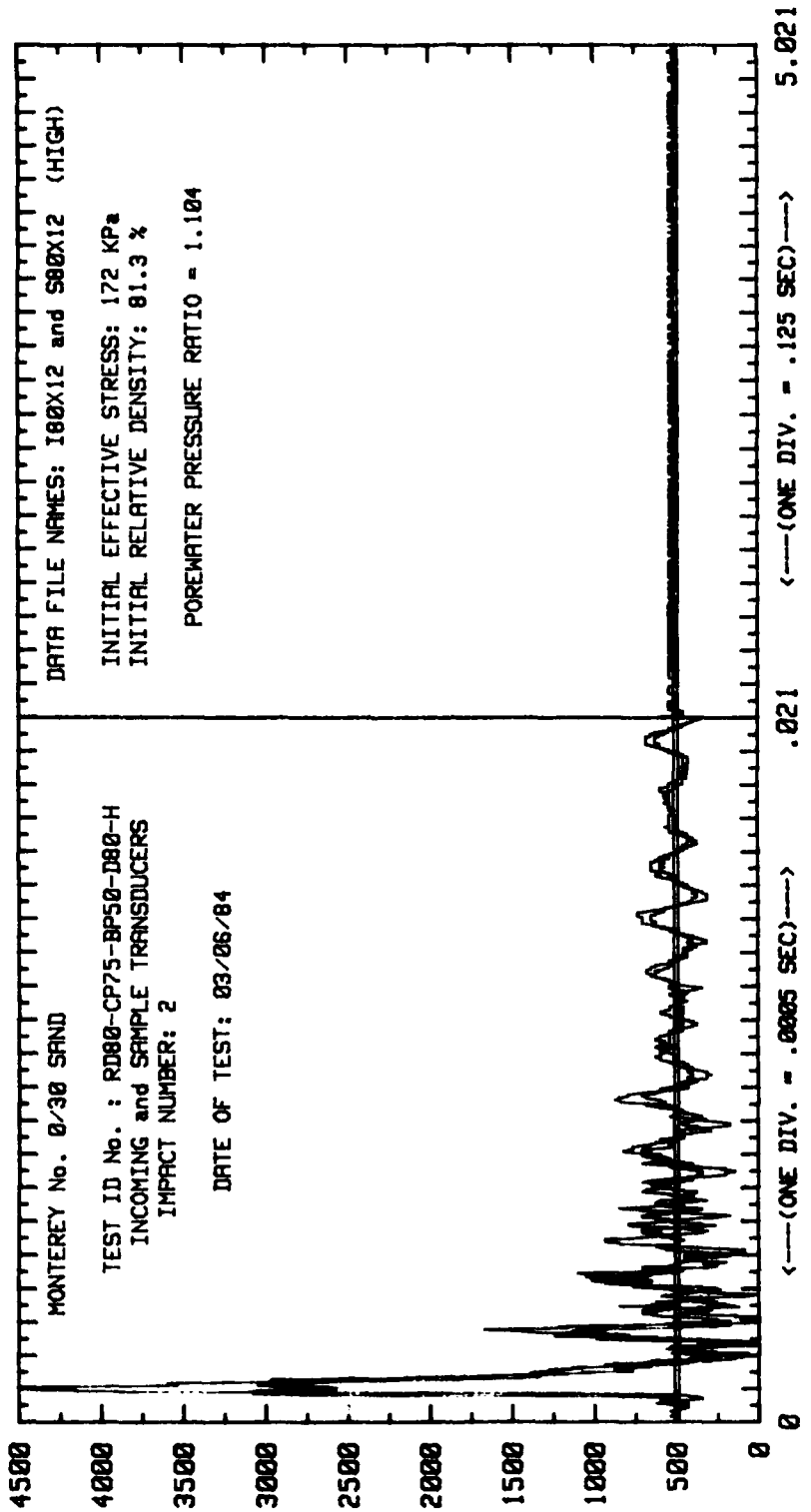

Figure 5.26 Pressure-Time Histories for D_r = '80%' Series and σ'_o = 172 KPa (High Impact Stress-Second Impact)

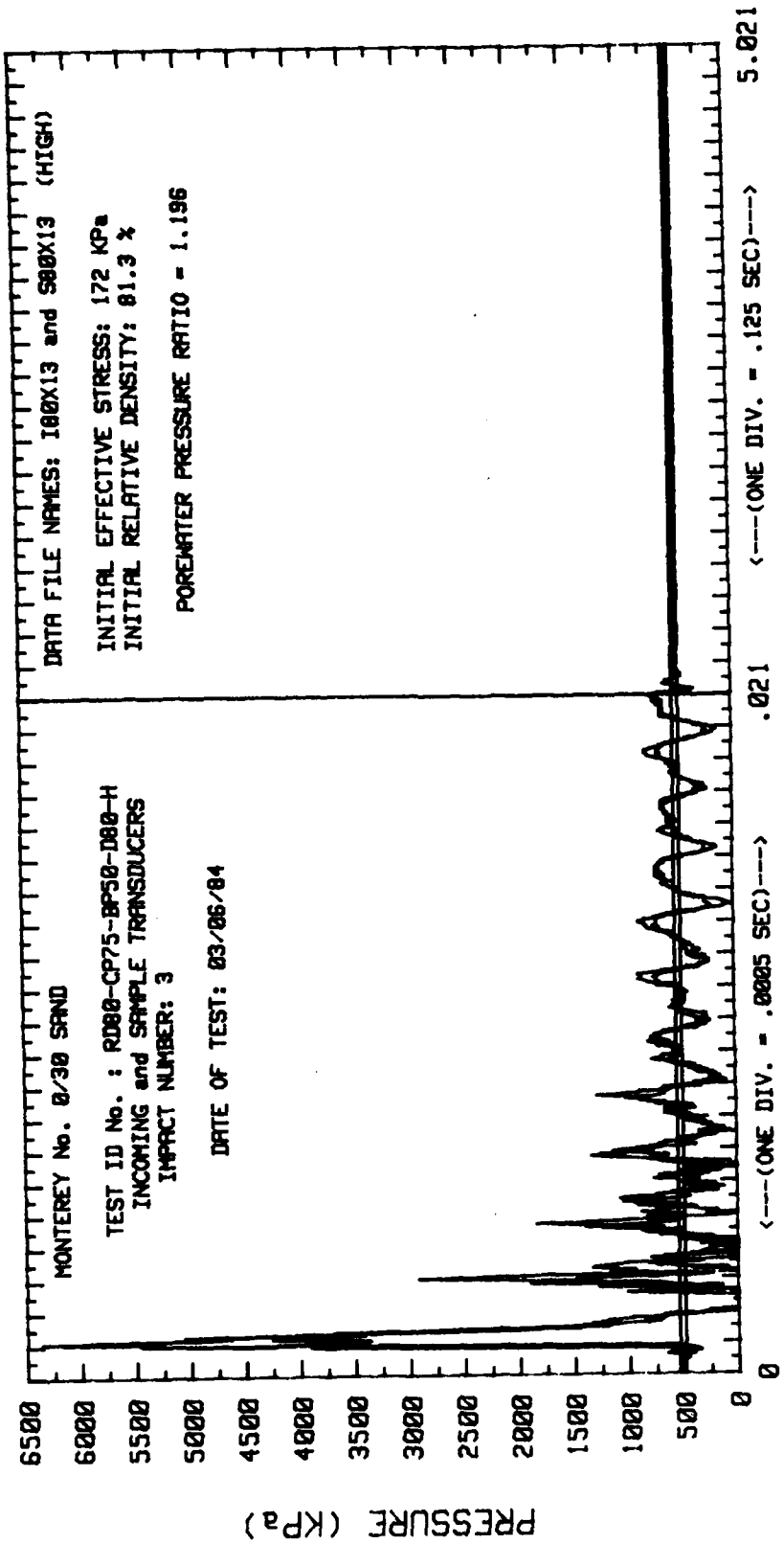

Figure 5.27 Pressure-Time Histories for D_r = '80%' Series and σ'_o = 172 KPa (High Impact Stress-Third Impact)

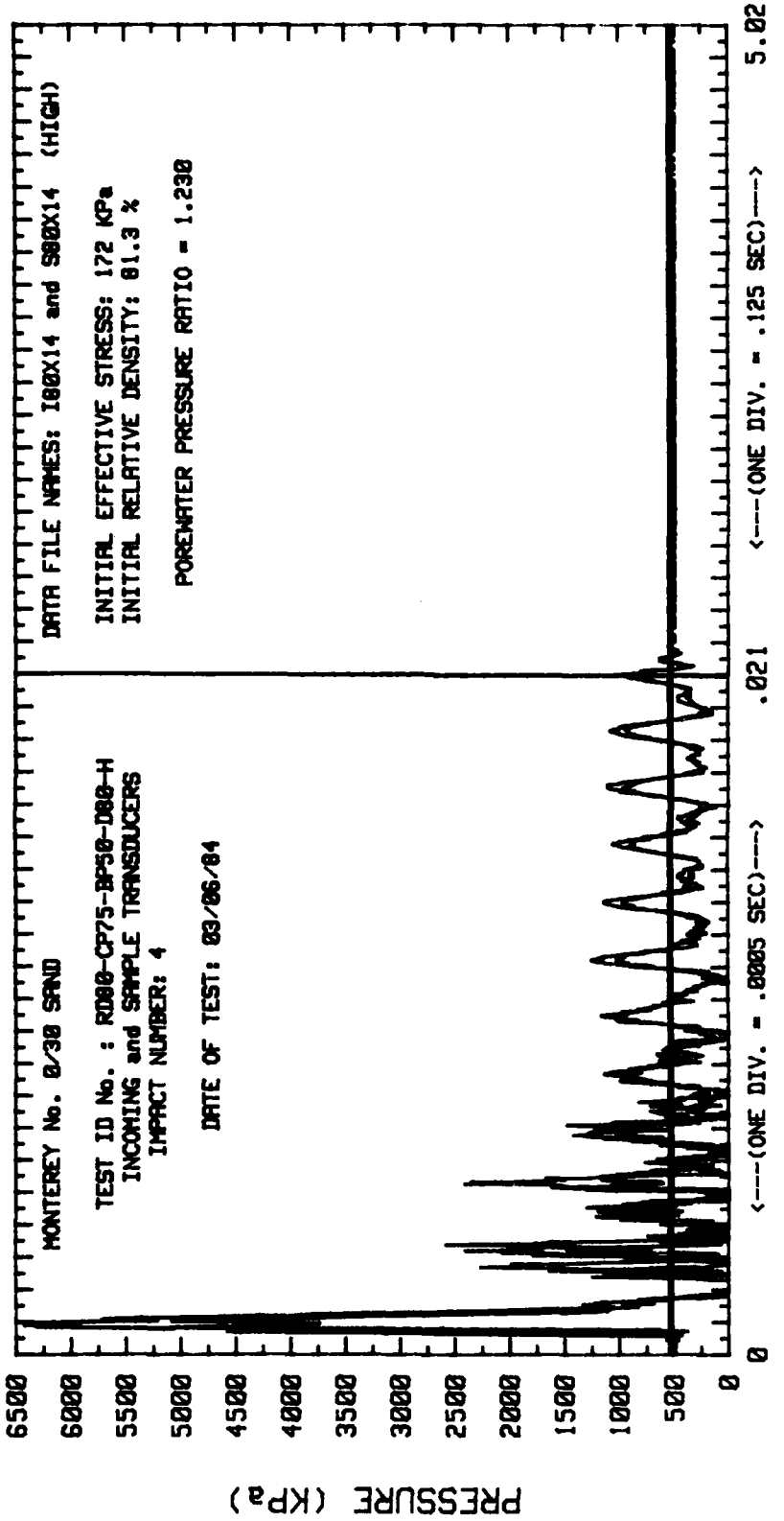

Figure 5.28 Pressure-Time Histories for D_r = '80%' Series and σ'_o = 172 KPa (High Impact Stress-Fourth Impact)

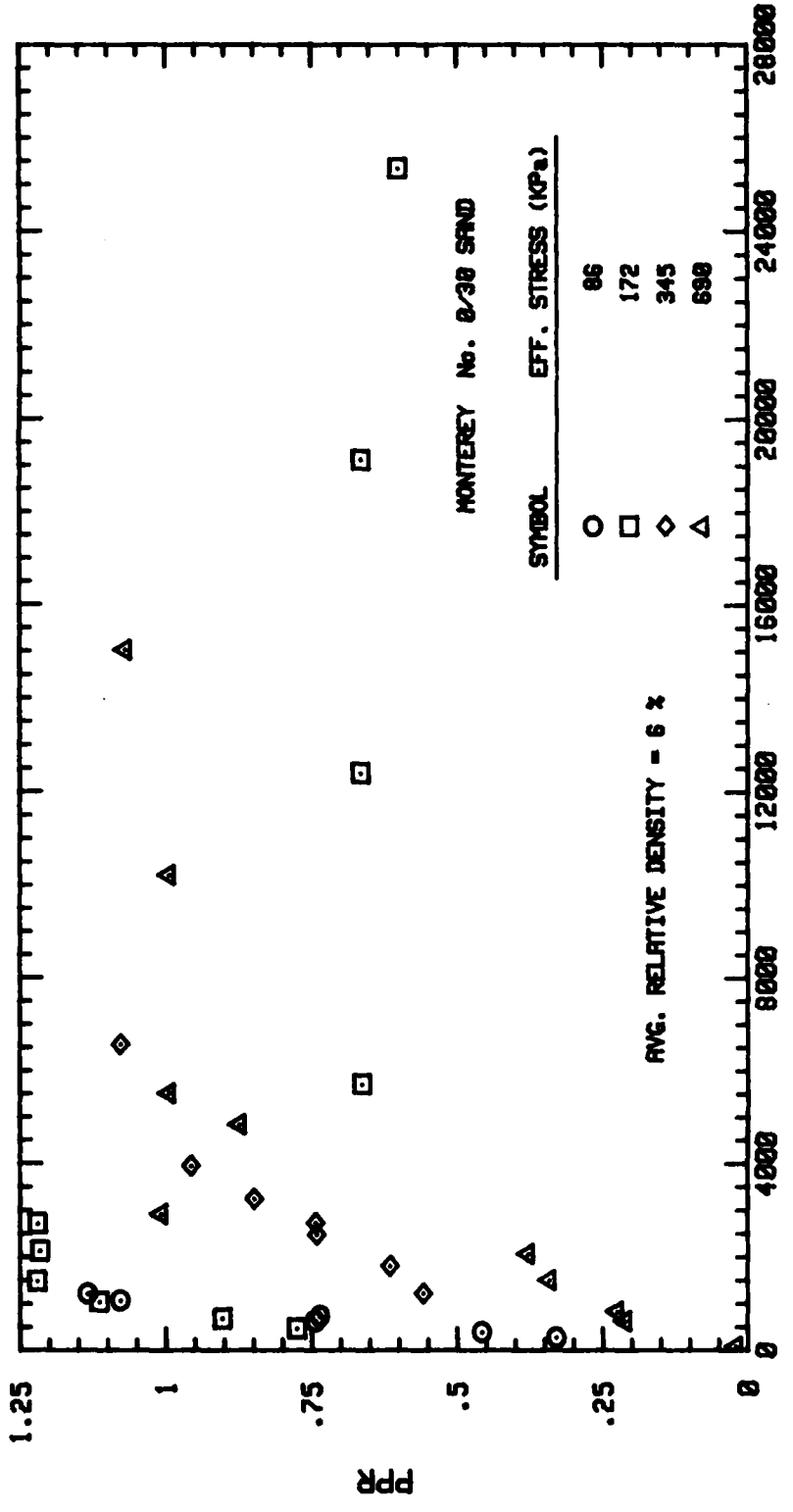

Figure 5.29 Porewater Pressure Ratio as a Function of the Sum of the Peak Porewater Pressures for Monterey No. 0/30 Sand and the D_r = '0%' Series

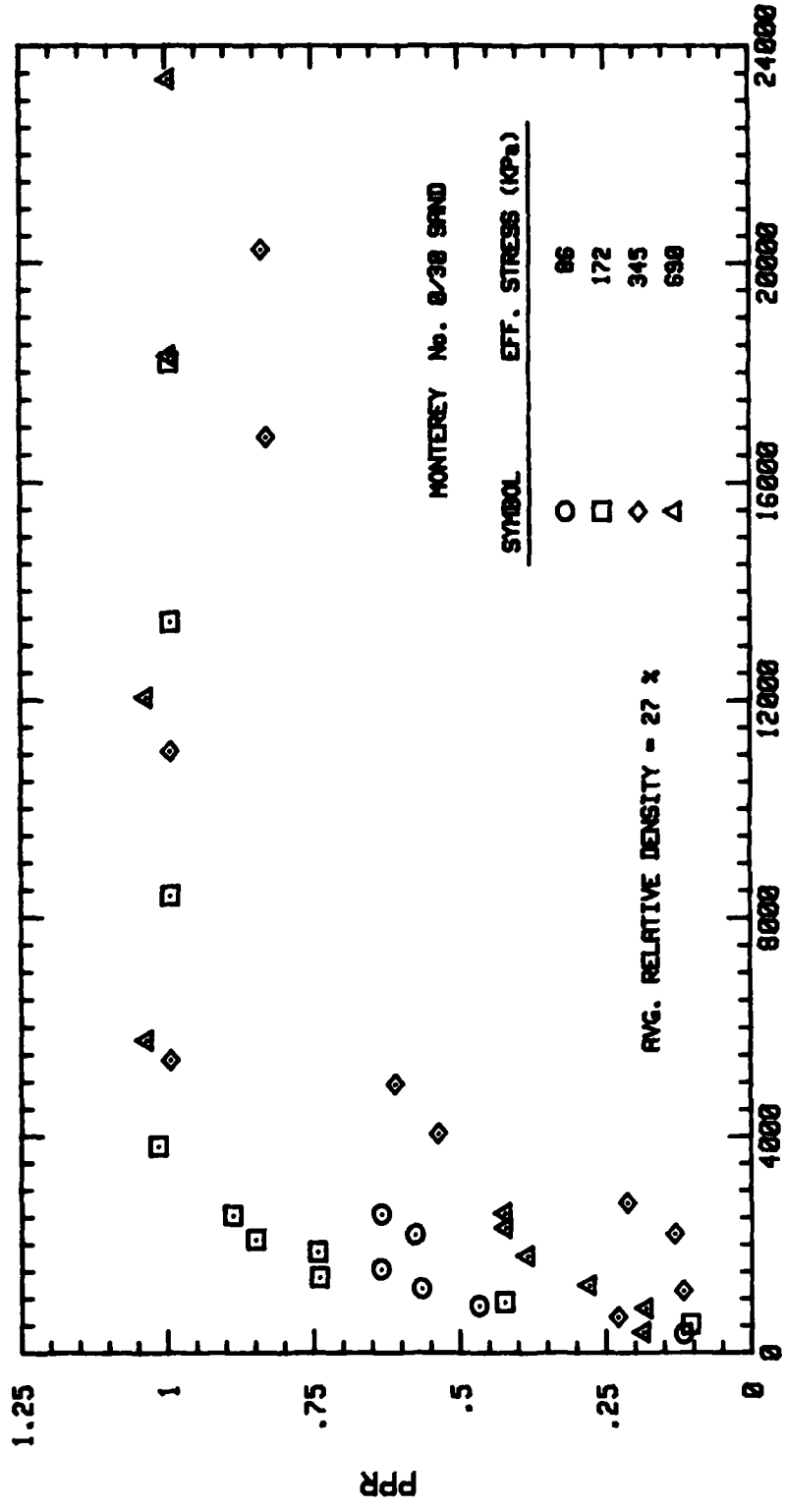

Figure 5.30 Porewater Pressure Ratio as a Function of the Sum of the Peak Porewater Pressures for Monterey No. 0/30 Sand and the D_r = '20%' Series

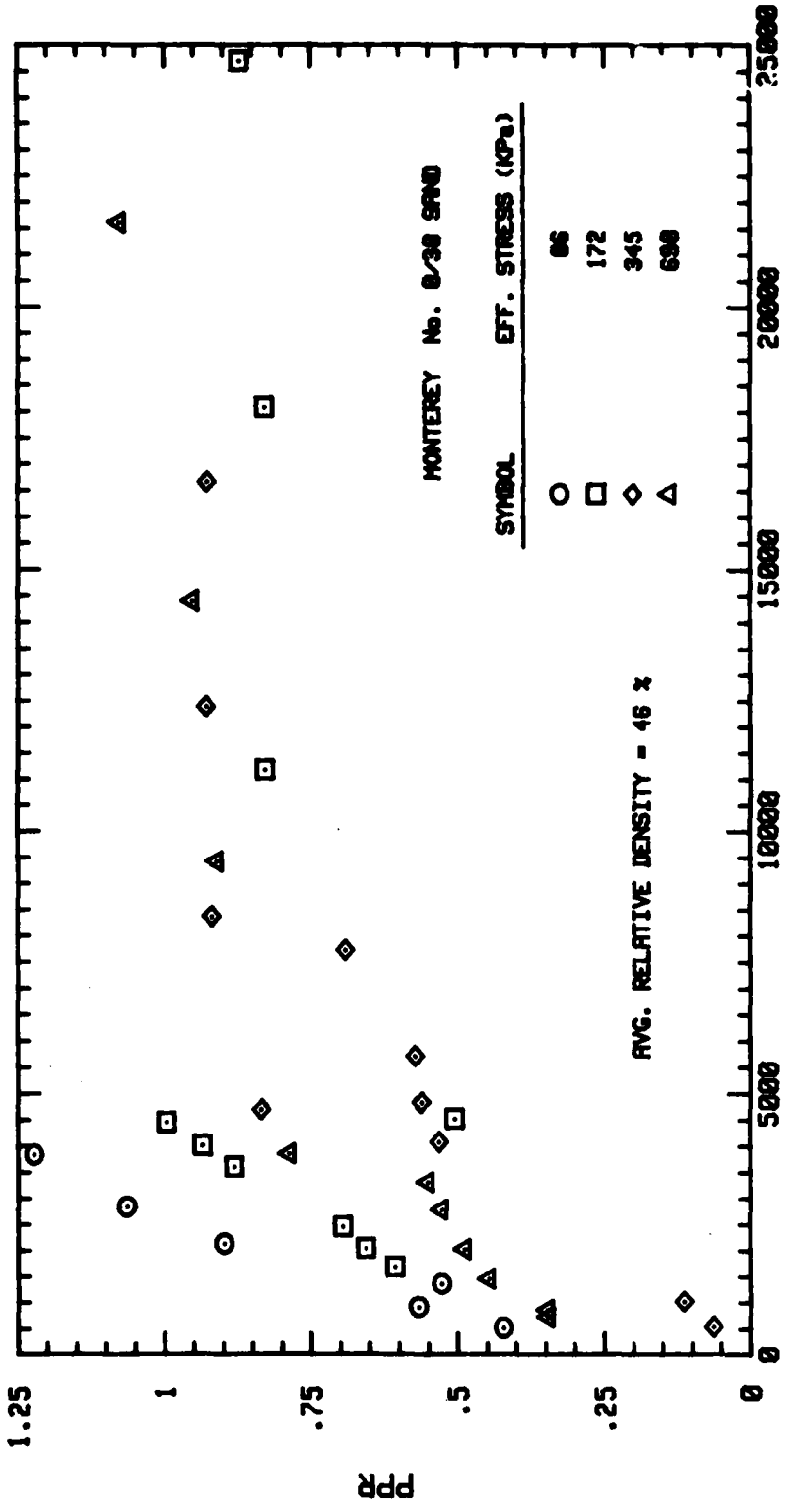

Figure 5.31 Porewater Pressure Ratio as a Function of the Sum of the Peak Porewater Pressures for Monterey No. 0/30 Sand and the D_r = '40%' Series

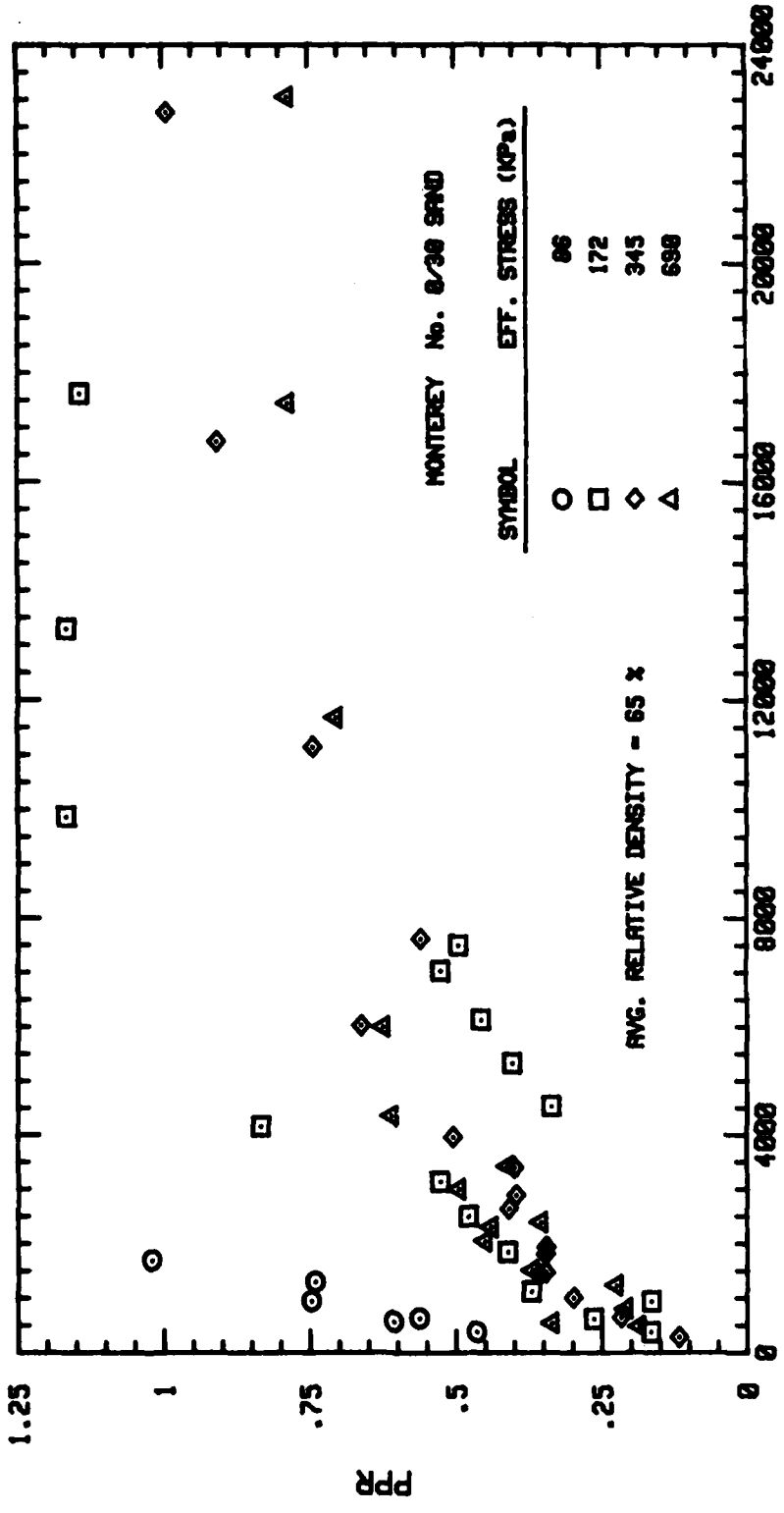

Figure 5.32 Porewater Pressure Ratio as a Function of the Sum of the Peak Porewater Pressures for Monterey No. 0/30 Sand and the D_r = '60%' Series

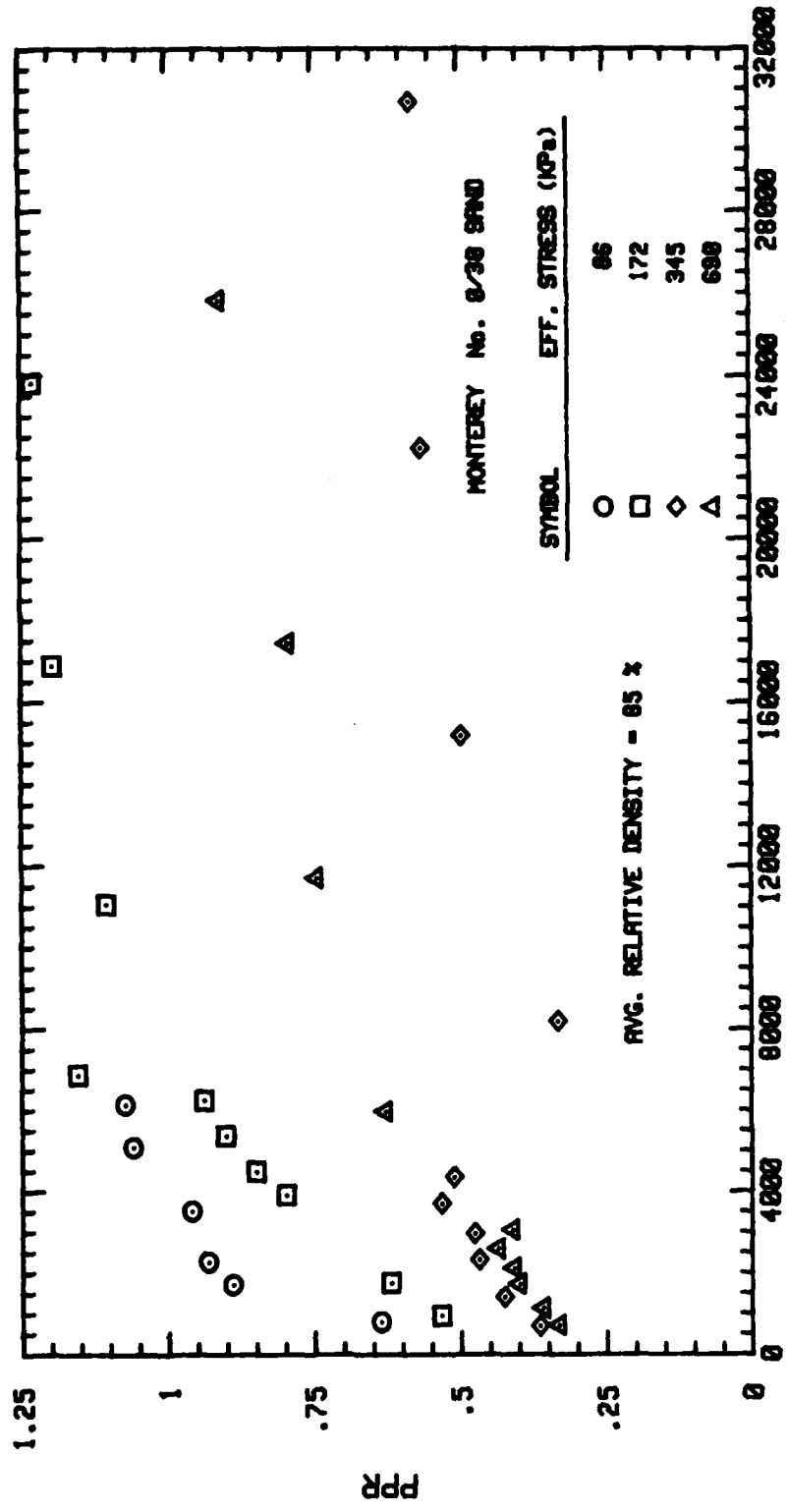

Figure 5.33 Porewater Pressure Ratio as a Function of the Sum of the Peak Porewater Pressures for Monterey No. 0/30 Sand and the D_r = '80%' Series

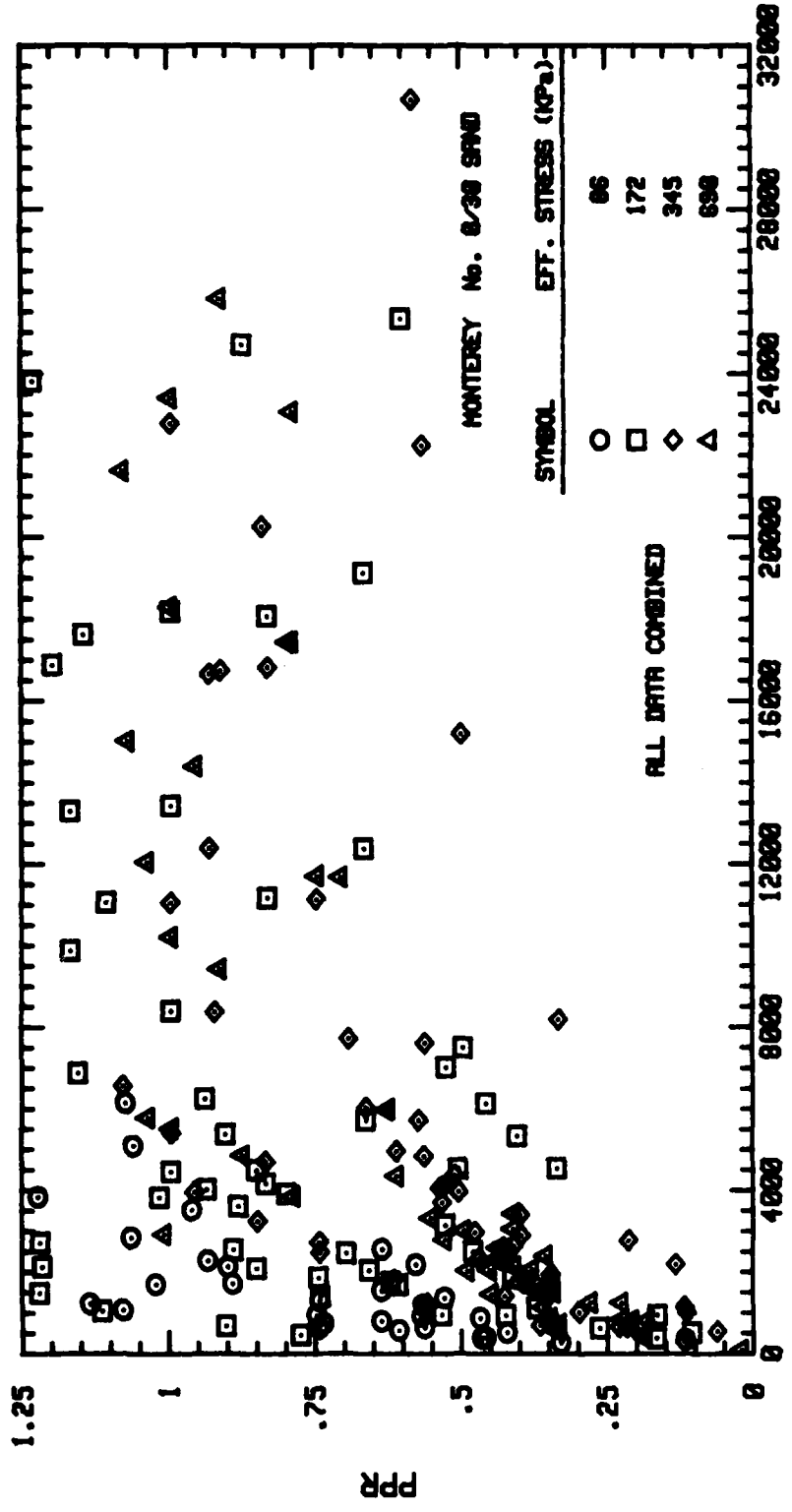

Figure 5.34 Porewater Pressure Ratio as a Function of the Sum of the Peak Sample Porewater Pressures in Terms of Relative Density for All Data Combined (Monterey No. 0/30 Sand)

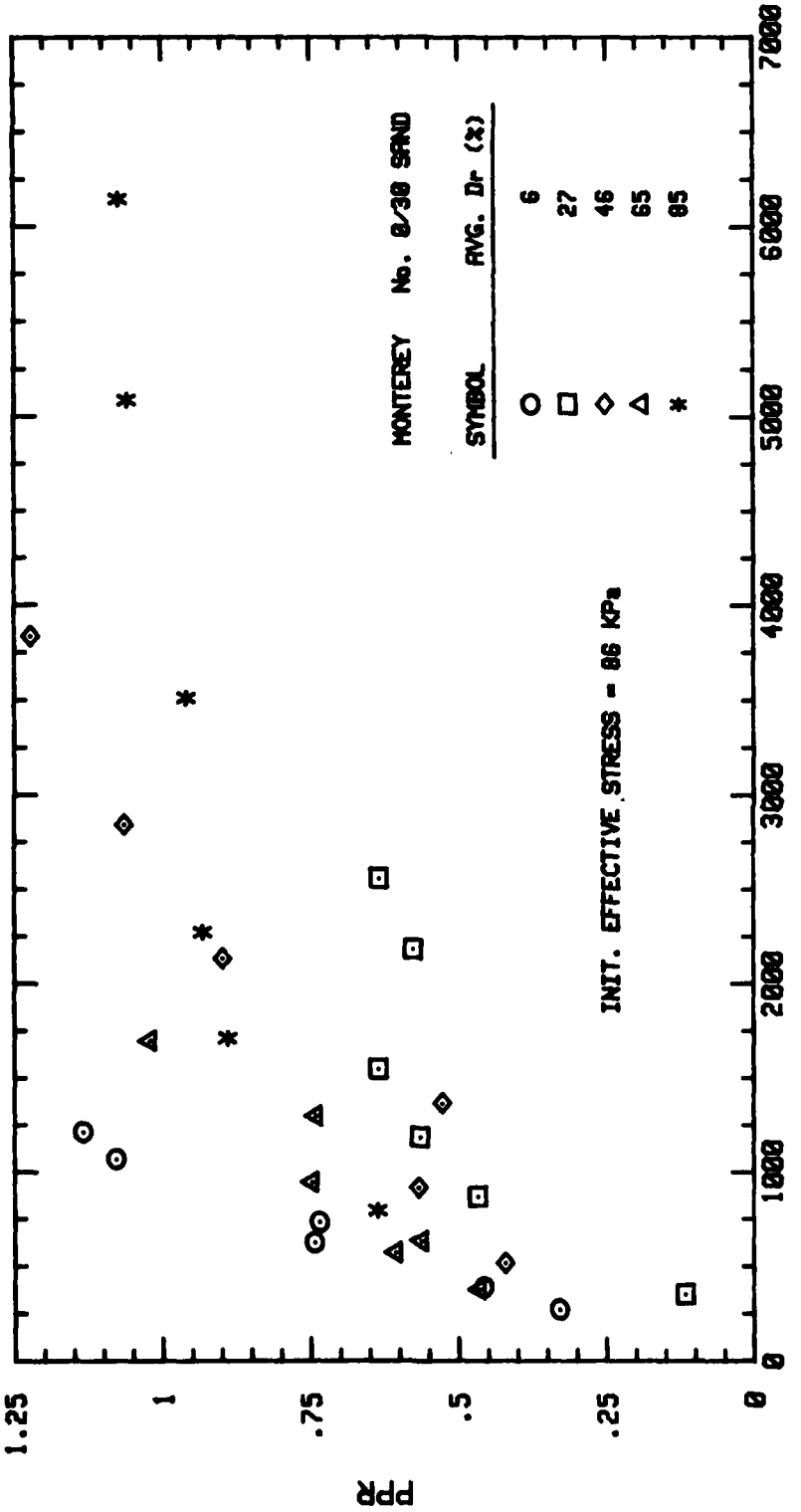

Figure 5.35 Porewater Pressure Ratio as a Function of the Sum of the Peak Porewater Pressures for Monterey No. 0/30 Sand at σ'_o = 86 KPa

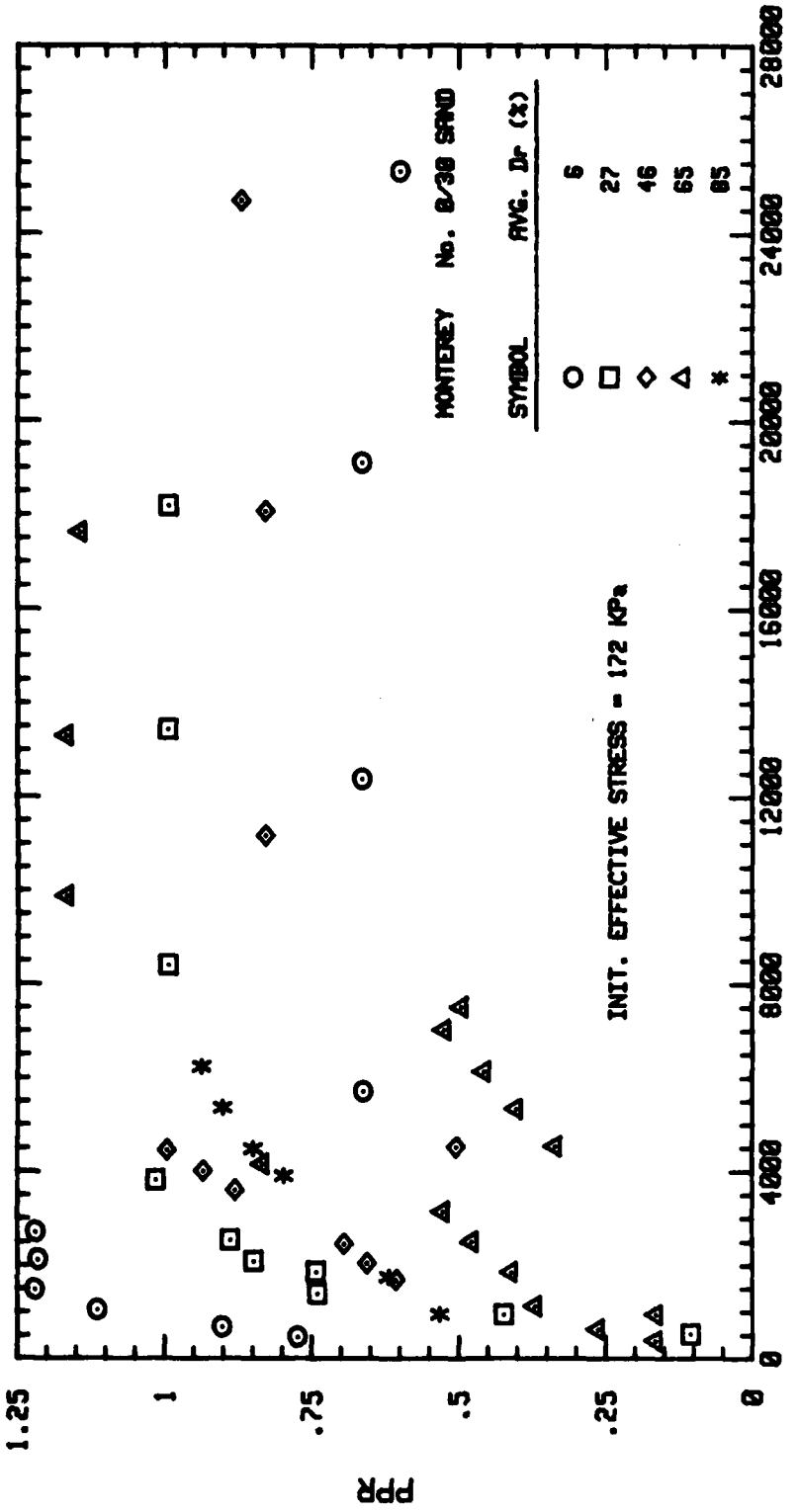

Figure 5.36 Porewater Pressure Ratio as a Function of the Sum of the Peak Porewater Pressures for Monterey No. 0/30 Sand at σ_o' = 172 KPa

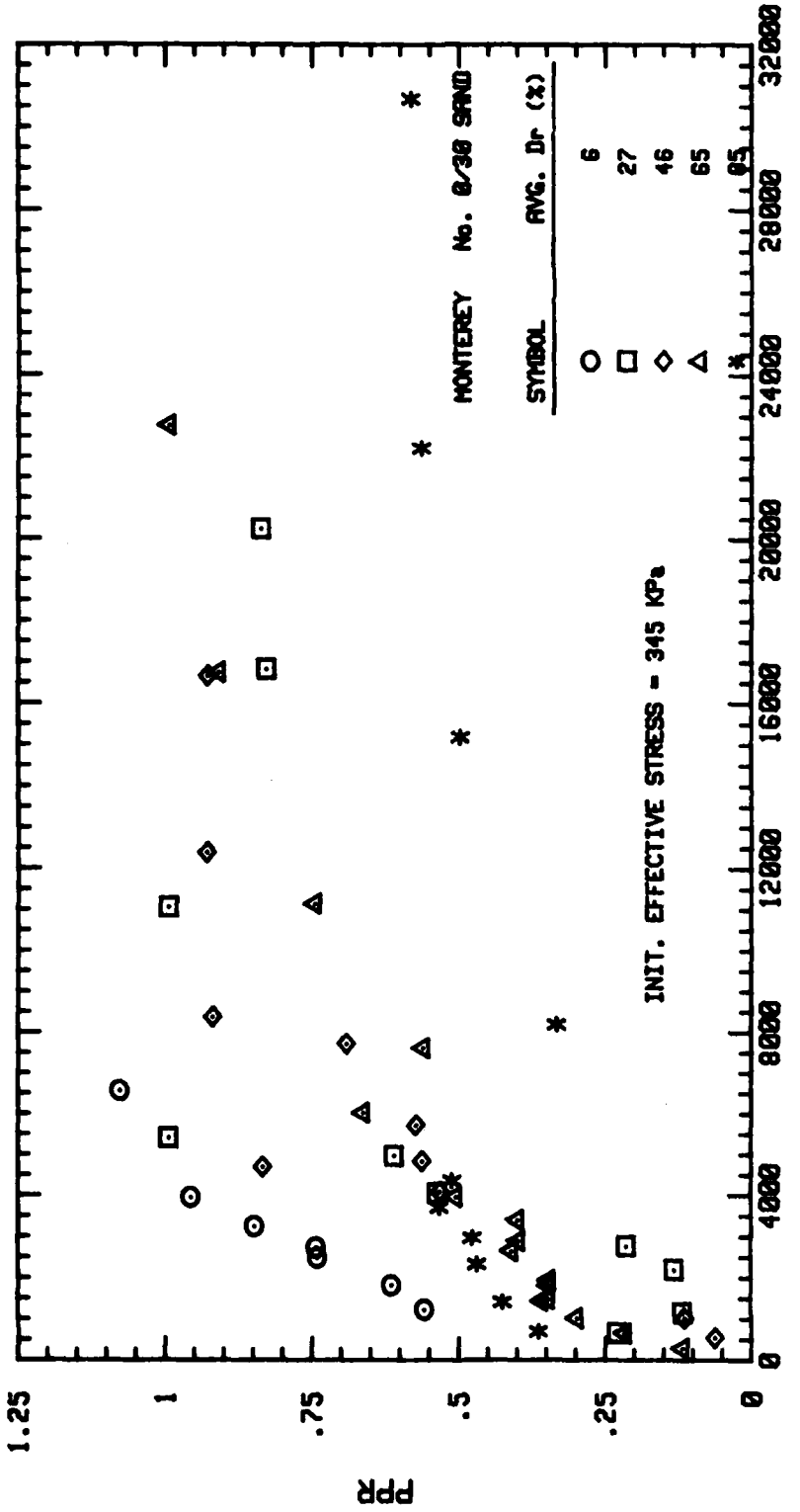

Figure 5.37 Porewater Pressure Ratio as a Function of the Sum of the Peak Porewater Pressures for Monterey No. 0/30 Sand at $\sigma_o' = 345$ KPa

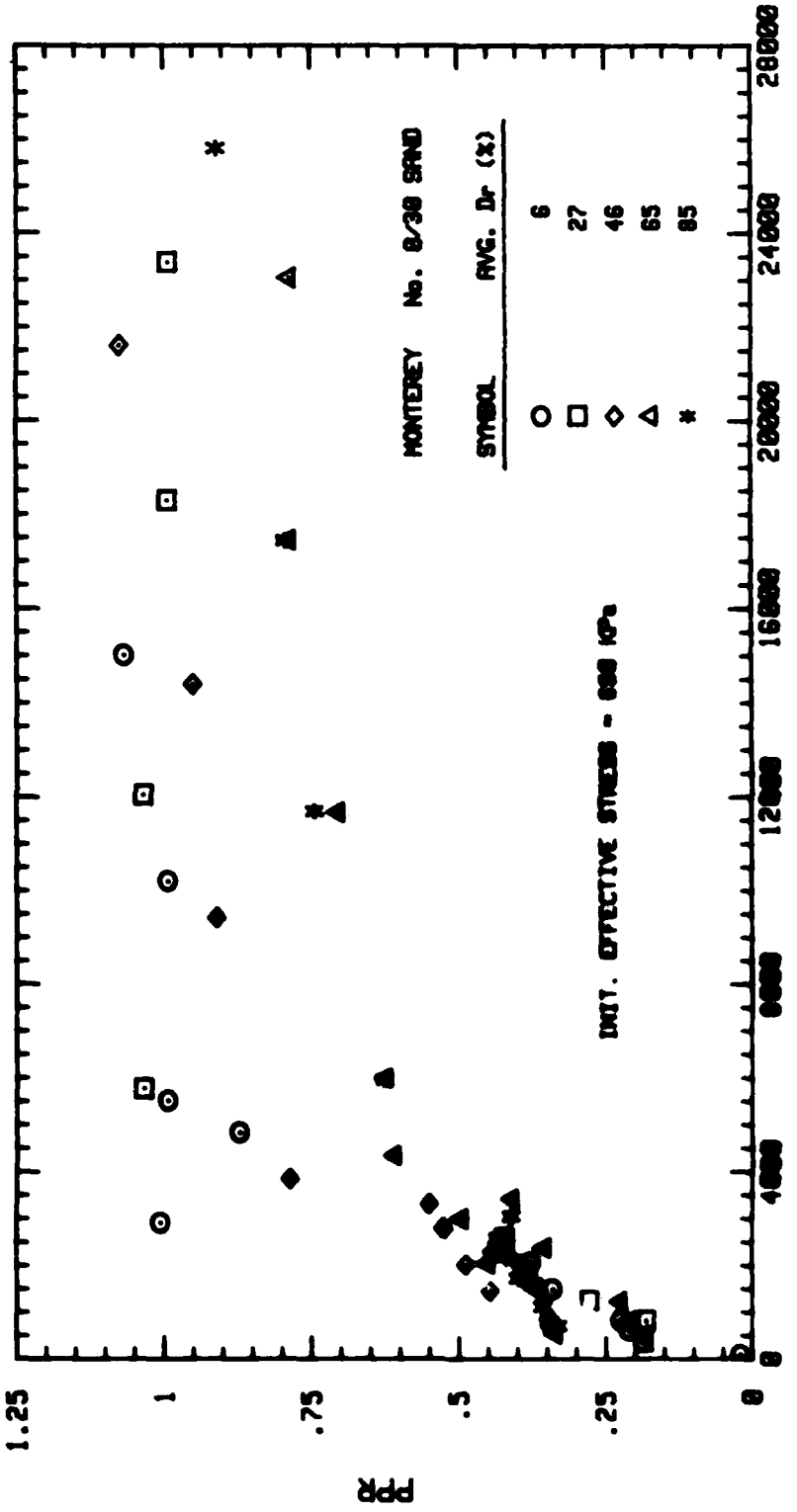

Figure 5.38 Porewater Pressure Ratio as a Function of the Sum of the Peak Porewater Pressures for Monterey No. 0/30 Sand at σ'_o = 690 KPa

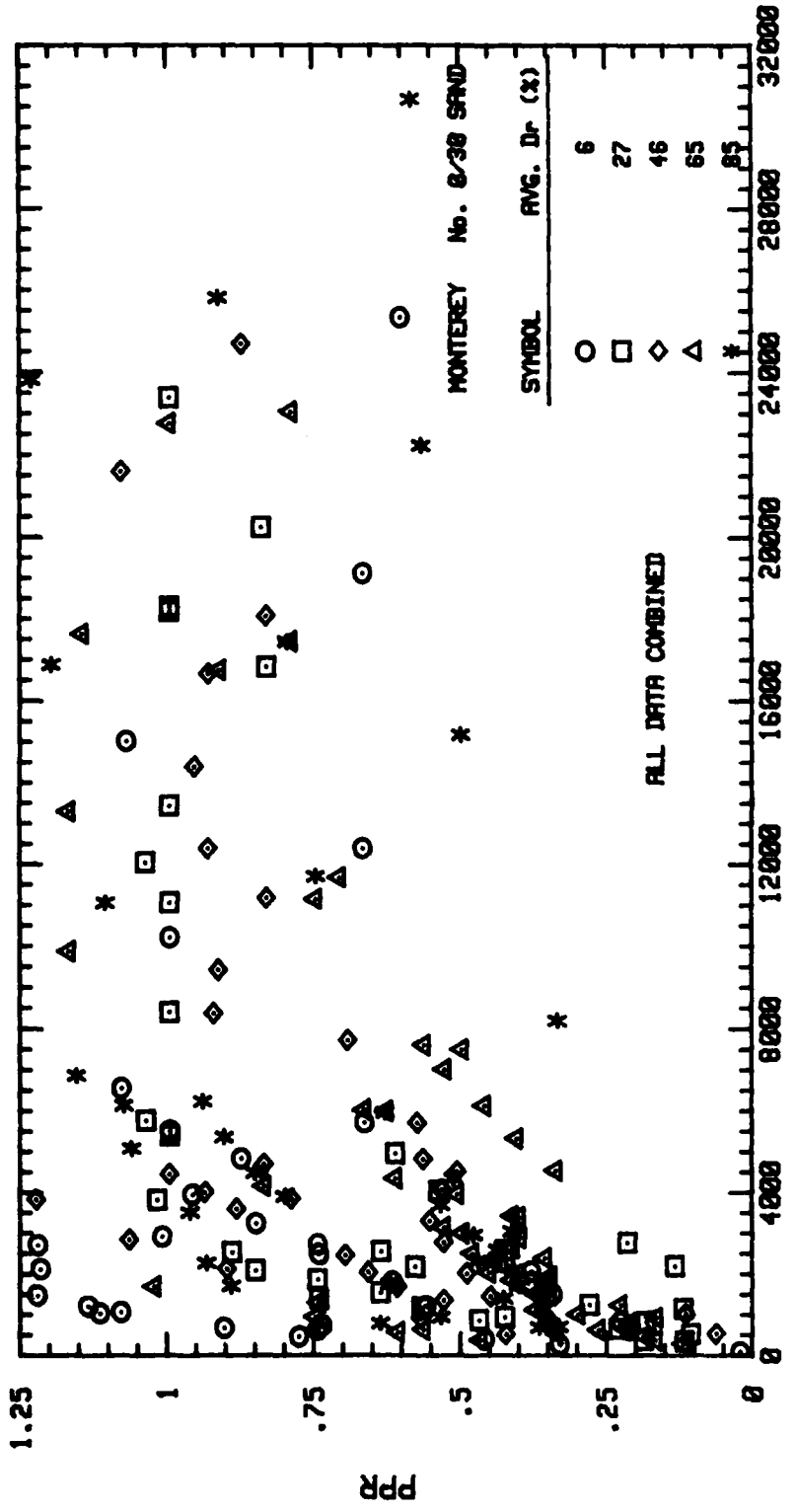

Figure 5.39 Porewater Pressure Ratio as a Function of the Sum of the Peak Sample Porewater Pressures in Terms of Relative Density for All Data Combined (Monterey No. 0/30 Sand)

VI. ANALYSIS AND APPLICATION OF RESULTS

A. Bulk Modulus and Compressive Stress Wave Propagation

The water saturated sand samples used in this experimental investigation represent a two-phase medium for stress wave propagation. The presence of the solid sand particles in the water increases the fluid density and also affects the compressibility of the soil-water mixture. The changes in fluid density and mixture compressibility need to be considered in evaluating the compressive stress wave propagation velocity in a mixture. A procedure presented by Richart et al. (1970) was followed and will be outlined here.

The total mass density, ρ_t , of a soil-water mixture can be determined from:

$$\rho_t = \rho_w \frac{G_s + e}{1 + e} \qquad \text{(Eq. 6.1)}$$

where, G_s is the specific gravity of the solid particles, ρ_w is the mass density of water and e is the void ratio.

The compressibility of a soil-water mixture, considering the solid particles to be suspended in the water, consists of two contributing factors: the compressibility of the solid particles and the compressibility of the fluid. The mixture compressibility can be determined from:

$$\frac{1}{B_{mix}} = \frac{1}{B_w}\left(\frac{e}{1+e}\right) + \frac{1}{B_s}\left(\frac{1}{1+e}\right) \qquad \text{(Eq. 6.2)}$$

where, B_w is the bulk modulus of the water and B_s is the bulk modulus of the soil particles. For quartz particles, B_s is about 30680 MPa and for distilled, de-aired fresh water at 20 degrees Celsius, B_w is about 2140 MPa (Richart et al.,1970). It should be noted that the theory of mixtures assumes that the solid particles are suspended in the water. However, the total stress will be somewhat larger since the solid particles are actually in contact with one another. For small strain conditions, this difference is small and can be neglected.

Using the bulk modulus and the total mass density for the mixture, the compressive stress wave propagation velocity through the mixture, V_{mix}, can be found from:

$$V_{mix} = \left[\frac{B_{mix}}{\rho_t}\right]^{0.5} \qquad \text{(Eq. 6.3).}$$

The value of V_{mix} includes the effects of density and compressibility. Calculated values for the Monterey No. 0/30 sand used in this experimental investigation are given in Table 6.1. Figure 6.1 shows the acoustic impedance as a function of void ratio and Figure 6.2 shows the compressive stress wave propagation velocity as a function of void ratio.

B. Peak Particle Velocity and Peak Strain

Two values of particular interest that are useful in interpreting the results of this investigation, are the peak particle velocity and the peak compressive strain. For saturated, sandy soils the peak

Table 6.1 Stress Wave Propagation Parameters for Monterey No. 0/30 Sand

D_r (%)	e	ρ_t (Kg/M^3)	B_{mix} (KPa)	V_{mix}	V_{mix}/V_w (M/sec)	$\rho_t V_c$ ($Kg/(M^2-sec)$)
0	.803	1915	4421407	1519	1.013	2908885
10	.779	1926	4485912	1526	1.017	2940602
20	.755	1940	4554171	1532	1.021	2972080
30	.731	1953	4626521	1539	1.026	3005667
40	.707	1967	4703343	1546	1.031	3040982
50	.683	1980	4785064	1555	1.037	3078900
60	.659	1995	4872167	1563	1.042	3118185
70	.635	2009	4965202	1572	1.048	3158148
80	.611	2024	5064797	1582	1.055	3201968
90	.587	2040	5171672	1592	1.061	3247680
100	.563	2056	5286654	1604	1.069	3297824

Note: V_w = the compressive stress wave velocity in fresh water (V_w = 1500 M/sec at 20 degrees Celsius)

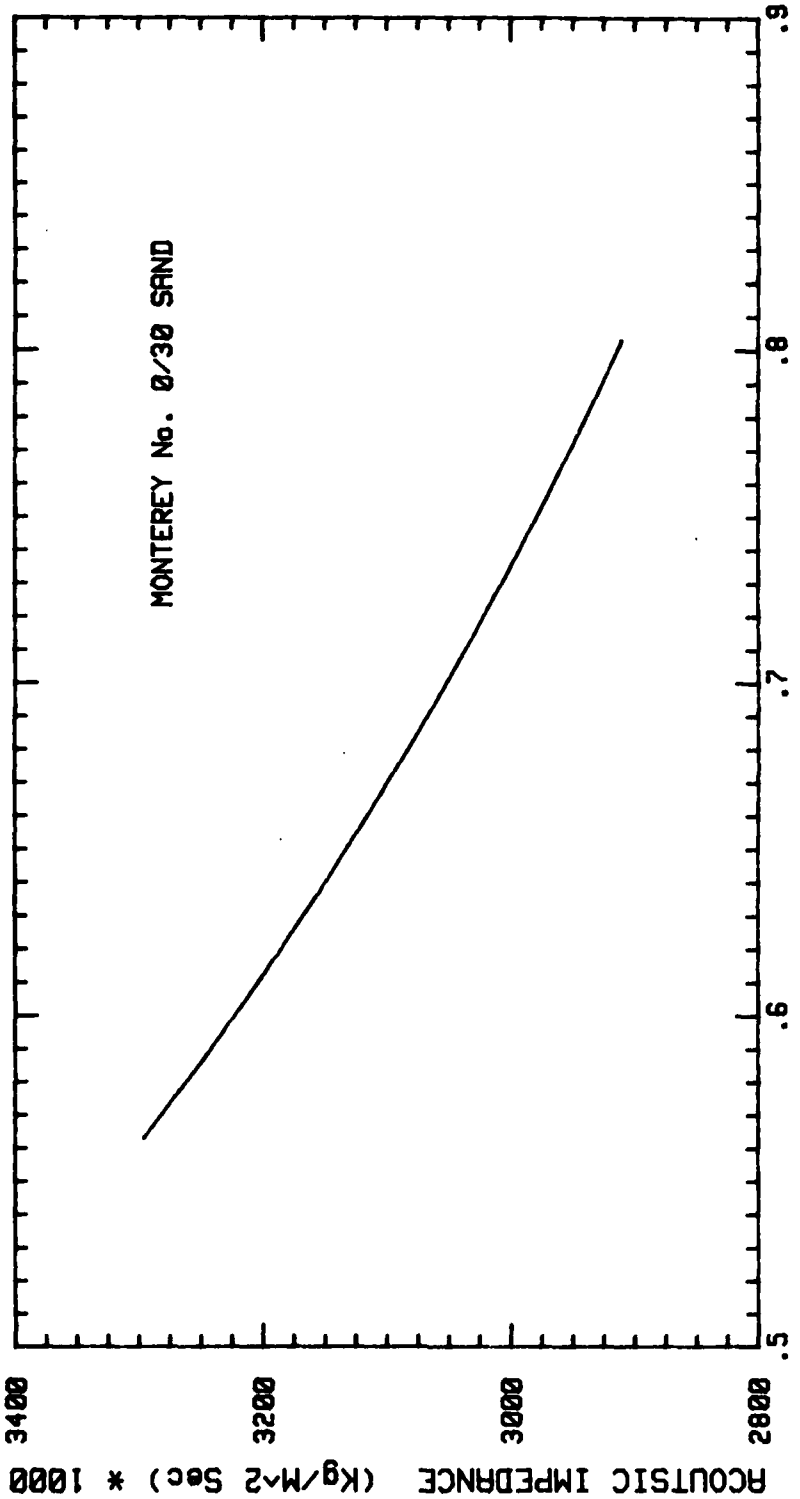

Figure 6.1 Acoustic Impedance as a Function of Void Ratio for Monterey No. 0/30 Sand

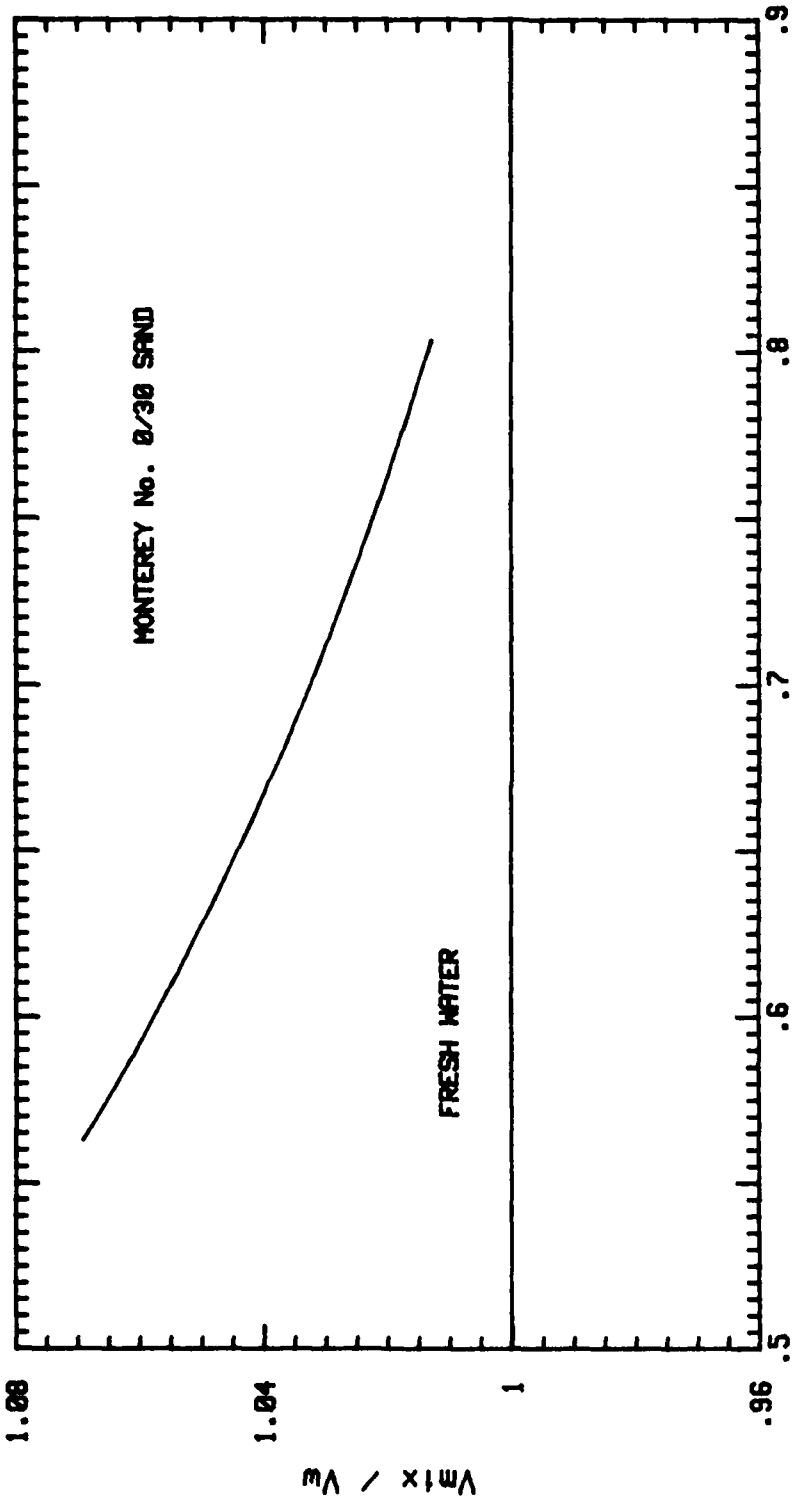

Figure 6.2 Compressive Stress Wave Propagation Velocity as a Function of Void Ratio for Monterey No. 0/30 Sand

particle velocity, V_{pk} , can be determined by using Equation 6.3 and rewriting Equation 2.19 in terms of the peak porewater pressure response, u_{pk} , as follows:

$$u_{pk} = (\rho_t V_{mix}) V_{pk} \qquad \text{(Eq. 6.4).}$$

The peak particle velocity, V_{pk} , can then be obtained by rearranging Equation 6.4:

$$V_{pk} = \frac{u_{pk}}{(\rho_t V_{mix})} \qquad \text{(Eq. 6.5)}$$

where, V_{mix} is calculated from Equation 6.3.

The peak compressive strain, ε_{pk} , can then be determined by combining Equations 2.19 and 6.5 as follows:

$$\varepsilon_{pk} = \frac{V_{pk}}{V_c} = \frac{u_{pk}}{\rho_t (V_c)^2} \qquad \text{(Eq. 6.6).}$$

Tables 6.2 through 6.12 summarize the results of this experimental investigation. In general, the experimental results show that liquefaction occurred when the sum of the peak compressive strains exceeded about $1x10^{-1}$ percent. When the sum of the peak compressive strains was less than about $1x10^{-2}$ percent, substantial porewater pressure increases did not occur. These values suggest threshold compressive strain limits for Monterey No. 0/30 sand at the relative densities and effective stresses examined in this experimental investigation.

It was possible to obtain porewater pressure ratios greater than one in several of the experimental results. Other researchers have

Table 6.2 Peak Porewater Pressures and Peak Compressive Strains for Monterey No. 0/30 Sand for Low Impact Stress Loading and D_r = '0%' Series

Test I.D.	σ'_o (KPa)	D_r (%)	Impact	u_{pk} (1) (KPa)	ε_{pk} (2) (%)	PPR (1)
S00X*	86	10.0	1	272	.00606	.329
			2	118	.00263	.457
			3	235	.00524	.743
			4	108	.00241	.735
			5	335	.00747	1.078
			6	145	.00323	1.134
S00X1	172	4.6	1	461	.01030	.774
			2	217	.00485	.902
			3	362	.00808	1.114
			4	443	.00990	1.220
			5	643	.01435	1.215
			6	588	.01314	1.219
S00X2	345	7.5	1	1222	.02734	.557
			2	588	.01316	.614
			3	670	.01498	.740
			4	244	.00546	.742
			5	516	.01154	.848
			6	917	.02052	.956
S00X4	690	7.5	1	81	.00182	.020
			2	543	.01214	.211
			3	208	.00466	.225
			4	670	.01498	.341
			5	561	.01256	.378
			6	2786	.06232	.873

Note: (1) Measured
(2) Calculated from Equation 5.6

Table 6.3 Peak Porewater Pressures and Peak Compressive Strains for Monterey No. 0/30 Sand for Low Impact Stress Loading and D_r = '20%' Series

Test I.D.	σ'_o (KPa)	D_r (%)	Impact	u_{pk} (1) (KPa)	ε_{pk} (2) (%)	PPR (1)
S20X*	86	29.2	1	353	.00764	.116
			2	516	.01116	.467
			3	316	.00685	.565
			4	362	.00783	.635
			5	634	.01371	.576
			6	379	.00821	.634
S20X1	172	27.9	1	524	.01136	.105
			2	416	.00903	.423
			3	452	.00981	.740
			4	469	.01017	.743
			5	226	.00490	.849
			6	452	.00981	.889
S20X2	345	29.6	1	661	.01429	.229
			2	489	.01057	.117
			3	1048	.02267	.132
			4	570	.01233	.213
			5	1276	.02760	.536
			6	914	.01977	.609
S20X4	690	28.8	1	380	.00823	.185
			2	441	.00956	.181
			3	425	.00921	.278
			4	543	.01175	.384
			5	516	.01117	.422
			6	272	.00588	.423

Note: (1) Measured
(2) Calculated from Equation 5.6

Table 6.4 Peak Porewater Pressures and Peak Compressive Strains for Monterey No. 0/30 Sand for Low Impact Stress Loading and D_r = '40%' Series

Test I.D.	σ'_o (KPa)	D_r (%)	Impact	u_{pk} (1) (KPa)	ε_{pk} (2) (%)	PPR (1)
S40X*	86	46.7	1	517	.01087	.421
			2	398	.00836	.567
			3	448	.00942	.527
			4	769	.01617	.898
			5	706	.01484	1.064
			6	996	.02093	1.222
S40X1	172	47.1	1	1692	.03554	.606
			2	353	.00742	.656
			3	416	.00875	.695
			4	1140	.02396	.881
			5	407	.00856	.935
			6	443	.00931	.996
S40X2	345	45.9	1	543	.01142	.062
			2	480	.01010	.114
			3	3061	.06444	.531
			4	751	.01581	.562
			5	878	.01848	.572
			6	2006	.04224	.691
S40X4	690	46.7	1	724	.01522	.345
			2	136	.00286	.347
			3	597	.01255	.447
			4	570	.01199	.488
			5	760	.01597	.527
			6	525	.01103	.551

Note: (1) Measured
(2) Calculated from Equation 5.6

Table 6.5 Peak Porewater Pressures and Peak Compressive Strains for Monterey No. 0/30 Sand for Low Impact Stress Loading and D_r = '60%' Series (First Set)

Test I.D.	σ'_o (KPa)	D_r (%)	Impact	u_{pk} (1) (KPa)	ε_{pk} (2) (%)	PPR (1)
S60X*	86		*****	No Data Retrieved		*****
S60X1	172	66.7	1	941	.01908	.164
			2	3592	.07281	.336
			3	796	.01614	.403
			4	796	.01614	.457
			5	896	.01815	.525
			6	480	.00973	.495
S60X2	345	67.5	1	652	.01319	.216
			2	823	.01666	.346
			3	335	.00678	.346
			4	832	.01684	.409
			5	751	.01520	.399
			6	4220	.08540	.560
S60X4	690	65.4	1	543	.01103	.335
			2	965	.01961	.369
			3	534	.01084	.450
			4	263	.00534	.439
			5	697	.01416	.495
			6	1339	.02721	.610

Note: (1) Measured
(2) Calculated from Equation 5.6

Table 6.6 Peak Porewater Pressures and Peak Compressive Strains for Monterey No. 0/30 Sand for Low Impact Stress Loading and D_r = '60%' Series (Second Set)

Test I.D.	σ'_o (KPa)	D_r (%)	Impact	u_{pk} (1) (KPa)	ε_{pk} (2) (%)	PPR (1)
S60X*	86	67.5	1	349	.00767	.464
			2	190	.00385	.606
			3	63	.00128	.562
			4	308	.00622	.747
			5	352	.00712	.741
			6	398	.00805	1.021
S60X1	172	67.1	1	380	.00769	.165
			2	244	.00494	.263
			3	498	.01008	.370
			4	724	.01466	.411
			5	652	.01320	.478
			6	643	.01302	.527
S60X2	345	66.3	1	290	.00587	.117
			2	724	.01469	.298
			3	416	.00845	.357
			4	507	.01028	.345
			5	950	.01927	.397
			6	1077	.02185	.504
S60X4	690	65.8	1	480	.00974	.185
			2	325	.00661	.208
			3	434	.00882	.225
			4	1149	.02333	.354
			5	1031	.02094	.410
			6	No Data Recorded this Impact		

Note: (1) Measured
(2) Calculated from Equation 5.6

Table 6.7 Peak Porewater Pressures and Peak Compressive Strains for Monterey No. 0/30 Sand for Low Impact Stress Loading and D_r = '80%' Series

Test I.D.	σ'_o (KPa)	D_r (%)	Impact	u_{pk} (1) (KPa)	ε_{pk} (2) (%)	PPR (1)
S80X*	86	85.8	1	796	.01554	.636
			2	914	.01784	.890
			3	561	.01095	.932
			4	1240	.02418	.960
			5	1575	.03072	1.060
			6	1057	.02066	1.073
S80X1	172	87.9	1	950	.01845	.532
			2	805	.01564	.619
			3	2151	.04178	.798
			4	579	.01125	.850
			5	878	.01705	.902
			6	878	.01705	.938
S80X2	345	85.4	1	697	.01361	.364
			2	715	.01396	.424
			3	914	.01785	.468
			4	643	.01255	.476
			5	733	.01431	.532
			6	661	.01290	.511
S80X4	690	86.3	1	715	.01394	.331
			2	416	.00812	.358
			3	597	.01164	.399
			4	389	.00758	.408
			5	470	.00917	.435
			6	461	.00899	.411

Note: (1) Measured
(2) Calculated from Equation 5.6

Table 6.8 Peak Porewater Pressures and Peak Compressive Strains for Monterey No. 0/30 Sand for High Impact Stress Loading and D_r = '0%' Series

Test I.D.	σ'_o (KPa)	D_r (%)	Impact	u_{pk} (1) (KPa)	ε_{pk} (2) (%)	PPR (1)
S00X1	172	4.6	1	5711	.12832	.662
			2	6674	.14997	.664
			3	6730	.15121	.664
			4	6219	.13974	.600
S00X2	345	3.8	1	6585	.14813	1.077
			2	6757	.15201	1.593
			3	6985	.15713	1.276
			4	5400	.12148	1.310
S00X4	690	5.8	1	2912	.06532	1.007
			2	2601	.05835	.994
			3	4693	.10527	.994
			4	4807	.10780	1.068

Note: (1) Measured
(2) Calculated from Equation 5.6

– No loadings were done for $\sigma'_o \approx 86$ KPa

Table 6.9 Peak Porewater Pressures and Peak Compressive Strains for Monterey No. 0/30 Sand for High Impact Stress Loading and D_r = '20%' Series

Test I.D.	σ'_o (KPa)	D_r (%)	Impact	u_{pk} (1) (KPa)	ε_{pk} (2) (%)	PPR (1)
S20X1	172	23.8	1	3817	.08332	1.015
			2	4580	.09999	.994
			3	5033	.10986	.994
			4	4750	.10369	.994
S20X2	345	27.5	1	5400	.11719	.994
			2	5655	.12271	.994
			3	5768	.12517	.828
			4	3421	.07425	.837
S20X4	690	22.1	1	5768	.12624	1.035
			2	6274	.13733	1.035
			3	6247	.13673	.994
			4	5089	.11139	.994

Note: (1) Measured
(2) Calculated from Equation 5.6

\- No loadings were done for σ'_o = 86 KPa

Table 6.10 Peak Porewater Pressures and Peak Compressive Strains for Monterey No. 0/30 Sand for High Impact Stress Loading and D_r = '40%' Series

Test I.D.	σ'_o (KPa)	D_r (%)	Impact	u_{pk} (1) (KPa)	ε_{pk} (2) (%)	PPR (1)
S40X1	172	44.2	1	4524	.09550	.504
			2	6647	.14032	.829
			3	6902	.14571	.829
			4	6619	.13974	.871
S40X2	345	46.7	1	4693	.09866	.834
			2	3676	.07727	.919
			3	4015	.08440	.929
			4	4269	.08974	.928
S40X4	690	46.7	1	3845	.08083	.787
			2	5570	.11708	.911
			3	4976	.10460	.952
			4	7212	.15160	1.076

Note: (1) Measured
(2) Calculated from Equation 5.6

\- No loadings were done for σ'_o = 86 KPa

Table 6.11 Peak Porewater Pressures and Peak Compressive Strains for Monterey No. 0/30 Sand for High Impact Stress Loading and D_r = '60%' Series

Test I.D.	σ'_o (KPa)	D_r (%)	Impact	u_{pk} (1) (KPa)	ε_{pk} (2) (%)	PPR (1)
S60X1	172	61.1	1	4156	.08504	.834
			2	5711	.11686	1.166
			3	3421	.07000	1.166
			4	4326	.08851	1.143
S60X2	345	64.2	1	6022	.12265	.662
			2	5117	.10422	.745
			3	5598	.11401	.909
			4	6019	.12259	.994
S60X4	690	62.5	1	5994	.12245	.624
			2	5681	.11607	.704
			3	5771	.11790	.787
			4	5599	.11438	.787

Note: (1) Measured
(2) Calculated from Equation 5.6

\- No loadings were done for σ'_o = 86 KPa

Table 6.12 Peak Porewater Pressures and Peak Compressive Strains for Monterey No. 0/30 Sand for High Impact Stress Loading and D_r = '80%' Series

Test I.D.	σ'_o (KPa)	D_r (%)	Impact	u_{pk} (1) (KPa)	ε_{pk} (2) (%)	PPR (1)
S60X1	172	81.3	1	6867	.13525	1.154
			2	4185	.08241	1.104
			3	5824	.11470	1.196
			4	6929	.13647	1.230
S60X2	345	83.3	1	8198	.16076	.332
			2	6985	.13697	.497
			3	7040	.13805	.564
			4	8453	.16576	.581
S60X4	690	83.8	1	5966	.11688	.627
			2	5737	.11240	.745
			3	5737	.11240	.794
			4	8371	.16400	.911

Note: (1) Measured
(2) Calculated from Equation 5.6

\- No loadings were done for σ'_o = 86 KPa

also reported porewater pressure ratios greater than one in the field (Kok,1977,1978b; Studer and Kok 1980, Fragaszy et al.,1983) and in the laboratory (Ruygrok and Van der Kogel,1980; Van der Kogel et al.,1981). A ratio greater than one suggests that the porewater pressure has exceeded the total stress and the effective stress has become negative. Theoretically, the porewater pressure ratio should not exceed a value of one. Part of the increase can be explained by the limitations of the electronic measurement and recording systems part can be attributed to random experimental errors. Beyond these reasons, it is not clear why the porewater pressure ratio should have exceeded unity.

C. Volume Decrease Potential and Relative Density

The increase in porewater pressure in a saturated soil occurs as a result of the tendency for the soil skeleton to decrease in volume under an applied load. As the volume decrease takes place, the pore spaces reduce in size and the porewater pressure increases. The potential for soil skeleton volume changes is usually quantified in terms of the relative density, D_r, which relates a soil's density to the maximum and minimum values. For soils having similar particle types, shapes and grain size distributions, the relative density is a useful index parameter that can be estimated in the field by a standard penetration test (ASTM D1586). Soils having relative densities below 65 percent have been observed to have a high liquefaction potential for both explosive-induced ground motions and seismic-induced ground motions. However, when the grain characteristics mentioned differ considerably, Lee and Fitton (1968) observed differing resistances to liquefaction at the same relative density for cyclic loading of

saturated sands. Therefore, in such cases the relative density data would not provide a useful indicator for estimating liquefaction potential. Ishihara and Watanabe (1976) explained the variations in liquefaction potential in terms of a soil's 'volume decrease potential (VDP).'

Figure 6.3 shows two elements of equal volumes for two different sands at the same relative density. The soil in diagram a, has a much smaller potential for volume decrease than does the soil in diagram b, even though they are at the same relative density. The potential for volume change can be observed by noting the change in void ratio possible for each soil to achieve 100 percent relative density packing. Based on their relative densities, both soils would appear to have the same potential for liquefaction. However, their void ratio data indicates the contrary. The larger the volume reduction possible, the larger the potential porewater pressure increase and potential for liquefaction. Ishihara and Watanabe (1976) present the volume decrease potential concept in equation form as:

$$VDP = e - e_{min} = (1 - D_r)(e_{max} - e_{min}) \qquad \text{(Eq. 6.7)}$$

where, e is the sample void ratio, e_{min} is the minimum void ratio, e_{max} is the maximum void ratio and D_r is the relative density as a decimal. The term $(e_{max} - e_{min})$ accounts for variations in sand types at similar relative densities. Whenever information on void ratio limits for a granular soil is available, it would be preferable to use Equation 6.7 to estimate volume change potential. However, in the field often the only available density information is the relative density. Two

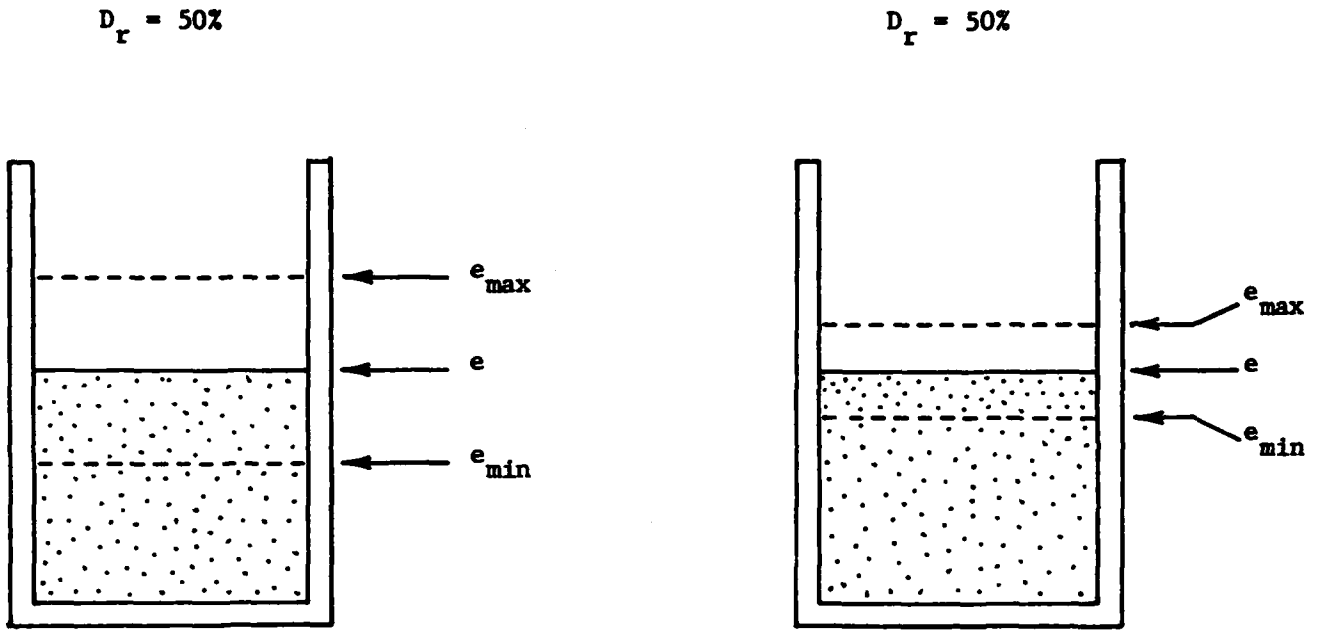

a.) Large Dilatancy

b.) Small Dilatancy

Figure 6.3 Illustration of Volume Decrease Potential Concept (Ishihara and Watanabe,1976)

models, one using relative density and one using the volume decrease potential concept, have been proposed and are presented in the next section.

D. Multivariate Regression Analysis

In conducting this experimental investigation, three important factors that influence liquefaction were examined. They were, the initial effective stress, the initial sample density and the applied compressive stress or compressive strain. To evaluate the influence of each factor, a statistical analysis of the data was performed to develop a model for predicting the porewater pressure ratio, PPR. The porewater pressure ratio , is a nondimensionalized factor defined as:

$$PPR = \frac{\sigma'_r - \sigma'_o}{\sigma'_o} = \frac{\Delta u}{\sigma'_o} = \frac{u_r}{\sigma'_o} \qquad \text{(Eq. 6.8)}$$

where,

σ'_r = the residual effective stress after the passage of the compressive stress wave,

σ'_o = the initial effective stress,

Δu = the change in porewater pressure and equal to the change in effective stress, and

u_r = the residual excess porewater pressure.

In nondimensionalized form, the changes in porewater pressure due to loading of soils having differing initial effective stresses and relative densities can be compared. The results from laboratory and field investigations can also be compared.

1. Porewater Pressure Ratio Predictor Model

One method of evaluating liquefaction potential as a numerical result, is to examine the porewater pressure ratio increase from an applied loading. The larger the ratio becomes the closer the soil is to being liquefied. When the soil has liquefied, the porewater pressure ratio equals unity. The ratio can be related to the initial effective stress, initial sample density and the sample strain from the applied compressive loading.

Considering these factors, a series of predictor models was investigated to find one that would be intuitively correct from an engineering standpoint and would also fit the data well statistically. Two models were developed, one including relative density and one including the volume decrease potential which would provide flexibility in applying the models to other laboratory and field studies. A linear, multivariate, regression analysis was performed using a model of the form:

$$\log (PPR) = \log a + b \log c + d \log f + g \log h \quad \text{(Eq. 6.9)}$$

where,

PPR = the porewater ratio, defined as the ratio of the residual excess porewater pressure to the initial effective stress,

a = the constant coefficient,

c = the initial effective stress in KPa,

f = the initial relative density in percent, or the volume decrease potential,

h = the sum of the applied peak compressive strains in percent, and

b, d, g = the exponents for each model.

The linear, multivariate, regression analysis was performed using the program 'MINITAB' (Ryan et al.,1976,1982). Table 6.13 presents the six models used in analyzing the data and Table 6.14 gives two selected statistical parameters used to evaluate the models. The two parameters are the standard error of estimate, S, and the coefficient of determination, R^2. The standard error of estimate is a measure of how much the measured value deviates from the average value predicted by the regression equation. In other words, S is a measure of the accuracy of the predictions. The smaller the deviation the closer the equation predicts the data. If the standard error of estimate was zero, then the equation would match the data exactly. The R^2 value is a measure of how much of the variation in the data is explained by the regression equation. The higher the R^2 value, the closer the prediction of observed behavior. If the coefficient of determination was 100 percent, then all of the data could be explained by the regression equation. Based on the results of the statistical analysis presented in Table 6.14, two models were selected. In terms of the volume decrease potential, the porewater pressure ratio predictor model has the following form:

$$PPR = (11.39)\ (\Sigma\varepsilon_{pk})^{.321}\ (\sigma'_o)^{-.305}\ (VDP)^{.149} \qquad \text{(Eq. 6.10)}$$

where, ε_{pk} is in percent and σ'_o is in KPa. In terms of relative density, the porewater pressure ratio predictor model has the following form:

Table 6.13 Experimental Porewater Pressure Ratio Predictor Models

Model
(a) $PPR = (11.76)\left[\frac{(\Sigma\, \varepsilon_{pk})\,(VDP)}{\sigma'_o}\right]^{.278}$
(b) $PPR = (16.95)\left[\frac{\Sigma\, \varepsilon_{pk}}{(\sigma'_o)\,(D_r)}\right]^{.277}$
(c) $PPR = (9.41)\,(\Sigma\, \varepsilon_{pk})^{.315}\,(\frac{VDP}{\sigma'_o})^{-.238}$
(d) $PPR = (12.71)\,(\Sigma\, \varepsilon_{pk})^{.325}\,(\sigma'_o\, D_r)^{-.232}$
(e) $PPR = (11.39)\,(\Sigma\, \varepsilon_{pk})^{.321}\,(\sigma'_o)^{-.305}\,(VDP)^{.149}$
(f) $PPR = (16.30)\,(\Sigma\, \varepsilon_{pk})^{.331}\,(\sigma'_o)^{-.308}\,(D_r)^{-.179}$

Note: - ε_{pk} and D_r are in percent
- σ'_o is in KPa

Table 6.14 Coefficient of Determination and Standard Error of Estimate for Porewater Pressure Ratio Predictor Models in Table 6.13

Model	R^2 (%)	S
a	55.0	.206
b	61.1	.193
c	57.6	.207
d	63.8	.191
e	59.8	.205
f	65.9	.187

Note: R^2 = the coefficient of determination
S = the standard error of estimate

$$PPR = (16.30)\ (\Sigma\varepsilon_{pk})^{.331}\ (\sigma'_o)^{-.308}\ (D_r)^{-.179} \quad \text{(Eq. 6.11)}$$

where, D_r and ε_{pk} are both in percent, and σ'_o is in KPa.

The equations presented in Table 6.13 are the statistical best fits for all the experimental data combined. The ε_{pk} term represents the total strain applied to the sample at a given impact loading including the strain from previous impacts. Therefore, the $\Sigma\varepsilon_{pk}$ quantity is a cumulative strain value for a sample. Equation 6.11 represents the statistical best fit of all the models examined and has been selected for use in the analysis presented in this chapter. Figure 6.4 shows the variation of residuals about the regression line for Equation 6.11. Tables 6.15 and 6.16 give compressive strains predicted by Equation 6.11 for a porewater pressure ratio of 0.25 and 1.0 respectively.

It would be useful if the summation of measured peak compressive strains could be used to represent the strain from a series of successive impact loadings or a single large impact loading. To investigate this, the two models given by Equations 6.10 and 6.11 were evaluated considering only the data from the first impact loadings from each data set. In terms of the volume decrease potential, the porewater pressure ratio predictor model has the following form:

$$PPR = (10.90)\ (\varepsilon_{pk})^{.321}\ (\sigma'_o)^{-.305}\ (VDP)^{.149} \quad \text{(Eq. 6.12)}$$

where, ε_{pk} is in percent and σ'_o is in KPa. In terms of relative density, the porewater pressure ratio predictor model has the following form:

$$PPR = (16.00)\ (\varepsilon_{pk})^{.331}\ (\sigma'_o)^{-.308}\ (D_r)^{-.179} \quad \text{(Eq. 6.13)}$$

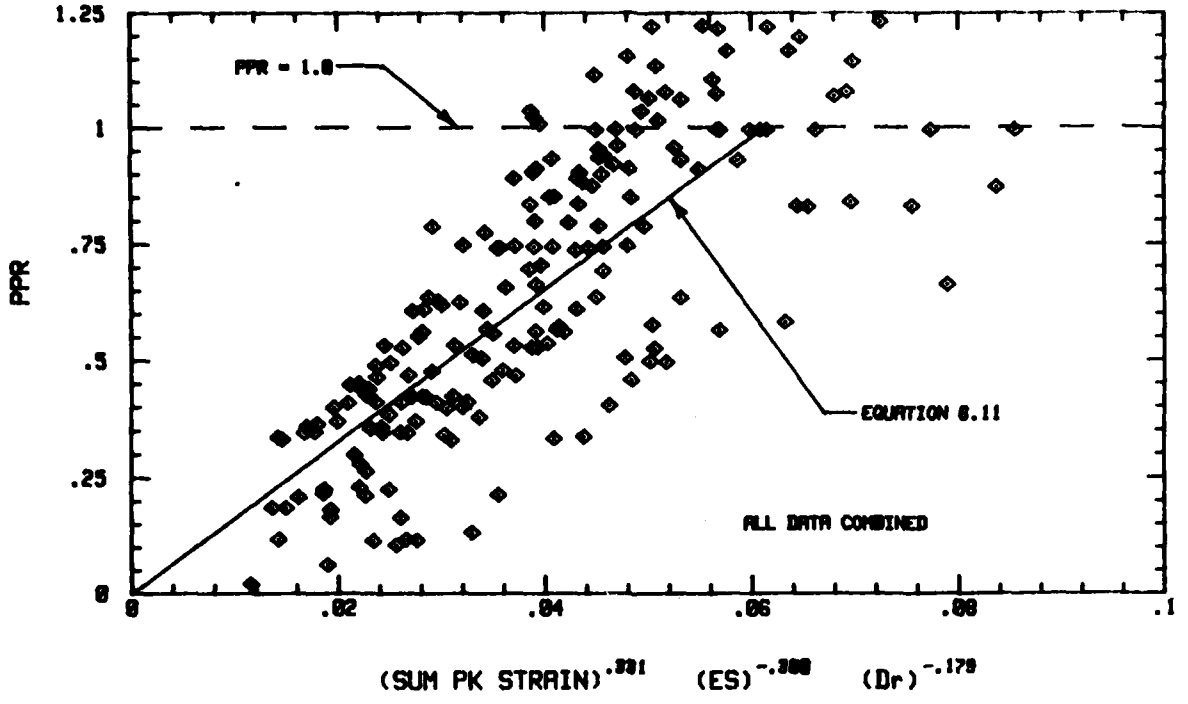

Figure 6.4a. Variation of Residuals About the Regression Line for Equation 6.11.

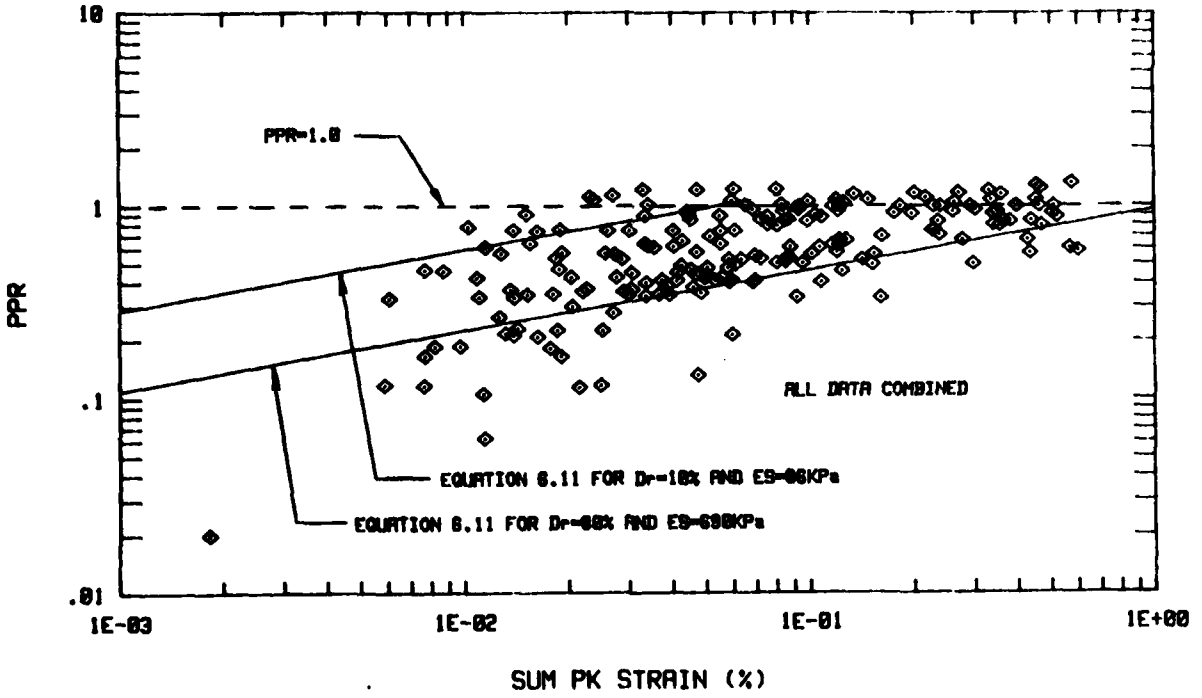

Figure 6.4b. Porewater Pressure Ratio for Equation 6.11 as a Function of Density and Effective Stress.

Table 6.15 Compressive Strains Predicted by Equation 6.11 for PPR = 0.25 (Monterey No. 0/30 Sand)

	D_r (%)				
σ'_o (KPa)	10	20	40	60	80
86	.00072	.00105	.00153	.01908	.00223
172	.00138	.00201	.00292	.00364	.00425
345	.00264	.00384	.00558	.00695	.00812
690	.00503	.00731	.01064	.01325	.01548

Note: Predicted strains are in percent

Table 6.16 Compressive Strains Predicted by Equation 6.11 for PPR = 1.0 (Monterey No. 0/30 Sand)

	D_r (%)				
σ_o' (KPa)	10	20	40	60	80
86	.04772	.06942	.10098	.12574	.14691
172	.09094	.13230	.19247	.23966	.27800
345	.17381	.25285	.36783	.45801	.53511
690	.33127	.48191	.70107	.87294	1.01989

Note: Predicted strains are in percent

where, D_r and ε_{pk} are both in percent, and σ'_o is in KPa. The standard error of estimate for Equation 6.12 was 0.193 and the standard error of estimate for Equation 6.13 was 0.186.

In comparing Equations 6.10 and 6.11 with 6.12 and 6.13, it can be seen that they vary slightly in their coefficients and that the standard deviations are nearly the same. This leads to the conclusion that Equations 6.10 and 6.11 are valid for use with the compressive strain from a single large loading or from a succession of smaller loadings leading to the same total peak compressive strain value.

Intuitively, these four Equations, 6.10, 6.11, 6.12 and 6.13 correctly represent the observed behavior in that the porewater pressure ratio varied inversely with the initial effective stress and relative density, and directly with the volume decrease potential. As was shown in Figures 5.4, 5.5, 5.6 and 5.7 and Table 5.2, the soil skeleton stiffness also varied directly with increasing initial effective stress and relative density and inversely with volume decrease potential.

2. Physical Interpretation of Model

The initial attempt of the model was to predict the porewater pressure ratio as a function of peak compressive strain and relative density or volume decrease potential for each data set at a given initial effective stress. The results from the initial models indicated a definite trend with variations in the initial effective stress. However, these results gave four separate equations of the same form with different constants and were only applicable to the four particular initial effective stresses examined. Therefore, a more

general form of the model was developed to include the initial effective stress as a variable.

The variation in initial effective stress and initial sample density can be viewed as an extension of the relationships into a third dimension as is shown in Figure 6.5. In the figure, it can be seen that a three-dimensional curved planar surface extends along the third axis. The surface does not have constant end points along the extended edges. For a given initial effective stress and initial density, the three-dimensional surface becomes a plane whose abscissa is the peak compressive strain and ordinate is the porewater pressure ratio.

E. Finite Difference Approximation

A finite difference solution approximation was investigated to simulate the laboratory measured pressure-time histories using the equations for a one-dimensional, confined compressive loading. Equations were developed to model both the transient and long-term porewater pressure response in the soil mass. These equations are based on the developments presented by Biot (1956a,b,1962) and a general approach given by Ishihara (1967). The finite difference recursion formulas used were adapted from Biggs (1964) for a single degree of freedom, viscoelastic system. Appropriate modifications were made to the solution to model the soil as a two-phase material and to include the experimental boundary conditions.

1. Rheologic Model

The rheologic model consists of masses, springs and dashpots used to represent the applied compressive stress wave propagation through

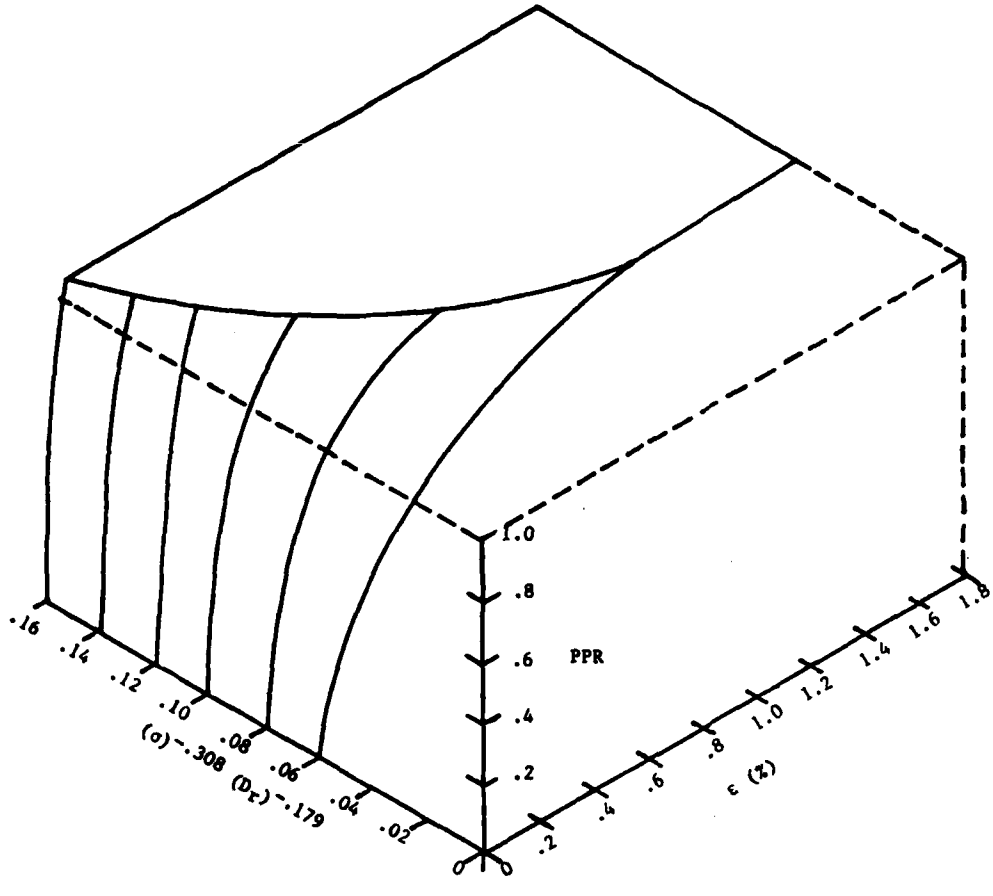

Figure 6.5 Illustration of Three-Dimensional Porewater Pressure Ratio Predictor Model

the confining pressure tube, the saturated soil sample and the PVC momentum trap. Figure 6.6 shows a schematic of the mass-spring-dashpot system. The confining tube was treated as a constrained 'bar' of water having three mass elements connected by linear elastic springs whose stiffness corresponded to the bulk modulus of water. The PVC momentum trap was treated in the same way as the confining tube using two elements and the bulk modulus for PVC.

In modeling the soil-water system, consideration was given to including the stiffness of the mixture, the stiffness of the soil skeleton and material damping. The bulk modulus of the mixture was evaluated as described in section A of this chapter. The soil skeleton was treated in two parts, with a separate value for loading and unloading to account for permanent deformations of the soil skeleton. The skeleton stiffness values were determined from one-dimensional, confined compression loadings of dry Monterey No.0/30 sand as described in section A, part 5 of Chapter V. A viscous damping term was also included to account for the compressive stress wave energy dissipation due to system and material damping.

2. Finite Difference Solution Formulation

The finite difference approximation uses Biot's (1962) theory for stress wave propagation in a porous elastic medium. Biot's theory was coupled with a soil skeleton model that decreases in volume whenever the applied compressive loading produces a compressive strain that exceeds a threshold value.

Biot's modified general equations for a porous medium have the following forms for the component parts:

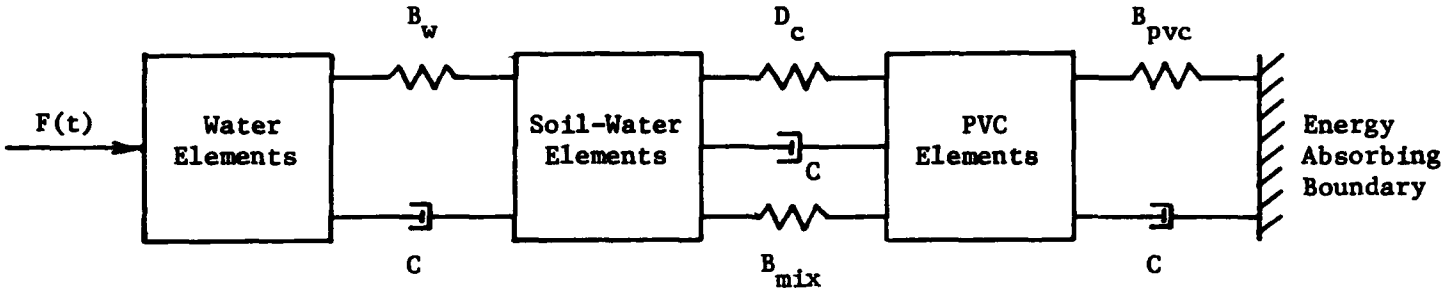

F(t) = Applied Force as a Function of Time
B_w = Bulk Modulus of Water
B_{pvc} = Bulk Modulus of PVC
D_c = Constrained Modulus of the Soil Skeleton (Loading or Unloading)
B_{mix} = Bulk Modulus of the Soil-Water Mixture
C = System Damping

In The Model There Are:

3 Water Elements
6 Soil-Water Elements
3 PVC Elements

Figure 6.6 Rheologic Model Used in Finite Difference Approximation

a. overall system equilibrium:

$$\sigma_{ij,j} + \rho_t g_i = \rho_t \ddot{u}_i + \rho_w \ddot{w}_i \qquad \text{(Eq. 6.14)}$$

b. liquid equilibrium:

$$-P_{,i} + \rho_w g_i = \rho_w \ddot{u}_i + \frac{\beta}{n} \rho_w \ddot{w}_i + \frac{\rho_w g_i \dot{w}_i}{k} \qquad \text{(Eq. 6.15)}$$

c. porous solid equilibrium:

$$\sigma'_{ij,j} = \sigma_{ij,j} + \delta_{i,j} P_{,i} \qquad \text{(Eq. 6.16)}$$

d. stress-strain (fluid and porous solid):

$$\varepsilon_{ij} = \frac{1}{2} (u_{i,j} + u_{j,i}) \qquad \text{(Eq. 6.17)}$$

$$\theta = w_{i,i} \qquad \text{(Eq. 6.18)}$$

where,

$\sigma_{ij,j}$ = the total stress tensor,

ρ_t = the total mass density,

g_i = the components of the gravitational constant,

$\ddot{u}_i$ = the acceleration vector of the solid skeleton,

ρ_w = the mass density of the fluid,

$\dot{w}_i$ = the velocity vector of the fluid,

$\ddot{v}_i$ = the acceleration vector of the fluid,

β = a kinetic energy correction factor,

n = the porosity of the soil skeleton,

k = Darcy's coefficient of permeability,

$\sigma'_{ij,j}$ = the effective stress tensor,

$P_{,i}$ = the porewater pressure tensor,

$\delta i,j$ = the Kronecker delta,

ε_{ij} = the strain tensor of the solid skeleton,

u = the displacement vector of the solid skeleton,

Θ = the variation of the fluid content

$w_{i,i}$ = the displacement vector of the water with respect to the solid skeleton

For the case of one-dimensional strain with undrained loading conditions, Equations 6.14, 6.15 and 6.16 reduce to:

$$\frac{d\sigma}{dx} = \rho_t \ddot{u} \qquad \text{(Eq. 6.19)}$$

$$-\frac{dP}{dx} = \rho_w \ddot{u} \qquad \text{(Eq. 6.20)}$$

$$\sigma' = \sigma + P \qquad \text{(Eq. 6.21).}$$

The stress-strain conditions (Equations 6.17 and 6.18) reduce to:

$$\Delta\sigma = (B_{mix} + D_c)\,\Delta\varepsilon^T \qquad \text{(Eq. 6.22)}$$

$$\Delta\sigma' = \Sigma(D_c \ \Delta\varepsilon^p) \qquad \text{(Eq. 6.23)}$$

where,

D_c = the constrained modulus for loading or unloading of the soil skeleton,

B_{mix} = the bulk modulus of the soil-water mixture calculated from Equation 6.2,

$\Delta\varepsilon^T$ = the volumetric strain of the mix, and

$\Delta\varepsilon^p$ = the inelastic volumetric strain of the mix.

The following recurrence formulas presented by Biggs (1964), were used to evaluate the terms for displacement, velocity and acceleration:

a. displacement (y):

$$y^{(s+1)} = 2y^{(s)} - y^{(s-1)} + \ddot{y}^{(s)} \ (\Delta t)^2 \qquad \text{(Eq. 6.24)}$$

b. velocity ($\dot{y}$):

$$\dot{y}^{(s)} = \frac{y^{(s)} - y^{(s-1)}}{\Delta t} + \ddot{y}^{(s)} \ \frac{\Delta t}{2} \qquad \text{(Eq. 6.25)}$$

c. acceleration ($\ddot{y}$):

$$\ddot{y}^{(s)} = \frac{\left[\frac{F^{(s)} - K^{(s)} - (C)(y^{(s)} - y^{(s-1)})}{\Delta t}\right]}{M^{(s)} + C\,(\Delta t)^2} \qquad \text{(Eq. 6.26)}$$

where,

s = the time at any step in the iteration,

Δt = the time increment for the iteration,

K = the equivalent spring stiffness,

C = the viscous damping coefficient,

F = the applied force, and

M = the mass.

The viscous damping coefficient, C, was calculated for the system at each time step from:

$$C = (2)\,(D)\,\left[(K)\,(M)\right]^{0.5} \qquad \text{(Eq. 6.27).}$$

The damping ratio, D, was evaluated from the pressure-time history data of the laboratory experiments and had an average value of 0.0167.

F. Comparison of Solution With Experimental Results

The finite difference approximation was used to compare a theoretical analysis with observed behavior in the laboratory. A series of computer runs using a triangular loading pulse was performed for the first impact loadings of two laboratory samples at two

different initial effective stresses. The initial relative densities used were 40 and 80 percent and the initial effective stresses used were 172 KPa and 690 KPa. The respective loading and unloading constrained moduli were obtained from Figures 5.4, 5.5, 5.6 and 5.7. The moduli were determined at strains corresponding to the experimental laboratory results and their numerical values are given in Table 5.2.

Figures 6.7, 6.8, 6.9, and 6.10 show the results of the finite difference analysis. In comparing these figures with the experimental pressure-time histories presented in section D of Chapter V, similar behavior is evident for the porewater pressure response both during and after the applied loading. There is also a marked increase in the residual excess porewater pressure. Table 6.17 presents a comparison of the finite difference approximation results and the experimental results. Variations in the results can be attributed to the use of a static constrained modulus for the soil skeleton ibn the model and laboratory boundary conditions that could not be exactly simulated by the finite difference approximation.

G. Application of Results

In Chapter II, several empirical scaling equations were presented for predicting the peak compressive stress developed by a buried charge as a function of radial distance from the detonation point and charge weight. Equations 6.4, 6.5 and 6.6 developed the relationship between peak compressive strain and peak compressive stress. Since the peak compressive strain can be estimated, the statistical models developed in this experimental investigation can be used to approximate the resulting porewater pressure ratio as a function of effective stress

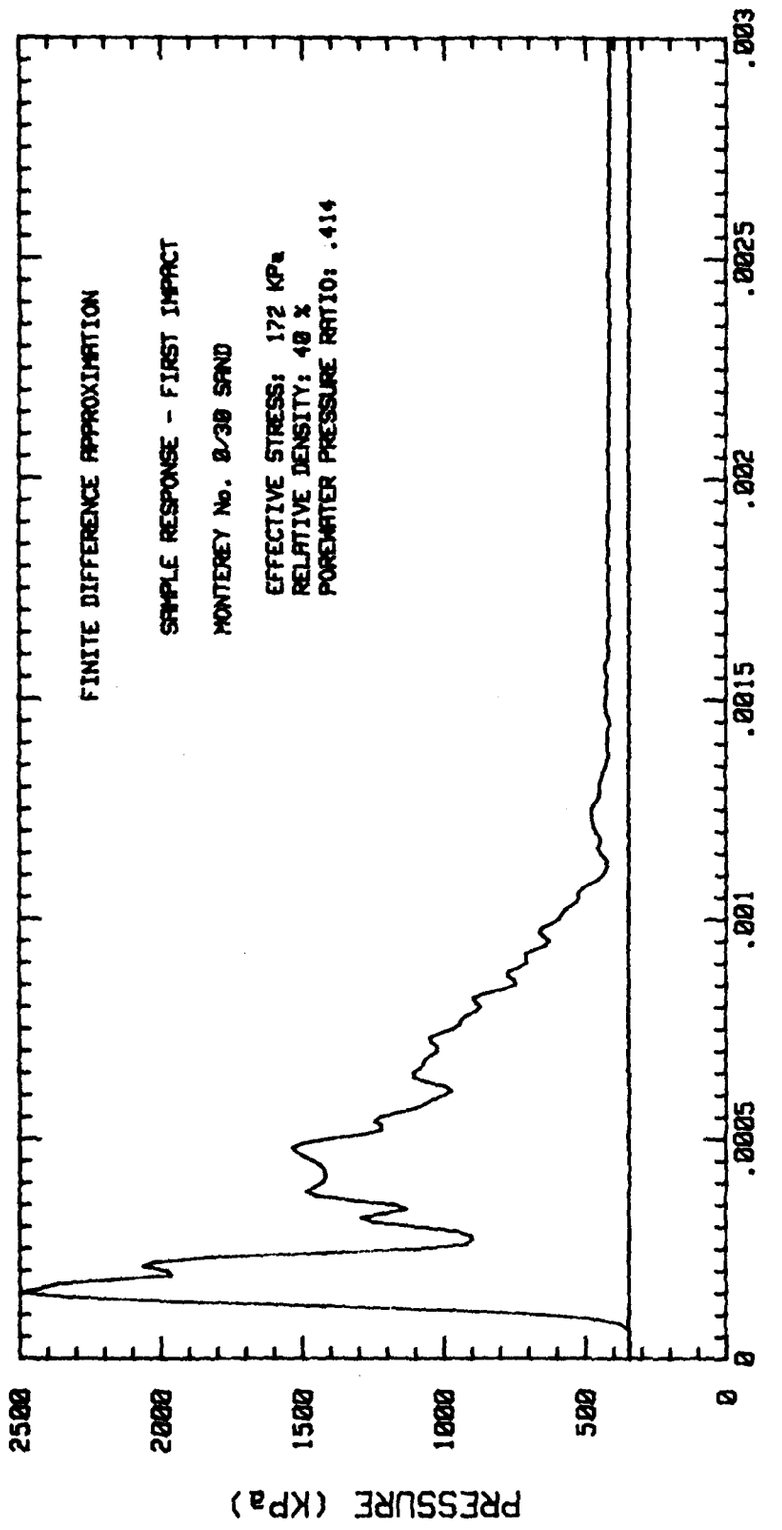

Figure 6.7 Sample Porewater Pressure Response as Predicted by Finite Difference Approximation for Monterey No. 0/30 Sand at σ_o' = 172 KPa and D_r = 40% (First Impact)

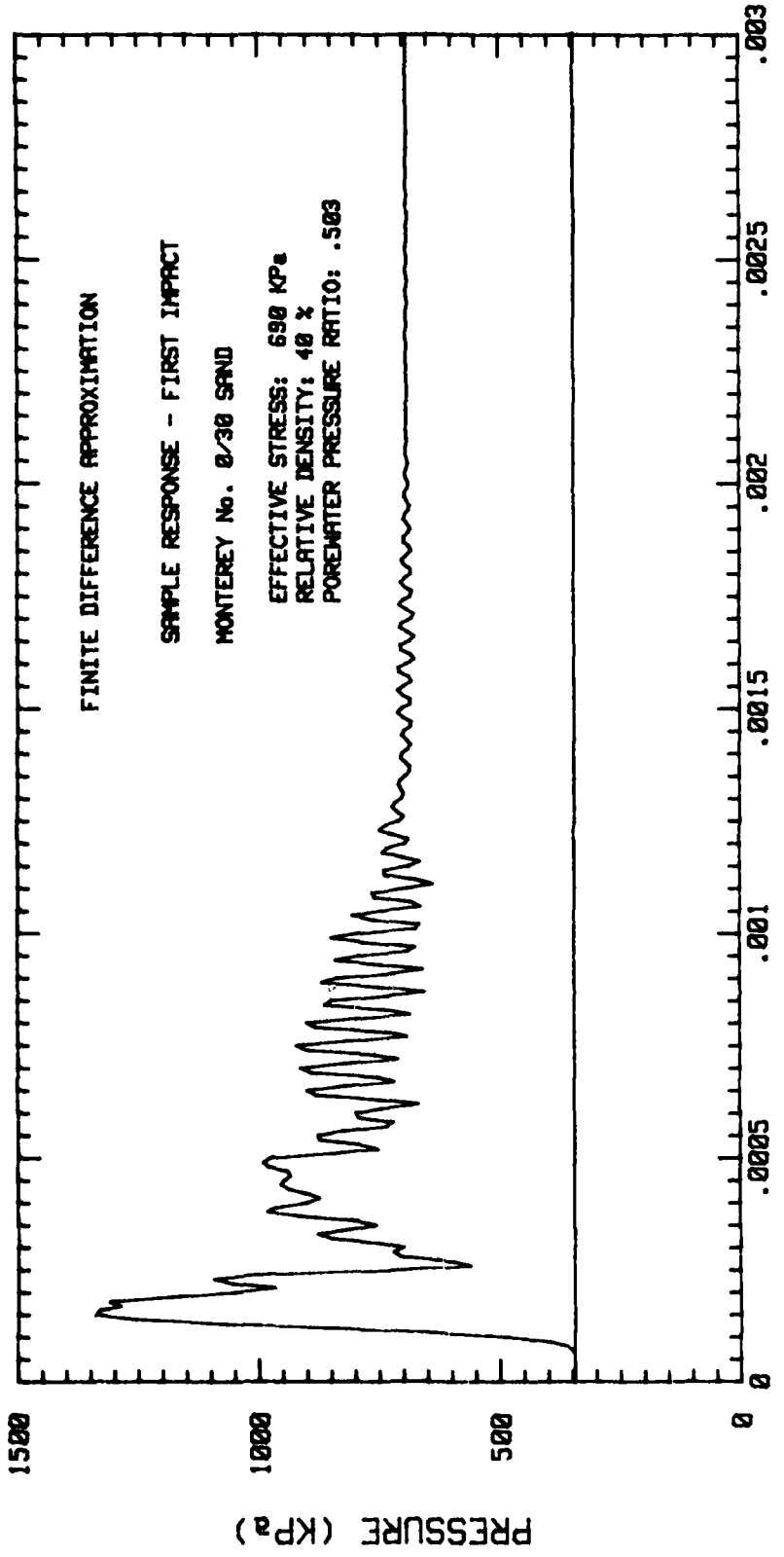

Figure 6.8 Sample Porewater Pressure Response as Predicted by Finite Difference Approximation for Monterey No. 0/30 Sand at σ_o' = 690 KPa and D_r = 40% (First Impact)

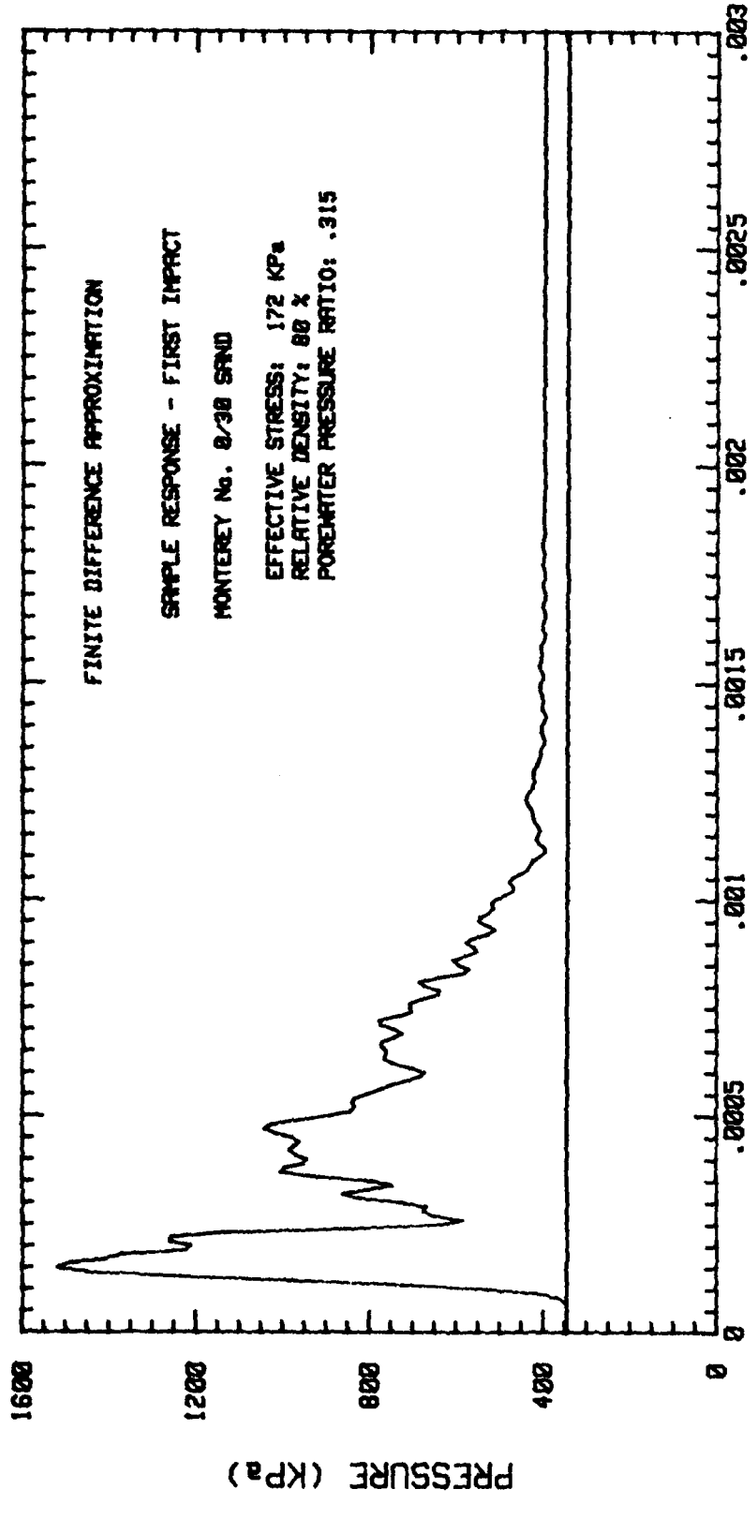

Figure 6.9 Sample Porewater Pressure Response as Predicted by Finite Difference Approximation for Monterey No. 0/30 Sand at σ_o' = 172 KPa and D_r = 80% (First Impact)

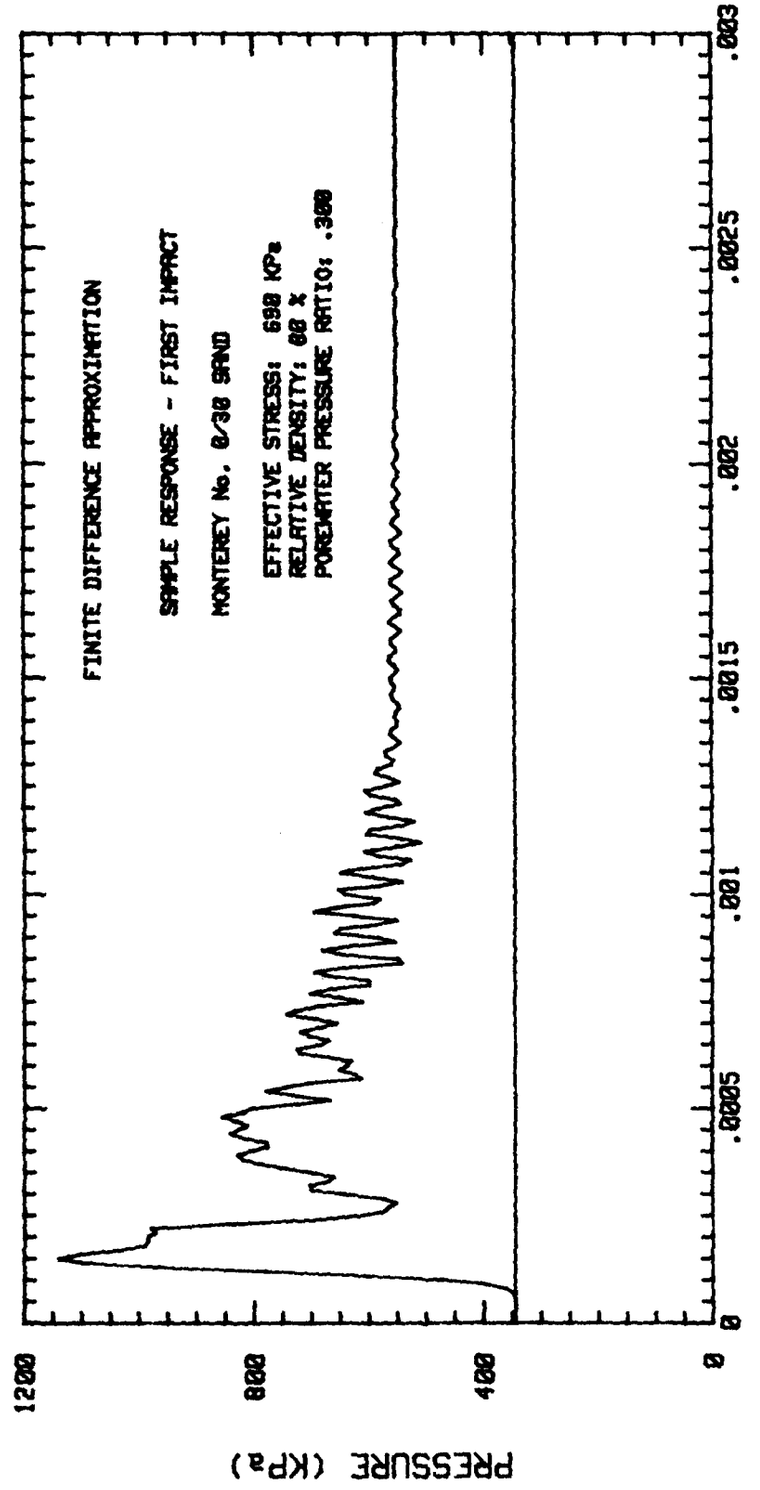

Figure 6.10 Sample Porewater Pressure Response as Predicted by Finite Difference Approximation for Monterey No. 0/30 Sand at σ_o' = 690 KPa and D_r = 80% (First Impact)

AD-A173 137 BLAST INDUCED LIQUEFACTION POTENTIAL AND TRANSIENT POREWATER PRESSURE RES (U) COLORADO STATE UNIV FORT COLLINS DEPT OF CIVIL ENGINEERING W A CHARLIE ET AL 1/3

UNCLASSIFIED 15 OCT 85 AFOSR-TR-86-0946 AFOSR-80-0260 F/G 8/13 NL

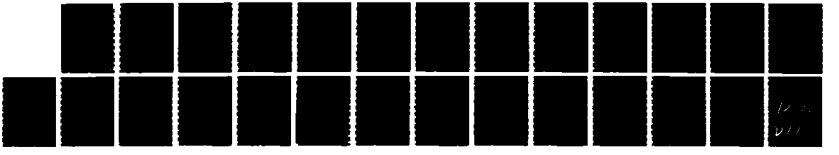

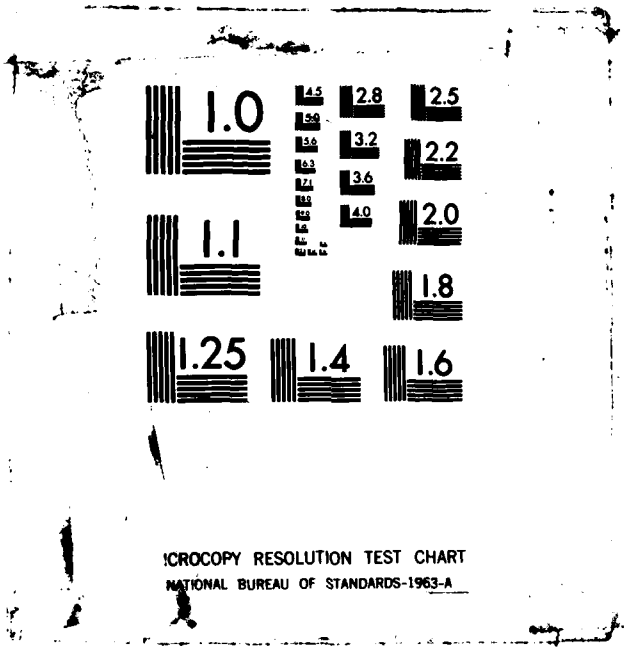
1.0
1.1
1.25
1.4
1.6
1.8
2.0
2.2
2.5
2.8
3.2
3.6
4.0
ICROCOPY RESOLUTION TEST CHART
NATIONAL BUREAU OF STANDARDS-1963-A

Table 6.17 Comparison of Porewater Pressure Ratios Predicted by Finite Difference Approximation and Equation 6.11 with Experimental Results for Monterey No. 0/30 Sand

D_r (%)	σ'_o (KPa)	σ_{pk} (KPa)	$PPR^{(1)}$	$PPR^{(2)}$	$PPR^{(3)}$
40	172	1476	.606	.414	.564
40	690	683	.345	.503	.285
80	172	800	.532	.315	.400
80	690	552	.331	.300	.231

Note: (1) Experimental Results
(2) Predicted by Finite Difference Analysis
(3) Predicted by Equation 6.11

and soil density. This provides a way to estimate the extent of regions of porewater pressure increases at distances outward from a buried charge. An example using this approach follows.

Example

To estimate the peak compressive strains from a buried charge, it was necessary to use one of the peak particle velocity scaling laws given in Chapter II with Equation 6.6. For this example, the scaling law selected was Equation 2.18 (Drake and Little, 1983). When Equation 2.18 is substituted into Equation 6.6, the following equation for peak compressive strain is obtained:

$$\varepsilon_{pk} = \frac{(5.6)\ (f)\ \left(\frac{R}{W^{1/3}}\right)^{-2.35}}{V_c} \qquad \text{(Eq. 6.28)}$$

where all terms are as previously defined.

If a charge placement depth of 5 meters is used, Equation 2.3 gives a charge weight of 7 kilograms to insure a contained explosion. For this depth and weight, the scaled depth of burst is 2.6 $M/Kg^{1/3}$ and since this is greater than 0.56 $M/Kg^{1/3}$ (Figure 2.3), the groundshock coupling factor, f, becomes 1.0. Assuming a saturated soil, the compressive stress wave velocity, V_c, can be taken as 1500 meters per second. Substituting these values into Equation 6.28 gives:

$$\varepsilon_{pk} = (0.086)\ (R)^{-2.35} \qquad \text{(Eq. 6.29)}$$

for a confined 7 kilogram charge in a saturated soil.

The porewater pressure ratio predictor model chosen for this example is that given by Equation 6.11. Two relative densities were used, 40 and 80 percent, and the effective stress and peak compressive strains were varied with the radial distance, R, from the buried charge depth. When the strains calculated from Equation 6.28 are used in Equation 6.11, the result gives the porewater pressure ratio as a function of depth and horizontal distance from the charge.

Since the porewater pressure ratio variation has been determined at points away from the buried charge depth, a series of contours can be drawn. These contours are symmetric about the charge location. Figures 6.11 and 6.12 show the porewater pressure ratio contours for the two relative densities examined. These results estimate the zones of potential porewater pressure increase. Figure 6.13 compares the maximum radius of liquefaction near the ground surface as predicted by the approach presented and Equation 2.7. The differences in the estimated maximum radius of liquefaction can be attributed to variations in soil type and boundary conditions between the experimental investigation and the field tests.

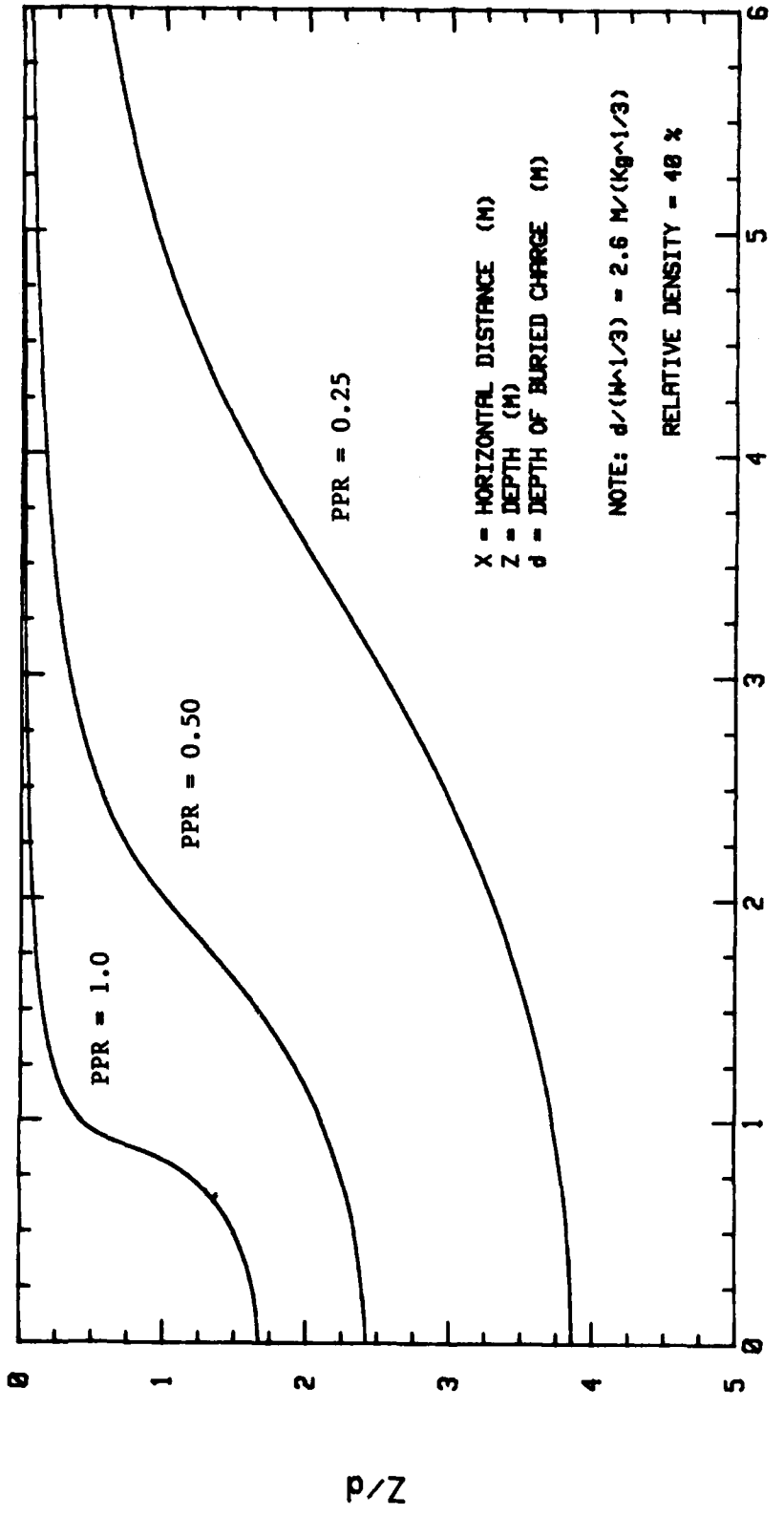

Figure 6.11 Porewater Pressure Ratio Contours for Monterey No. 0/30 Sand at D_r = 40%

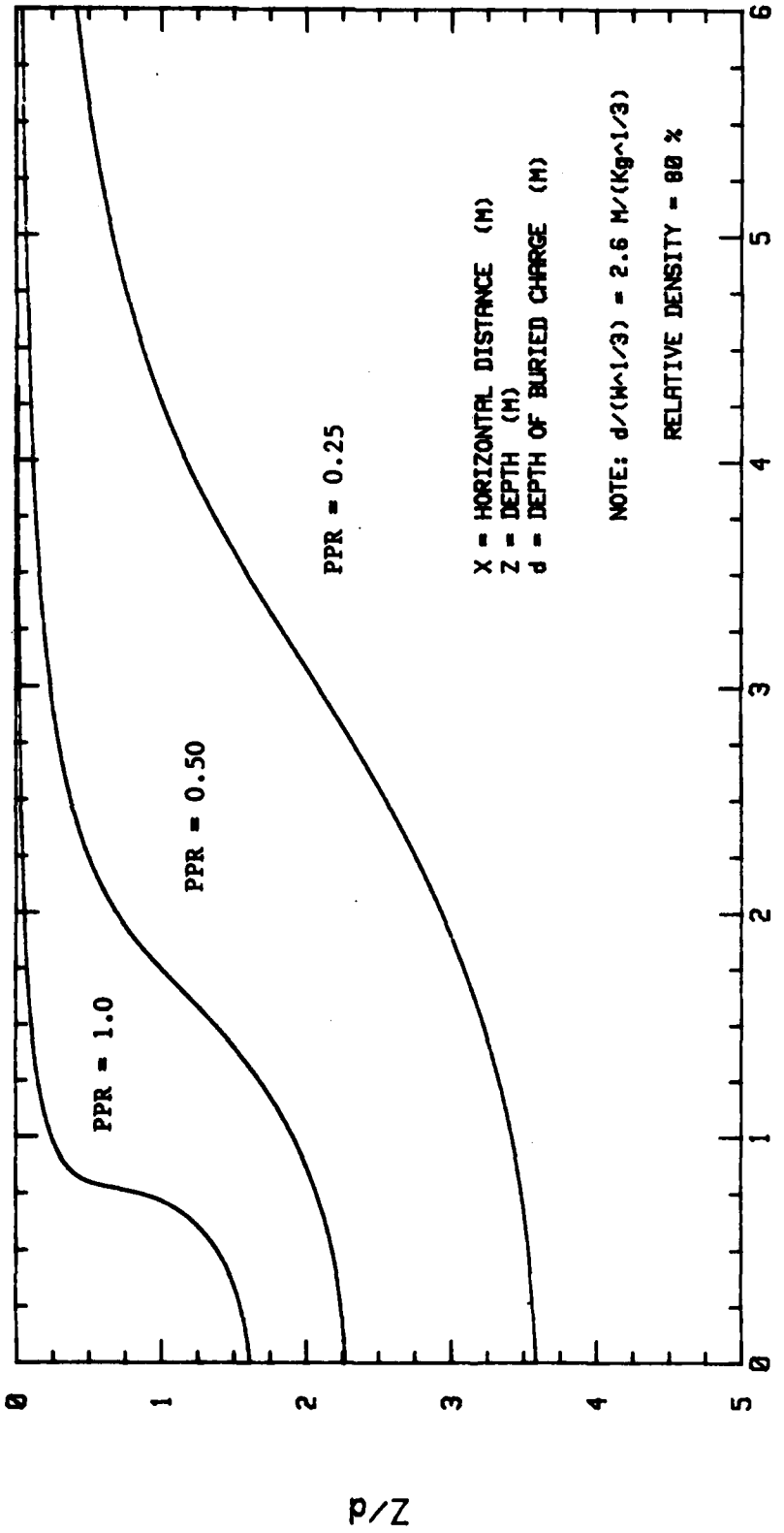

Figure 6.12 Porewater Pressure Ratio Contours for Monterey No. 0/30 Sand at D_r = 80%

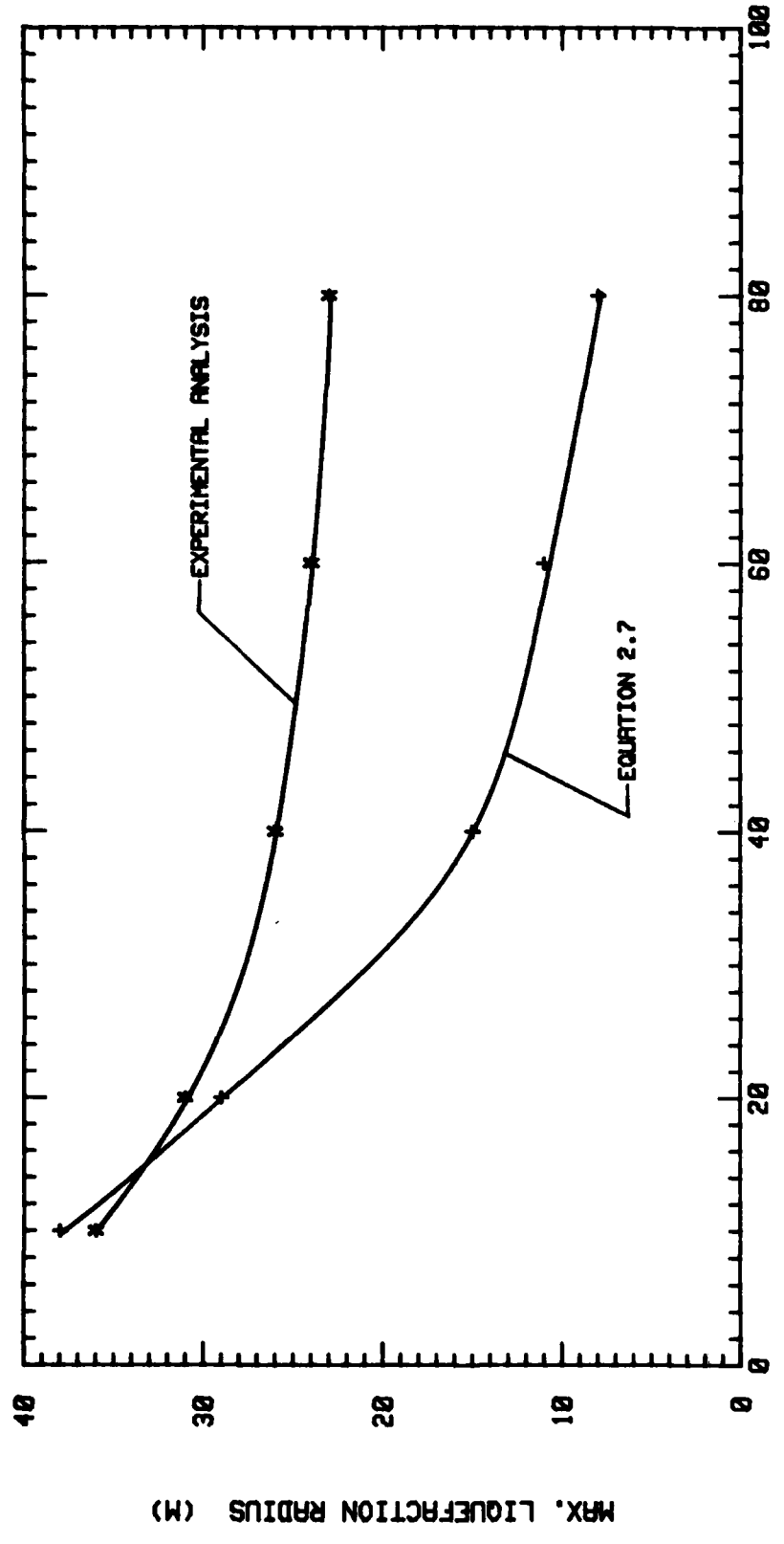

Figure 6.13 Comparison of Maximum Radius of Liquefaction at the Ground Surface as Predicted by Experimental Analysis and Equation 2.7

VII. SUMMARY, CONCLUSIONS AND RECOMMENDATIONS

A. Summary

The cause of earthquake-induced liquefaction is well understood and documented. Shear stress wave propagation is the primary cause of increases in porewater pressures. Although considerable research has been conducted on explosive-induced ground motions and effects, little work has been directed towards examining the phenomenon of explosive-induced liquefaction, hence, this phenomenon is not well understood. This experimental investigation represents an effort to examine and establish a fundamental understanding of compressionally-induced liquefaction.

A new experimental soil dynamics facility has been developed to investigate the transient and long-term porewater pressure response of saturated soils as a function of initial density, initial effective stress and applied load intensity. The facility is capable of generating compressive shock loadings on the order of 35000 KPa with millisecond rise times to peak stress. Samples of water saturated Monterey No. 0/30 sand were prepared at relative densities of approximately 0 , 20, 40, 60 and 80 percent and effective stresses of 86, 172, 345 and 690 KPa. Each sample was subjected to one-dimensional, confined, compressive loadings under undrained conditions. Experimental results have shown that it is possible to liquefy Monterey No. 0/30 sand under these conditions. Significant porewater pressure

increases were observed even at high densities and high effective stresses.

It is evident from this investigation that liquefaction becomes more difficult to induce with increasing density and effective stress, since greater energy is required for porewater pressure increases. The intensity of the applied load is important and liquefaction could be induced by a single high amplitude compressive loading or a series of less intense compressive loadings. Threshold compressive strain values, below which substantial porewater pressures should not occur, were determined to be less than about $1x10^{-2}$ percent. Liquefaction was generally observed at compressive strains greater than about $1x10^{-1}$ percent.

The data analysis has provided empirical models that can be used to estimate the compressive strain required to produce liquefaction in a saturated sand as a function of density and effective stress. One model, Equation 6.11, has been used with an empirical field explosive scaling equation to develop a method of approximating the extent of the liquefied zone in the field when buried, contained charges are detonated in a saturated soil. The results can be applied to estimate the locations of regions having various porewater pressure increases at points away from the explosion.

A finite difference approximation was used to model the porewater pressure response observed in the experimental investigation. The approximation considered the soil-water mixture as a two-phase material and included the nonlinear, inelastic behavior of the soil skeleton. The results were generally consistent with the laboratory behavior and showed a marked increase in the residual excess porewater pressure.

Variations in the results can be attributed to using a static constrained modulus for the soil skeleton in the model and laboratory boundary conditions that could not be exactly simulated by the finite difference approximation.

A number of significant factors that influence the occurrence of liquefaction have been reviewed. Both field and laboratory investigations using explosives have provided consistent observations about the behavior of saturated soils subjected to transient loadings. Empirical scaling equations to predict peak particle velocities, peak compressive strains and peak compressive stresses have been presented.

B. Conclusions

Based on the results of this experimental investigation as well as the discussion and review of other work, the following conclusions were drawn. These conclusions pertain to the laboratory investigation of saturated Monterey No. 0/30 sand under the experimental conditions as previously defined in the text and include the following.

Liquefaction can be induced by dynamic one-dimensional, confined compressive loadings under undrained conditions at the relative densities and effective stresses used in this investigation.

The experimental results show that it is possible to obtain significant porewater pressure increases even at high densities and effective stresses.

Liquefaction can be induced by a single large compressive loading or a series smaller compressive loadings.

The initial density and initial effective stress are significant factors that influence the occurrence of liquefaction. In general, a sample at a high initial relative density and high initial effective stress requires more applied energy to

produce liquefaction than does one at a lower initial effective stress and initial density.

Substantial increases in porewater pressure did not occur at compressive strains less than about $1x10^{-2}$ percent. Liquefaction could be induced at compressive strains greater than about $1x10^{-1}$ percent. Both single and multiple compressive loadings were observed to produce liquefaction.

The finite difference analysis indicates that liquefaction is dependent on the unloading constrained modulus of the soil skeleton which is in turn dependent on the initial density and initial effective stress. The unloading effects for the soil-water mixture are significant and liquefaction appears to occur during unloading due to the nonlinear, inelastic behavior of the soil skeleton.

The statistical models presented, when used with an empirical scaling equation for field explosive events, can be used to approximate the zone of liquefaction around a buried charge. The models need to be verified and modified to account for specific conditions in the field.

The results of this investigation have increased the state-of-the-art in understanding compressionally induced liquefaction and have extended the data base.

In considering the nature of explosions in the field and the results of this investigation, the following conclusions can be drawn relative to the use of buried charges in the field.

Current engineering designs are generally concerned with the peak particle velocity and damage produced by the explosion and do not consider any potential porewater pressure increases or liquefaction effects.

The damage from an explosion in the field may be disproportionate to the amount of energy released if liquefaction occurs. The damage would then include the direct effects of the explosion itself and liquefaction.

Liquefaction may occur at distances and/or peak particle velocities less than those associated with structural damage.

An estimate of field liquefaction zonation can be made by using the approach outlined. However, small scale field explosive tests are recommended to verify and appropriately adjust the equations to more closely match site specific conditions in the field.

C. Recommendations

The results of this investigation and the information currently available in the literature have provided insight into research needs to better understand the phenomenon of liquefaction as produced by intense compressive loadings. Based on this, a number of recommendations can be made.

Research efforts should be extended to investigate the effects of different soil types and varying degrees of saturation on liquefaction potential of soils under compressional loading. Attention also should be given to evaluating both two and three dimensional loading phenomenon.

Develop a series of fully instrumented, systematically controlled, small scale, field explosive tests under controlled conditions. This should involve the variation of initial density, effective stress, saturation and type of loading. Correlations can then be made between field and laboratory results.

The statistical models presented and the empirical equations for explosively produced peak particle velocities should be evaluated with respect to site specific conditions and modified accordingly to account for field conditions.

The effects of liquefaction and soil property changes should be further investigated and incorporated into engineering analysis and design procedures that consider explosive loading of soils and structures.

Develop finite element models that will account for the loading conditions and boundary conditions of this investigation and extend them to two and three dimensional analyses. Since many models treat the soil-water system as a one-phase material, it will be necessary to evaluate a given element of soil as a

two-phase and three-phase material to more accurately evaluate the behavior under loading.

Develop methods for evaluating the dynamic constrained modulus of a soil for both loading and unloading to be used in numerical models.

Establish a standard data set to be obtained from all field tests designed to investigate explosively-induced liquefaction. This should include a complete and appropriate set of information including soil index properties, sub-surface profile characterization, groundwater table location, degree of saturation of the soil and local geologic conditions. Detailed information should also be obtained for the explosive charge being used including type, location, weight, delay times and charge patterns.

Examine available field ground motion records from explosive events to define where the transition from one-dimensional loading to shear loading occurs and evaluate these findings in terms of their interaction in producing liquefaction.

REFERENCES

Abelev, Y. M. and Askalonov, V. V., (1957), "The Stabilization of Foundations of Structures on Loess Soils," Proc., 4th International Conference on Soil Mechanics and Foundation Engineering, London, England, August 12-14, pp. 259-263.

Al-Hussani, M. M., (1976), "Centrifuge Model Testing of Soils: A Literature Review," Miscellaneous Paper S-76-9, U.S. Army Corps of Engineers Waterways Experiment Station, Vicksburg, Mississippi, June.

Allen, N. F., (1975), "Fluid Wave Propagation in Saturated and Nearly Saturated Sands," Doctoral Dissertation, Department of Civil Engineering, University of Michigan, Ann Arbor, Michigan, December.

Allen, N. F., Richart, F. E. and Woods, R. D., (1980), "Fluid Wave Propagation in Saturated and Nearly Saturated Sands," Journal of the Geotechnical Engineering Division, American Society of Civil Engineers, Vol. 106, No. GT 3, March, pp. 235-254.

Ambraseys, N. N. and Hendron, A. J., (1968), "Dynamic Behavior of Rock Masses," Rock Mechanics in Engineering Practice, edited by K. G. Stagg and O. C. Zienkiewicz, John Wiley and Sons, New York, New York.

Arya, A. S., Nandakumaran, P., Puri, V. K. and Mukerjee, S., (1978), "Verification of Liquefaction Potential by Field Blast Tests," Proc., 2nd International Conference on Microzonation for Safer Construction, San Francisco, California, Vol. 1, November 26 - December 1, pp. 865-869.

Benson, K.A., (1983), "Mill Race: Cratering and Related Events," AFWL-TR-82-76, Air Force Weapons Laboratory, Kirtland Air Force Base, Albuquerque, New Mexico, January.

Biggs, J. M., (1964), Introduction to Structural Dynamics, McGraw-Hill, New York, New York.

Biot, M. A., (1956a), "Theory of Propagation of Elastic Waves in a Fluid-Saturated Porous Solid, Part I, Low Frequency Range," Journal of the Acoustical Society of America, Vol. 28, No. 2, pp. 158-178.

Biot, M. A., (1956b), "Theory of Propagation of Elastic Waves in a Fluid-Saturated Porous Solid, Part II, Higher Frequency Range," Journal of the Acoustical Society of America, March, Vol. 28, No. 2, pp. 158-178.

Biot, M. A., (1962), "Mechanics of Deformation and Acoustic Propagation in Porous Media," Journal of Applied Physics, April, Vol. 33, No. 4, pp. 1482-1498.

Blouin, S. E., (1978), "Liquefaction Evidence Observed in Various Explosive Events," Proc., International Workshop on Blast-Induced Liquefaction, Dames & Moore/U.S. Air Force, Maidenhead, United Kingdom, September 17-19, pp. 95-110.

Blouin, S. E. and Kim, K. J., (1983), "Explosion Produced Liquefaction in the Pacific Proving Grounds," Interim Report for the U.S. Air Force Office of Scientific Research, Applied Research Associates, Inc., South Royalton, Vermont, June.

Bruce, J. R., Lindberg, H. E. and Abrahamson, G. R., (1979), "Simulation of Strong Earthquake Motion With Contained Explosive Line Source Arrays," Proc., 2nd International Conference on Earthquake Engineering, Stanford University, Stanford, California, August 22-24, pp. 1134-1143.

Bruce, J. R., Lindberg, H. E. and Schwer, L. E., (1982), "Soil Motion From Contained Explosions," Physical Modeling of Soil Dynamics Problems, Session No. 67, American Society of Civil Engineers National Convention, Las Vegas Nevada, April 30.

Carnes, B. L., (1976), "The Influence of a Shallow Water Table on Cratering," Technical Report SL-81-6, Structures Laboratory, U.S. Army Corps of Engineers Waterways Experiment Station, Vicksburg, Mississippi, September.

Casagrande, A., (1936), "Characteristics of Cohesionless Soils Affecting the Stability of Slopes and Earth Fills," Journal of the Boston Society of Civil Engineers, Boston Society of Civil Engineers, Vol. 23, No. 1, pp. 257-276.

Charlie, W. A., (1978a), "Liquefaction Potential of Soils Under Blast Loads," Technical Report No. 40, AFOSR-TR-78-0349, Air Force Office of Scientific Research, Bolling, Air Force Base, Washington, D.C, August 15.

Charlie, W. A., (1978b), "The Dial Pack Event," Proc., International Workshop on Blast-Induced Liquefaction, Dames & Moore/U.S. Air Force, Maidenhead, United Kingdom, September 17-19, pp. 149-165.

Charlie, W. A., Muzzy, M. W., Tiedemann, D. A. and Doehring, D. O., (1984), "Cyclic Triaxial Behavior of Monterey Number 0 and Number 0/30 Sands," ASTM Geotechnical Testing Journal, Technical Note, American Society for Testing and Materials, Philadelphia, Pennsylvania, Vol. 7, No. 4, December, pp. 211-215.

Charlie, W. A., Shinn, J., Melzer, L. S., Martin, J. P. and Blouin, S. E., (1980), "Blast-Induced Liquefaction Phenomenon and Evaluation," Proc., International Symposium on Soils Under Cyclic and Transient Loading, Swansea, United Kingdom, January 7-11, pp 533-542.

Charlie, W. A., Veyera, G. E. and Abt, S. R., (1985), "Predicting Blast-Induced Porewater Pressure Increases in Soils," Journal of Civil Engineering for Practicing and Design Engineers, Vol. 4, No. 4, April, pp. 311-328.

Cole, R. H., (1948), "Underwater Explosions," Princeton University Press, Princeton, New Jersey.

Committee on Soil Dynamics of the Geotechnical Engineering Division, American Society of Civil Engineers, (1978), "Definition of Terms Related to Liquefaction," Journal of the Geotechnical Engineering Division, American Society of Civil Engineers, Vol. 104, No. GT 9, September, pp. 1197-1200.

Couch, R. F., Fetzer, J. A., Goter, E. R., Ristvet, B. L., Tremba, E. L., Walter, D. R. and Wendland V. P., (1975), "Drilling Operations on Enivetok Atoll During Project EXPOE," AFWL-TR-75-216, Air Force Weapons Laboratory, Kirtland Air Force Base, Albuquerque, New Mexico, September.

Crawford, R. E., Higgins, C. J. and Bultmann, E. A., (1974), The Air Force Manual for Design and Analysis of Hardened Structures, AFWL-TR-74-102, Air Force Systems Command, Kirtland Air Force Base, Albuquerque, New Mexico. 17th Printing, July, 1983.

Damitio, C., (1978a), "Field Experience on Blast-Induced Liquefaction," Proc., International Workshop on Blast-Induced Liquefaction, Dames & Moore/U.S. Air Force, Maidenhead, United Kingdom, September 17-29, pp. 137-148.

Damitio, C., (1978b), "Empirical Predictions of Blast-Induced Liquefaction," Proc., International Workshop on Blast-Induced Liquefaction, Dames & Moore/ U.S. Air Force, Maidenhead, United Kingdom, September 17-19, pp. 390-400.

D'Appolonia, E., (1968), "Dynamic Loadings," American Society of Civil Engineers Specialty Conference on Placement and Improvement of Soils to Support Structures, American Society of Civil Engineers, Massachusetts Institute of Technology, Cambridge, Massachusetts.

Das, B. M., (1983), Fundamentals of Soil Dynamics, Elsevier, New York, New York.

Dowding, C. H., (1985), Blast Vibration Control and Monitoring, Prentice-Hall, Englewood Cliffs, New Jersey.

Drake, J. L., (1978), "Results of Some Experiments Conducted Primarily for the Purpose of Understanding the Influence of Water Table Depth on the Size and Extent of Craters," Proc., International Workshop on Blast-Induced Liquefaction, Dames & Moore/U.S. Air Force, Maidenhead, United Kingdom,. September 17-19, pp. 250-266.

Drake, J. L. and Ingram, L. F., (1981), "Predictions of the Airblast and Ground Motions Resulting from Explosive Removal of the Bird's Point-New Madrid Fuze Plug Levee," Miscellaneous Paper SL-81-30, U.S. Army Corps of Engineers Waterways Experiment Station, Vicksburg, Mississippi, November.

Drake, J. L. and Little, C. D., (1983), "Ground Shock From Penetrating Conventional Weapons," Proc., Symposium on the Interaction of Non-Nuclear Munitions with Structures, U.S. Air Force Academy, Colorado Springs, Colorado, Part I, May 10-13, pp. 1-6.

Engineering News Record, (1932), "Blasting to Settle Swamp Fill Approaches Rational Practice," March 10, pp. 354-355.

Finn, W. D. L., (1972), "Liquefaction of Sands," Proc., 1st International Conference on Microzonation for Safer Construction Research and Application, Seattle, Washington, Vol. 1, October 30 - November 3, pp. 87-111.

Finn, W. D. L., (1981), "Liquefaction Potential: Developments Since 1976," Proc., International Conference on Recent Advances in Geotechnical Earthquake Engineering and Soil Dynamics, University of Missouri-Rolla, St. Louis, Missouri, April 26 - May 3, pp. 655-681.

Florin, V. A. and Ivanov, P. L., (1961), "Liquefaction of Saturated Sandy Soils," Proc., 5th International Conference on Soil Mechanics and Foundation Engineering, ISSMFE, Paris, France, Vol. 1, July 17-22, pp. 107-111.

Fragaszy, R. J. and Voss, M. E., (1981), "Laboratory Verification of Blast-Induced Mechanism," Final Report, Air Force Office of Scientific Research Grant No. 81-0085, Air Force Office of Scientific Research, Bolling Air Force Base, Washington, D.C., October.

Fragaszy, R. J., Voss, M. E., Schmidt, R. M. and Holsapple, K. A., (1983), "Laboratory and Centrifuge Modeling of Blast-Induced Liquefaction," Proc., 8th International Symposium on Military Applications of Blast Simulation, Gruppe fur Rustungsdienste, Spiez, Switzerland, pp. 1-20.

Gilbert, P. A., (1976), "Case Histories of Liquefaction Failures," Miscellaneous Paper 8-76-4, U.S. Army Corps of Engineers Waterways Experiment Station, Vicksburg, Mississippi, April.

Green, P.A. and Ferguson, P. A. S., (1971), "On Liquefaction Phenomenon, by Professor A. Casagrande: Report of Lecture," Geotechnique, The Institution of Civil Engineers, Vol. XXI, No. 3, September, pp. 197-202.

Hall, C. E., (1962), "Compacting a Dam Foundation by Blasting," Journal of the Soil Mechanics and Foundation Engineering Division, American Society of Civil Engineers, Vol. 88, No. SM 3, June, pp. 33-51.

Hendron, A. J., (1963), "The Behavior of Sand in One-Dimensional" Compression," Doctoral Dissertation, Department of Civil Engineering, University of Illinois at Urbana.

Henrych, J., (1979), The Dynamics of Explosion and Its Use, Elsevier, New York, New York.

Ishihara, K. J., (1967), "Propagation of Compressional Waves in a Saturated Soil," Proc., International Conference on Wave Propagation and Dynamic Properties of Earth Materials, University of New Mexico, Albuquerque, New Mexico, August 23-25, pp. 451-467.

Ishihara, K. J. and Watanabe T., (1976), "Sand Liquefaction Through Volume Decrease Potential," Japanese Society of Soil Mechanics and Foundation Engineering, Japan, Vol. 16, No. 4, pp. 61-70.

Ivanov, P. L., (1967), "Compaction of Noncohesive Soils by Explosions," Izdatel'stvor Literatury Po Stroitel'stvu, Leningrad, U.S.S.R., Translated by the Indian National Scientific Documentation Center, New Delhi, India, Published for the U.S. Department of the Interior, Bureau of Reclamation and National Science Foundation, Washington, D.C.

Ivanov, P. L., Sinitsin, A. P. and Musaelyan, A. A., (1981), "Characteristics of Soils at Cyclic and Shock Loads," Proc., 10th International Conference on Soil Mechanics and Foundation Engineering, Stockholm, Sweden, Vol. 3, June 15-19, pp. 239-243.

Jackson, J. G., (1978), "WES Dynamic Soil Property Test Equipment for Blast Oriented Problems," Proc., International Workshop on Blast-Induced Liquefaction, Dames & Moore/U.S. Air Force, Maidenhead, United Kingdom, September 17-19, pp. 211-230.

Jackson, J. G. , Erghott, J. Q. and Rohani, B., (1980), "Loading Rate Effects on Compressibility of Sand," Journal of the Geotechnical Engineering Division, American Society of Civil Engineers, Vol. 105, No. GT 8, August, pp. 839-852.

James, R. G., (1978), " Explosive Tests in the Centrifuge," Proc., International Workshop on Blast-Induced Liquefaction, Dames & Moore/U.S. Air Force, Maidenhead, United Kingdom, September 17-19, pp. 188-201.

Jones, G. H. S. , (1976), "Complex Craters in Alluvium," Proc., Symposium on Planetary Cratering Mechanics, U.S. Geologic Survey, Geologic Division Branch of Astrogeologic Studies, Flagstaff, Arizona, September 13-17, pp. 163-182.

Klohn, E. J., Garga, V. K. and Shukin, W., (1981), "Densification of Sand Tailings by Blasting," Proc., 10th International Conference on Soil Mechanics and Foundation Engineering, ISSMFE, Stockholm, Sweden. Vol. 3, June 15-19, pp. 725-730.

Kok, L., (1977), "The Effect of Blasting in Water-Saturated Sands," Proc., 5th International Symposium on Military Applications of Blast Simulation, Royal Swedish Fortifications Administration, Stockholm, Sweden, May 23-26, pp. 7:6:1-7:6:10.

Kok, L., (1978a), "Some Dutch Laboratory and Field Results on Blast-Induced Liquefaction," Proc. International Workshop on Blast-Induced Liquefaction, Dames & Moore/U.S. Air Force, Maidenhead, United Kingdom, September 17-19, pp. 71-94.

Kok, L., (1978b), "Empirical Predictions of Blast-Induced Liquefaction," Proc., International Workshop on Blast-Induced Liquefaction, Dames & Moore/U.S. Air Force, Maidenhead, United Kingdom, September 17-19, pp. 408-424.

Kok, L., (1978c), "Explosive Densification and Vertical Drainage as Soil Consolidation Techniques for Harbour Building," Proc., 7th International Harbour Congress, Antwerp, Belgium, May 22-26, pp. 1.04/1-1.04/7.

Kolsky, H., (1963), Stress Waves In Solids, Dover, New York, New York.

Kummeneje, O. and Eide, O., (1961), "Investigation of Loose Sand Deposits by Blasting," Proc., 5th International Conference on Soil Mechanics and Foundation Engineering, ISSMFE, Paris, France, Vol 1., July 17-22, pp. 491-497.

Kurzeme, M., (1971), "Liquefaction of Saturated Granular Soils," Proc. 1st Australia-New Zealand Conference on Geomechanics, Australian Geomechanics Society, Melbourne, Australia, Vol. 1, August 9-13, pp 45-53.

Ladd, R. S., (1978), "Preparing Test Specimens Using Undercompaction," American Society for Testing and Materials Geotechnical Testing Journal, American Society for Testing and Materials, Philadelphia, Pennsylvania, Vol. 1, No. 1, March, pp 16-23.

Lambe, W. T. and Whitman, R. V., (1969), Soil Mechanics, John Wiley and Sons, New, York, New York.

Langley, N. P., Smith, C. R. and Pfefferle, W., (1972), "DIAL PACK - Soil Pore Pressure and Shear Strength Test," Aerospace Report No. TOR-0172-(S2970-20)-1, The Aerospace Corporation, San Bernadino, California, Space and Missile Systems Organization, U.S. Air Force Systems Command, U.S. Air Force Unit Post Office, Los Angeles, California, February.

Lee, K. L. and Fitton, J. A., (1968), "Factors Affecting the Dynamic Strength of Soils," Vibration Effects of Earthquakes on Soils and Foundations, ASTM STP 450, American Society for Testing and Materials, Philadelphia, Pennsylvania.

Long, H., Ries, E. R. and Michalapoulos, A. P., (1981), "Potential for Liquefaction Due to Construction Blasting," Proc., International Conference on Recent Advances in Geotechnical Engineering and Soil Dynamics, University of Missouri-Rolla, St. Louis, Missouri, April 26 - May 3, pp. 191-194.

Lyakhov, G. M., (1961), "Shock Waves in the Ground and the Dilatency of Water Saturated Sand," Zhurnal Prikladnoy Mekhanik i Tekhnicheskoy Fiziki, Moscow, U.S.S.R., No. 1, pp. 38-46.

Lyman, A. K. B., (1942), "Compaction of Cohesionless Foundation Soils by Explosives," Transactions of the American Society of Civil Engineers, Vol. 68, No. 8, Part 2, Transactions No. 107, October, pp. 1330-1348.

Marti, J., (1978), "Blast-Induced Liquefaction: A Survey," Technology Report No. TR-78-3, Dames & Moore, London, United Kingdom, U.S. Air Force Office of Scientific Research, Bolling Air Force Base, Washington, D.C., May 25.

Melzer, L. S., (1978a), "Blast-Induced Liquefaction of Materials," Nuclear Technology Digest, AFWL-TR-78-110, Air Force Weapons Laboratory, Kirtland Air Force Base, Albuquerque, New Mexico, August, pp. 21-38.

Melzer, L. S., (1978b), "The Nature and Effects of Explosions in Soils," Proc., International Workshop on Blast-Induced Liquefaction, Dames & Moore/U.S. Air Force, Maidenhead, United Kingdom, September 17-19, pp. 24-55.

Mitchell, J. K., (1970), "In-Place Treatment of Foundation Soils," Journal of the Soil Mechanics and Foundation Engineering Division, American Society of Civil Engineers, Vol. 96, No. SM 1, January, pp. 73-110.

Mitchell, J. K. and Katti, R. K., (1981), "Soil Improvement - State-of-the-Art Report (Preliminary)," Proc., 10th International Conference on Soil Mechanics and Foundation Engineering, ISSMFE, Stockholm, Sweden, June 15-19, pp. 261-317.

Mueller, O., (1971), "Soil Compaction by Blasting," Proc., 4th Budapest Conference on Soil Mechanics and Foundation Engineering, Akademiai Kiado, Budapest, Hungary, October 12-15, pp. 463-468.

Muzzy, M. W., (1983), "Cyclic Triaxial Behavior of Monterey No. 0 and No. 0/30 Sands," Master's Thesis, Department of Civil Engineering, Colorado State University, Ft. Collins, Colorado, May.

Obermeyer, J. R., (1980), "Monitoring Uranium Tailings Dams During Blasting Program," Proc., 3rd Symposium on Uranium Mill Tailings Management, Colorado State University, Ft. Collins, Colorado, November 24-25, pp. 513-527.

Oriard, L. L., (1976), "Vibrations Due to Blasting," Report No. DOT-TST-76-91, Proc., Workshop on Construction Blasting for Tunnels, Underground Research Council, American Society of Civil Engineers, Published by U.S. D.O.T., Washington, D.C., November 11-13, pp. 200-221.

Perry, E. B., (1972), "Movement of Variable-Density Inclusions in Wet Sand Under Blast Loading," Miscellaneous Paper S-72-37, U.S. Army Corps of Engineers Waterways Experiment Station, Vicksburg, Mississippi, September.

Piekutowski, A. J., (1976), Cratering Mechanisms Observed in Laboratory-Scale High-Explosive Experiments," Proc., Symposium on Planetary Cratering Mechanics, U.S. Geologic Survey, Geologic Division Branch of Astrogeologic Studies, Flagstaff, Arizona, September 13-17, pp. 67-102.

Prakash, S. and Gupta, M. K., (1970), "Blast Tests at Tenughat Dam Site," Journal South East Asian Society of Soil Engineering, Southeast Asian Society of Soil Engineers, Bangkok, Thailand, Vol. 1, No. 1, June, pp. 41-85.

Prater, E. G., (1977), "Pressure Wave Propagation in a Saturated Soil Layer With Special Reference to Soil Liquefaction," Proc., 5th International Symposium on Military Applications of Blast Simulation, Royal Swedish Fortifications Administration, Stockholm, Sweden, May 23-26, pp. 7:3:1-7:3:23.

Prugh, B. J., (1963), Densification of Soils by Explosive Vibrations," Journal of the Construction Division, American Society of Civil Engineers, Vol. 89, No. CO 1, March, pp. 79-100.

Puchkov, S. V., (1962), "Correlation Between the Velocity of the Seismic Oscillations of Particles and the Liquefaction Phenomenon of Saturated Sands," Problems of Engineering Seismology, Issue No. 6, Study No. 21, Edited by S. V. Medvedev, translated by Consultants Bureau, New York, New York, pp. 92-94.

Quaak, M. P., (1978), "Shock Tube Tests at TNO," Proc., International Workshop on Blast-Induced Liquefaction, Dames & Moore/U.S. Air Force, Maidenhead, United Kingdom, September 17-19, pp. 231-238.

Queiroz, L. A., Oliveira, H. G. and Nazario, F. A. S., (1967), "Foundation Treatment of Rio Casca III Dam," Proc., 9th International Congress on Large Dams, International Commission on Large Dams, Istanbul Turkey, Vol. 1, Question No. 32, September 4-8, pp. 321-333.

Richart, F. E., Hall, J. R. and Woods, R. D., (1970), Vibrations of Soils and Foundations, Prentice-Hall, Englewood Cliffs, New Jersey.

Rinehart, J. S., (1975), Stress Transients in Solids, Hyperdynamics, Inc., Santa Fe, New Mexico.

Rischbieter, F., (1977), "Soil Liquefaction - A Survey of Research," Proc., 5th International Symposium on Military Applications of Blast Simulation, Royal Swedish Fortifications Administration, Stockholm, Sweden, May 23-26, pp. 7:1:1-7:1:24.

Rischbieter, F., (1978), "Liquefaction Tests on Refilled, Partly Saturated Soils," Proc., International Workshop on Blast-Induced Liquefaction, Dames & Moore/U.S. Air Force, Maidenhead, United Kingdom, September 17-19, pp. 65-70.

Rischbieter, F., Corvin, P., Metz, K. and Schaepermeier, E., (1977), "Studies of Soil Liquefaction by Shock Wave Loading," Proc., 5th International Symposium on Military Applications of Blast Simulation, Royal Swedish Fortifications Administration, Stockholm, Sweden, May 23-26, pp. 7:4:1-7:4:12.

Ristvet, B. L., Tremba, E. L., Couch, R. F., Fetzer, J. A., Goter, E. R., Walter, D. R. and Wendland, V. P., (1978), "Geologic and Geophysical Investigations of the Eniwetok Nuclear Craters," AFWL-TR-77-242, Air Force Weapons Laboratory, Kirtland Air Force Base, Albuquerque, New Mexico, September.

Roddy, D. J., (1976a), "Tabular Comparisons of the Flynn Creek Impact Crater, United States, Steinhein Impact Crater, Germany and SNOWBALL Explosion Crater, Canada," Proc., Symposium on Planetary Cratering Mechanics, U.S. Geologic Survey, Geologic Division Branch of Astrogeologic Studies, Flagstaff, Arizona, September 13-17, pp. 125-161.

Roddy, D. J., (1976b), "Large-Scale Impact and Explosion Craters: Comparisons of Morphological and Structural Analogs," Proc., Symposium on Planetary Cratering Mechanics, U.S. Geologic Survey, Geologic Division Branch of Astrogeologic Studies, Flagstaff, Arizona, September 13-17, pp. 185-246.

Ruygrok, P. A. and Van der Kogel, H. (1980), "Some Results of Experiments on Nearly Saturated and Dry Sand," Proc., International Symposium on Soils Under Cyclic and Transient Loading, Swansea, United Kingdom, January 7-11, pp. 211-224.

Ryan, T. A., Joiner, B. L. and Ryan, B. F., (1976), MINITAB Student Handbook, Duxbury Press, North Scituate, Massachusetts.

Ryan, T. A., Joiner, B. L. and Ryan, B. F., (1982), MINITAB Reference Manual, Statistics Department, The Pennsylvania State University, University, Park, Pennsylvania.

Sanders, S. G., (1982), "Assessment of the Liquefaction Hazards Resulting from Explosive Removal of the Bird's Point New-Madrid Fuze Plug Levee," Miscellaneous Paper No. GL-82-5, U.S. Army Corps of Engineers Waterways Experiment Station, Vicksburg, Mississippi, April.

Schaepermeier, E., (1978a), Liquefaction Produced by Compressional Waves," Proc., International Workshop on Blast-Induced Liquefaction, Dames & Moore/U.S. Air Force, Maidenhead, United Kingdom, September 17-19, pp. 57-64.

Schaepermeier, E., (1978b), "Soil Liquefaction Test in Meppen Proving Ground, 1978," Proc., 6th International Symposium on Military Applications of Blast Simulation, Cahors, France, pp. 7.4.1-7.4.5.

Schaepermeier, E., (1978c), "Soil Liquefaction Field Test in Meppen Proving Ground, 1978: Structure Response," Proc., 6th International Symposium on Military Applications of Blast Simulation, Cahors, France, pp. 7.5.1-7.5.27.

Schmidt, R. M., (1976),"A Centrifuge Cratering Experiment: Development of a Gravity-Yield Parameter," Proc., Symposium on Planetary Cratering Mechanics, U.S. Geologic Survey, Geologic Division Branch of Astrogeologic Studies, Flagstaff, Arizona, September 13-17, pp. 1261-1296.

Schmidt, R. M., Fragaszy, R. J. and Holsapple, K. A., (1981), "Centrifuge Modeling of Soil Liquefaction Due to Airblast," Proc., 7th International Symposium on Military Applications of Blast Simulation, Defense Research Establishment Suffield, Medicine Hat, Alberta, Canada, July 13-17.

Seaman, L., (1983), "Evaluation of WES One-Dimensional Dynamic Soil Testing Procedures," Miscellaneous Paper SL-83-8, U.S. Army Corps of Engineers Waterways Experiment Station, Vicksburg, Mississippi, June.

Seed, H. B., (1968), "The Fourth Terzaghi Lecture: Landslides During Earthquakes Due to Soil Liquefaction," Journal of the Soil Mechanics and Foundation Engineering Division, American Society of Civil Engineers, Vol. 94, No. SM 5, September, pp. 1053-1122.

Seed, H. B., (1976), "Evaluation of Soil Liquefaction Effects on Level Ground During Earthquakes," Liquefaction Problems in Geotechnical Engineering, American Society of Civil Engineers Annual Convention and Exposition, Philadelphia, Pennsylvania.

Seed, H. B., (1979), "Soil Liquefaction and Cyclic Mobility Evaluation for Level Ground During Earthquakes," Journal of the Geotechnical Engineering Division, American Society of Civil Engineers, Vol. 105, No. GT 2, February, pp. 201-255.

Seed, H. B., (1981), "Earthquake Resistant Design of Earth Dams," Proc., International Conference on Recent Advances in Geotechnical Engineering and Soil Dynamics, University of Missouri-Rolla, St. Louis, Missouri, April 26 - May 3, pp. 1157-1173.

Seed, H. B. and Booker, J. R., (1976), "Stabilization of Potentially Liquefiable Sand Deposits Using Gravel Drain Systems," Report No. EERC 76-10, Earthquake Engineering Research Center, University of California, Berkeley, California, April.

Seed, H. B. and Idriss, I. M., (1967), "Analysis of Soil Liquefaction: Niigata Earthquakes," Journal of the Soil Mechanics and Foundation Engineering Division, American Society of Civil Engineers, Vol. 93, No. SM 3, May, pp. 83-108.

Seed, H. B. and Idriss, I. M., (1971), "Simplified Procedure for Evaluating Soil Liquefaction Potential," Journal of the Soil Mechanics and Foundation Engineering Division, American Society of Civil Engineers, Vol. 97, No. SM 9, September, pp. 1249-1273.

Seed, H. B. and Lundgren, R., (1954), "Investigation of the Effect of Transient Loading on the Strength and Deformation Characteristics of Saturated Sands," Proc., 57th Annual Meeting of the American Society for Testing and Materials, Vol. 54, pp. 1288-1360.

Silver, M. L., (1981), "Load, Deformation and Strength Behavior of Soils Under Dynamic Loadings," Proc., International Conference on Recent Advances in Geotechnical Earthquake Engineering and Soil Dynamics, University of Missouri-Rolla, St. Louis, Missouri, April 26 - May 3.

Solymar, Z. V., (1984), "Compaction of Alluvial Sands by Deep Blasting," Canadian Geotechnical Journal, National Research Council of Canada, Vol. 21, No.3, August, pp 305-321.

Solymar, Z. V., Iloabachie, B. C., Gupta, R. C. and Williams, L. R., (1984), "Earth Foundation Treatment at Jebba Dam Site," Journal of the Geotechnical Engineering Division, American Society of Civil Engineers, Vol. 110, No. 10, October, pp. 1415-1431.

Studer, J., (1978), "Laboratory and Field Shock Tube Tests," Proc., International Workshop on Blast-Induced Liquefaction, Dames & Moore/U.S. Air Air Force, Maidenhead, United Kingdom, September 17-19, pp. 167-187.

Studer, J. and Hunziker, E., (1977), "Experimental Investigation on Liquefaction of Saturated Sand Under Shock Loading," Proc., 5th International Symposium on Military Applications of Blast Simulation, Royal Swedish Fortifications Administration, Stockholm, Sweden, May 23-26, pp. 7:2:1-7:2:9.

Studer, J. and Kok, L., (1980), "Blast-Induced Excess Porewater Pressures and Liquefaction: Experience and Application," Proc., International Symposium on Soils Under Cyclic and Transient Loading, Swansea, United Kingdom, January 7-11, pp. 581-593.

Studer, J., Kok, L. and Trense, R. W., (1978), "Soil Liquefaction Field Test - Meppen Proving Ground 1978 Free Field Response," Proc., 6th International Symposium on Military Applications of Blast Simulation, Cahors, France, pp. 7.3.1-7.3.18.

Studer, J. and Prater, E. G., (1977), "An Experimental and Analytical Study of the Liquefaction of Saturated Sands Under Blast Loads," Proc., International Conference on Numerical Methods in Soil and Rock Mechanics, Karlsruhe, Germany, Vol. 2, September 5-16, pp. 217-238.

Tanimoto, K., (1967), "Liquefaction of Sand Layer Subjected to Shock and Vibratory Loads," Proc., 3rd Asian Regional Conference on Soil Mechanics and Foundation Engineering, Haifa, Israel, Vol. 1, September 25-28, pp. 362-365.

Terzaghi, K., (1943), Theoretical Soil Mechanics, John Wiley and Sons, New York, New York.

Terzaghi, K., (1956), "Varieties of Submarine Slope Failures," Proc., 8th Texas Conference on Soil Mechanics and Foundation Engineering, Special Publication No. 29, Bureau of Engineering Research, University of Texas, Austin, Texas, September 14-15.

Terzaghi, K. and Peck, R. B., (1948), Soil Mechanics in Engineering Practice, John Wiley and Sons, New York, New York.

Timoshenko, S. P. and Goodier, J. W., (1970), Theory of Elasticity, McGraw-Hill, New York, New York.

Trense, R. W., (1977), "Soil Liquefaction - New Results From Dutch Tests," Proc., 5th International Symposium on Military Applications of Blast Simulation, Royal Swedish Fortifications Administration, Stockholm, Sweden, May 23-26, pp. 7:5:1-7:5:6.

True, D. G., (1967), "A Study of Pore Pressure Propagation in Sand," Proc., International Symposium on Wave Propagation and Dynamic Properties of Earth Materials, University of New Mexico, Albuquerque, New Mexico, August 23-25, pp. 541-544.

True, D. G., (1969), "Dynamic Pore Pressure Propagation in Sand," Technical Report No. R-610, Naval Civil Engineering Laboratory, Port Hueneme, California.

Van der Kogel, H., Van Loon-Engels, C. H. and Ruygrok, P. A., (1981), "Wave Propagation in Porous Media, Shock Tube Experiments," Proc., 10th International Conference on Soil Mechanics and Foundation Engineering, ISSMFE, Stockholm, Sweden, Vol. 3, June 15-19, pp. 253-256.

Vesic, A. S., Boutwell, G. P. and Tai, Tein-Lie, (1967), Theoretical Studies of Cratering Mechanisms Affecting the Stability of Cratered Slopes, Technical Report No. 3-699, Report No.6, Phase III, Engineering Properties of Nuclear Craters, Final Report on Research by U.S. Army Nuclear Cratering Group and U.S. Army Corps of Engineers Waterways Experiment Station, Vicksburg, Mississippi, March.

Whitman, R. V., (1957), "The Behaviour of Soils Under Transient Loadings," Proc., 4th International Conference on Soil Mechanics and Foundation Engineering, ISSMFE, London, United Kingdom, Vol. 1, August 12-24, pp. 207-210.

Whitman, R. V., (1969), "The Current Status of Soil Dynamics," Applied Mechanics Reviews, Vol. 22, No. 1, January, pp. 1-8.

Whitman, R. V., and Healy K. A., (1962), "Shear Strength of Sands During Rapid Loading," Journal of the Soil Mechanics and Foundation Engineering Division, American Society of Civil Engineers, Vol. 88, No. SM 2, April, pp. 99-129.

Whitman, R. V., Miller, E. T. and Moore, P. J., (1964), "Yielding and Locking of Confined Sands," Journal of the Soil Mechanics and Foundation Engineering Division, American Society of Civil Engineers, Vol. 90, No. SM 4, July, pp. 57-84.

Wild, P. A. and Haslam, E. F., (1962), "Towers and Foundations for Project EHV," Journal of the Power Division, American Society of Civil Engineers, Vol. 88, No. PO 2, July, pp. 69-105.

Workman, J. W., Trulio, J. G. and Stokes, E. S., (1981), "Trajectory Analysis, An Aid in Defining the MX System Ground Motion," AFWL-TR-80-56, Air Force Weapons Laboratory, Kirtland Air Force Base, Albuquerque, New Mexico.

Yamamura, K. and Koga, Y., (1974), "Estimation of Liquefaction Potential by Means of Explosion Test," Proc., 6th Joint Panel Conference of the U.S.-Japan Cooperative Program in Natural Resources, National Bureau of Standards, Washington, D.C., May, pp III-38 - III-51.

Yang, I-Min, (1973), "Ground Surface Waves," Tetra-Tech Report No. TT-P-260- 73-1, Report for Defense Nuclear Agency, Tetra-Tech, Inc., Pasadena, California, February.

END

12-86

DTIC